AD 297 946

WADD-TR-60-646
PART II

CARBONIZATION OF PLASTICS AND REFRACTORY MATERIALS RESEARCH

TECHNICAL REPORT NO. WADD-TR-60-646, PART II

January 1963

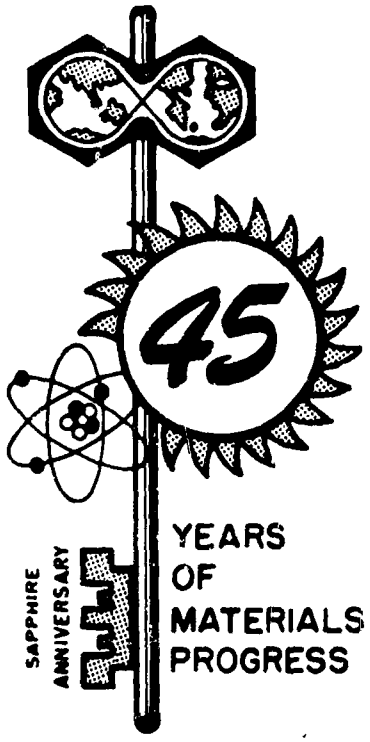

Directorate of Materials and Processes
Aeronautical Systems Division
Air Force Systems Command
Wright-Patterson Air Force Base, Ohio

Project No. 4776

(Prepared under Contract No. AF 33(616)-6841 by
General Electric Company, Cincinnati, Ohio
J. A. Coffman, G. M. Kibler, T. F. Lyon,
B. D. Acchione, authors)

NOTICES

When Government drawings, specifications, or other data are used for any purpose other than in connection with a definitely related Government procurement operation, the United States Government thereby incurs no responsibility nor any obligation whatsoever; and the fact that the Government may have formulated, furnished, or in any way supplied the said drawings, specifications, or other data, is not to be regarded by implication or otherwise as in any manner licensing the holder or any other person or corporation, or conveying any rights or permission to manufacture, use, or sell any patented invention that may in any way be related thereto.

Qualified requesters may obtain copies of this report from the Armed Services Technical Information Agency, (ASTIA), Arlington Hall Station, Arlington 12, Virginia.

This report has been released to the Office of Technical Services, U.S. Department of Commerce, Washington 25, D.C., in stock quantities for sale to the general public.

Copies of this report should not be returned to the Aeronautical Systems Division unless return is required by security considerations, contractual obligations, or notice on a specific document.

B

20-453C, 700, 2-27-63

FOREWORD

This report was prepared by the Flight Propulsion Laboratory Department, General Electric Company, under USAF Contract No. AF 33(616)-6841. Presented herein are results of investigations performed under the auspices of the Department of Defense, through the Advanced Research Projects Agency Order No. 24-60, Task 6, Project No. 4776, "Material Thermal Properties." The work was administered under the direction of the Directorate of Materials and Processes, Deputy for Technology, Aeronautical Systems Division, Wright-Patterson Air Force Base, Ohio. Messrs H. Marcus, P. W. Dimiduk and I. Goldfarb were the project engineers.

This report covers work done from 1 July 1960 to 30 June 1961, inclusive, and as such, is a continuation of work begun earlier and reported in WADD Technical Report 60-646, Part I.

The over-all program during the period covered by the present work was under the direction of G. M. Kibler, Flight Propulsion Laboratory Department. The individual tasks were conducted as follows:

Task I - Carbonization of Plastics; directed by J. A. Coffman; work done by W. S. Horton, E. E. Stone, G. P. Brown, E. G. McGowan, G. P. Schacher, A. Goldman and H. Friedman.

Task II - Vapor Pressure of Refractory Materials; directed by G. M. Kibler; work done by T. F. Lyon, G. Vidale (now deceased), and M. S. Linevsky.

Task III - Spectral Emissivity of Refractory Materials; directed by K. L. Coulson; work bone by B. Acchione.

ABSTRACT

Presented in this report are the results of continuing investigations of the Carbonization of Plastics, the Vapor Pressure of Refractory Materials and the Spectral Emissivity of Refractories.

Studies of thermal degradation of phenolic, epoxy, polyphenylene and polynaphthalene resins were made utilizing, as earlier, the arc-image furnace, the fluidized bed reactor and the thermogravimetric analysis technique. The effect of semicarbonized materials used as fillers has been studied and a Bendix time-of-flight mass spectrometer has been adapted to the study of transient and stable species resulting from the flash-photolysed degradation of plastics. Properties of carbon residues have been measured.

Vapor pressure studies using the Langmuir evaporation technique, the matrix isolation method, and resonance line absorption spectroscopy have progressed. Rates of evaporation of tungsten carbides, hafnium carbide and titanium carbide have been measured; further conclusive measurements on zirconium carbide have been made. Preliminary application of the matrix isolation technique to thoria has been made. Resonance line absorption studies have been completed on zirconium carbide and titanium carbide and the accessible thermodynamic data have been deduced.

Normal spectral emissivities of W-2 coated molybdenum, siliconized ATJ graphite, tantalum, molybdenum, tungsten carbide and zirconium have been measured in the temperature range 1400 to 3100°K.

This report has been reviewed and is approved.

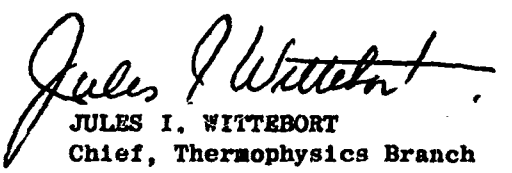

JULES I. WITTEBORT
Chief, Thermophysics Branch
Physics Laboratory
Directorate of Materials and Processes

TABLE OF CONTENTS

LIST OF ILLUSTRATIONS

LIST OF TABLES

I. INTRODUCTION

In November, 1959, work was undertaken to provide additional technology in the form of physical and chemical property data on selected refractory materials considered for possible future use in construction of uncooled nozzle components for solid propellant rocket motors. It was the intent of the investigation to alleviate some of the lack of design information which are also criteria for materials selection, and to add to the understanding of the complex mechanical, physical and chemical phenomena which accompany nozzle failure.

Three problem areas were recognized and research studies in each were defined. Three essentially independent investigations were initiated: The first involves a study of the process of plastics carbonization or degradation, including measurements of rates determination of possible mechanisms, and examination of the char and the volatile products resulting. The second concerns study of the rate of evaporation, determining the vapor pressure and the vapor species produced by refractory materials at very high temperatures. Together with the accessible thermodynamic data which can be deduced from these measurements, such information provides means for separating the effects of vaporization and chemical reaction from the complex process termed erosion. The third program involves measurement of normal spectral emissivities of refractory materials also at very high temperatures, in order to provide information on radiative heat transfer of importance at temperatures which are currently produced or projected by rocket exhausts.

Manuscript released by authors August 1961 for publication as a WADD Technical Report.

II. CARBONIZATION OF PLASTICS

A. Background

WADD Technical Report 60-646 Part 1 summarized the work accomplished on this task through 30 June 1960. Described in that report were the experimental techniques employed, the apparatus designed and built, the procedures used, and the results obtained during the first eight months of the project.

In the intervening year, work has continued on thermogravimetric analysis, arc-image furnace carbonization, fluid bed carbonization, and Time-of-Flight mass spectrometry investigations. In addition, some effort has been put into preparation of certain high carbon yield polymers study of semi-carbonized fillers, and formation of carbides from refractory metal filled resins.

This work has contributed, in some measure, to the gradually clarifying picture of the carbonization process. It seems likely too, that some of the leads which have been uncovered will, if followed on development projects, result in plastics of improved performance characteristics. Some progress has been made toward the goal of describing carbonization in more precise physical chemistry terms.

Carbonization is a complex process, differing substantially from other degradative processes in which only volatile species are formed. Attempts to define it mathematically tend to lead to unrealistic energies of activation and kinetic equations which are valid over only narrow ranges of conditions and for specific plastics. It might be helpful to describe briefly the process as precisely as possible in nonmathematical terms.

Consider a sample of phenolic resin which is to be carbonized. If well cured, it is already cross-linked together into essentially one molecule whose dimensions are those of the sample. That is, nearly all of the atoms in the sample are tied to each other by primary chemical bonds. After carbonization, the sample is still one molecule, now mostly carbon, with the proportion of other atoms and the degree of graphitization being dependent on the top temperature reached, and, to a lesser extent, on the time. In between these two states, by an almost infinite variety and number of steps, the hydrogen, oxygen, and some of the carbon atoms are torn loose as small molecules and radical fragments. These diffuse to the surface, sometimes undergoing further reaction on the way. The carbon skeleton shifts and shrinks and adjusts itself, and develops pores and fissures as the material changes from a resin to a coke, but never loses its one molecule character, unless, of course, the sample breaks into pieces.

As shown by Franklin [1] and Winslow et al. [2], materials such as phenolics, cellulose, and polvinylidene chloride, which are hydrogen-poor and form highly cross-linked structures at low temperatures, yield hard, amorphous cokes which show little graphitic character up to at least 1000°C. At the other extreme are fluid resins like coal tar pitch which condense to fairly large, planar aromatic ring structures before cross-linking; these yield soft, graphitic cokes. Between these extremes are many materials which yield cokes of intermediate character.

Barry and Sutton [3], for example, showed that certain epoxies yield an open-mesh primary char structure in which is deposited a great deal of pyrolytic carbon formed by thermal cracking of gaseous fragments as these diffuse outward to the surface. Similarly, Marolo [4] found evidence, in examination of phenolic-nylon laminate chars, for primary hard coke formation from the phenolic, and deposition in this structure of soft carbon derived from the thermoplastic nylon.

Most carbonizing plastics fall into this intermediate range of behavior, and there are variations even within a given resin family. For example, if a phenolic resin is made with a substantial portion of cresol, xylenol, or butylphenol, the resulting coke is softer and lower in yield than if straight synthetic phenol is used. Epoxies give, on the average, a fairly soft coke with a yield of about 25%. If a hydrogen-rich curing agent like diethylene triamine is used, the coke yield almost disappears. If a hydrogen-poor, strongly cross-linking curing agent like pyromellitic dianhydride is used with epoxies, a 40% yield of a harder coke is obtained.

In general, carbon yields are affected most strongly by two factors: 1) elemental composition, particularly carbon/hydrogen ratio, and 2) degree of cross-linking prior to the onset of carbonization. Of the two, the first is of greater importance. Details of molecular structure of the resin have some significance, but the effect is not usually large.

Polymers which do not carbonize are either so hydrogen-rich, like polyethylene, that all of the carbon is volatilized with the hydrogen, as hydro-carbons, or have such a high tendency to unzip, like polystyrene or poly-(methyl methacrylate), that all of the material is volatilized as monomer.

With this picture of carbonization in mind, it might be worthwhile to list those characteristics of a carbonizing plastic which seem most likely to give superior performance in rocket nozzles, the ultimate concern of this project.

1. High carbon yield

   It appears that the higher the carbon yield, the stronger, less porous, more dimensionally stable, and more erosion resistant is the coke that is formed.

2. Gradual carbonization process

   If the carbonization reactions occur over a fairly broad temperature range, there is less chance of blowing off the crust by a sudden outrush of gas.

3. Amorphous char

   It is probable that an amorphous coke will be harder, stronger, and have lower thermal conductivity than one which is more graphitic.

There is some evidence for these postulates from the data obtained in this and similar projects, but they have not as yet been proved in actual application. One more point might be made before turning to the experimental part of the report. Most of the tests of plastics in rocket nozzles have been based on commercial resins as used in nose cones. This is not surprising considering the spectacular success of plastics in solving the re-entry problem, but the two applications differ in many respects. Until plastics are specially formulated for maximum dimensional stability and erosion resistance, their range of usefulness in rocket nozzles cannot be adequately assessed.

B. Experimental Work

1. Thermogravimetric Analysis

The equipment used is a Chevenard thermobalance with X-Y recorder. Its construction and mode of operation were described in detail by Doyle [5]. Samples are about 200 mg in weight, the heating rate is 180°C per hour, the top temperature reached is 900°C, and the atmosphere is purified nitrogen.

Most of the experimentation has been done with powdered resin samples. However, for measurement of resistivity and density of semi-carbonized material, molded buttons were employed. When made from high carbon yield resins like synthetic phenolic or polyphenylene, these disks carbonized smoothly without formation of cracks, fissures, or macroscopic porosity. For electrical measurements, silver electrodes were painted on the flat surfaces and resistivities measured with a Keithley Electrometer at 100 volts Dc, 50% relative humidity, and 23°C. Densities were calculated from dimensional measurements.

2. Arc-Image Furnace Experiments

This equipment and its operation were pictured and described in the previous annual report[6]. Several modifications have been made during the past year to improve the focusing and general ease of operation, but the basic equipment is unchanged.

Heat flux to the carbonizing sample has been measured with an Arthur D. Little incident radiation calorimeter. With the calorimeter mounted at the usual specimen position, the average heat flux was 43.5 ± 1.2 cal/sec/cm^2. As might be expected, the value obtained is sensitive to movement of the calorimeter; but, with care in positioning, is quite reproducible At this heat flux, the temperature on the end of a carbonizing phenolic rod after about 20 sec. of operation is on the order of 2300°C, as measured by an optical pyrometer.

Higher heat flux is obtainable, if desired, by the use of larger carbons. In one run with these, a value of 61.3 cal/sec/cm^2 was measured. However, the lower heating rate has proved to be more satisfactory for the experimental work done to date.

3. Fluid Bed Experiments

This equipment and its operation were also described in the previous annual report [6]. One modification made since then was the replacement of the initially used Vycor tube with one made from fused silica. This permits operation of the column to a gas and powdered resin temperature of 900°C.

Another modification, suggested by personnel from the Allegany Ballistics Laboratory, was the use of molecular sieves in liquid nitrogen cooled traps to collect the most volatile species: hydrogen, carbon monoxide, and methane.

The resin powder size which has been found to be most satisfactory is material which will pass through a 200 mesh sieve but is held on a 325 mesh sieve. Such powder has an average diameter of about 0.09 mm. Finer powder has too great a tendency to float out of the column; coarser granules require so great a through-put of fluidizing gas that collection of evolved species from the carbonizing resin is made difficult.

Helium is customarily employed as the fluidizing gas. Nitrogen, first used, obscured identification of carbon monoxide, which has the same mass. There also seemed to be some chance of reaction of nitrogen with the carbonizing resin. Only thermoset resins can be studied in the fluid bed equipment. Thermoplastic polymers or thermosetting resins, which have not been previously cured, become sticky as the temperature of the column is raised, agglomerate, and either adhere to the walls or fall to the bottom of the column.

In a typical run, about 40 g. of powdered resin is placed in the column at room temperature. The flow of fluidizing gas is started and adjusted to give dense phase fluidization. The power to the furnace is then turned on, and the temperature gradually increased, usually at a rate of about 200°C per hour. As the temperature of the gas increases, the incoming gas flow is decreased to maintain constant pressure drop across the bed. At the appropriate intervals, usually every 50°C from 200° to 900°C, the temperature is maintained constant for about fifteen minutes while gas samples are being taken. Evolved gas, then, at the higher temperatures, comes from resin that has been gradually heated to that temperature over a period of several hours.

4. Time-of-Flight Mass Spectrometer

As reported previously [6], a Bendix Model 14-100 Time-of-Flight Mass Spectrometer had been made available to this project. During the past year, efforts have been directed toward adapting this mass spectrometer to yield reproducible mass spectra of pure gases, to provide accurate quantitative analysis of a mixture of stable gases of the type that are expected to form during degradation of plastics, and to yield time resolved mass spectra of gaseous products that were formed during degradation of plastics by flash photolysis.

Several instrument modifications and other factors led to the attainment of reproducible mass spectra. The most significant was the installation of a Bendix Model E-104 Trap Current Regulator The regulator was added so that the number of electrons that ionize the entering gases could be maintained nearly constant. A multiplier regulator circuit was installed so that the voltage on the electron multiplier is now held constant; this assures a constant ion multiplication factor. The installation of graphite insulated shielded cables from the multiplier anodes to the analog output appreciably reduced the noise level of the mass spectrum. A rhenium filament was used to replace the tungsten filament for the purpose of producing the electron beam. Installation of a Consolidated Vacuum Corp. Type GS-100 automatic liquid nitrogen level control was also helpful.

Additional improvements were produced by installing a Sola constant voltage transformer to regulate the power which operates the electronics, and by heating the source region of the instrument with insulated tape. As a result of these modifications it was possible to produce mass spectra where all but the minor fragment peaks could be reproduced to about 3 percent in day-to-day operation.

In the conduct of these experiments leading to reproducible mass spectra from known gases, gas samples were introduced to the mass spectrometer with the sampling system that is shown in Figure 1. Samples whose pressures were measured in a calibrated volume were isolated between a pair of stopcocks. They were then expanded into a calibrated 3,000 cc volume; from there they were allowed to enter the 2 mil diameter mass spectrometer leak. The small calibrated volume was of such size that the gas pressure on the sampling system side of the leak was about 100 microns. The mass spectrum was integrated with the Bendix Model 321 analog output scanner, and the analog signal was recorded with a Leeds and Northrup Speedomax G recorder.

In the course of studies performed to develop and/or improve the necessary procedures to obtain quantitative gas analyses, a group of two component mixtures was studied first. The knowledge gained from these simple mixtures was applied to a six-component mixture. In these studies it was found necessary to optimize the field strengths and positions of the magnets which surround the source and multiplier in order to achieve the appropriate level of compensation. When correctly compensated, the ions which arrived at the detector were truly representative of the mixture of ions which were originally formed by the electron beam. For example, if the compensation was incorrect, then perhaps a disproportionate number of light ions, e.g. hydrogen, may drift out of the mixture of ions before they strike the multiplier cathode. As a result, the hydrogen analysis would be too low. Another important factor was that a maximum leak diameter of 2 mils was required to produce molecular flow at the operating conditions that were described in the previous paragraph. The extent to which the development of quantitative analysis procedures for gas mixtures was successful is discussed, with the results obtained, in the next section of the report (Discussion of Results).

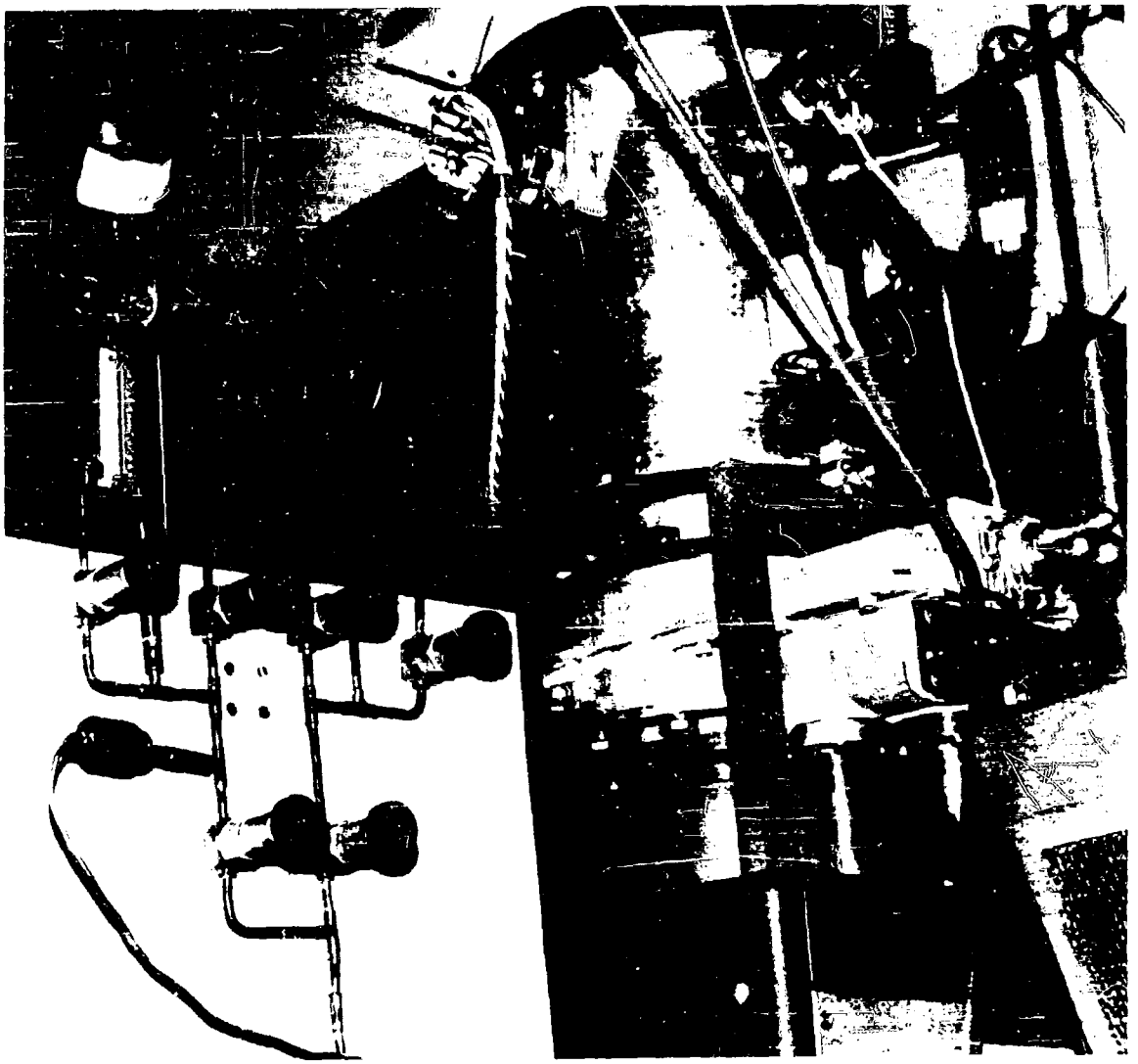

FIGURE 1. CONVENTIONAL SAMPLING SYSTEM FOR MASS SPECTROMETER.

Once it had been established that quantitative analysis could be performed with the mass spectrometer, plastic degradation studies commenced. Flash photolysis was selected as the method of heating. Nelson and coworkers [7] found that plastics could be heated rapidly to relatively high surface temperatures by use of this technique. A flash lamp and mounting assembly were designed and built which permitted the xenon filled flash lamp to be inserted into the evacuated mass spectrometer fast reaction chamber, where the plastic sample could be held close to the mass spectrometer leak. A schematic diagram of the apparatus is shown in Figure 2. Current experiments are carried out at 5 KV and 220 μf, with the flash lasting for about 1 millisecond. The behavior of the lamp indicates, however, that larger quantities of energy can be discharged through it. The flash is easily triggered with a spark coil and the lamp flash is readily synchronized with the photographic techniques that are employed.

In order to observe and to follow the changes in composition of the product gases during the photolysed degradation process, some means of photographing each of the succession of mass spectra produced is required. Drum camera techniques appear ideally suited to this purpose, and development of such techniques is proceeding. While not yet of the necessary analytical quality, an example of the mass spectra resulting after photolysis of an organic fiber-reinforced phenolic resin is shown in Figure 3. This photograph is not sharp and is of low intensity; however, examination shows that decomposition product mass spectra first begin to appear about 5000 μ seconds after the start of the flash, build up in quantity in a regular fashion, and continue to enter the mass spectrometer leak long after the flash is extinguished. Much effort has been and continues to be spent in improving drum camera photographs. Although some steps have produced improvements, notably in increasing the intensity of the photographs, the sharpness has not been improved very markedly. Recent photographs which have been taken on Kodak Royal Pan Recording Film (speed - 1250) are of high intensity. Efforts to improve the sharpness are continuing. The technique of using still photography to produce high quality photographs of single mass spectra, has also been used. An example of part of an organic fiber reinforced phenolic mass spectrum is shown in Figure 4, where a mixture of low molecular weight hydrocarbons, together with some water, hydrogen, and carbon monoxide can be seen. Of course, some peaks may represent free radicals, while others may be due to fragmentation during the ionization process. This will be determined in future experiments.

Several additional improvements were made in the mass spectrometer. The original multiplier header (with leaky ceramic feedthroughs) was replaced with a new header (with glass feedthroughs) which resulted in improved background pressure and mass spectra. A change was made in the electron beam electrode circuitry so that more accurate electron energies could be chosen by the electron energy selector. Since, in this work, it is important to differentiate between free radicals and ionization fragments, it will be necessary to do "appearance potential" work. In this, accurate

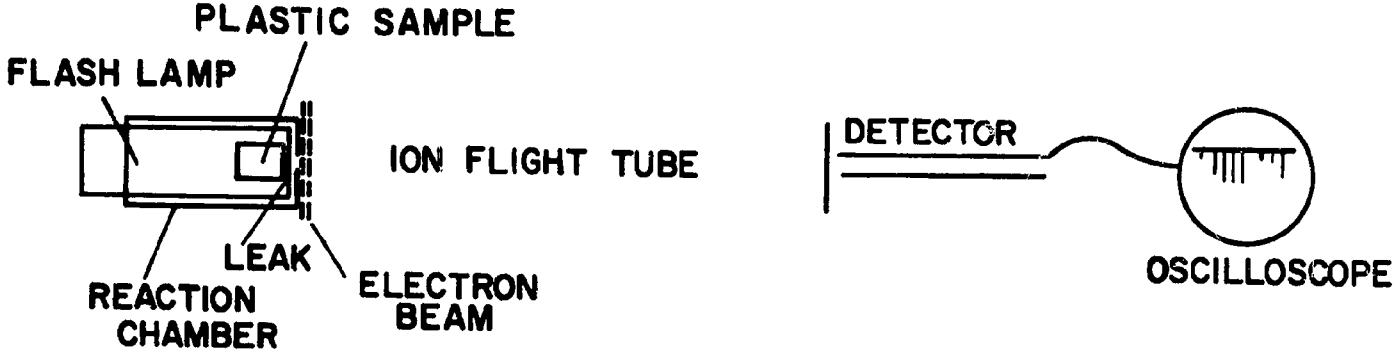

FIGURE 2. SCHEMATIC VIEW OF SAMPLE - FLASH LAMP - MASS SPECTROMETER ARRANGEMENT.

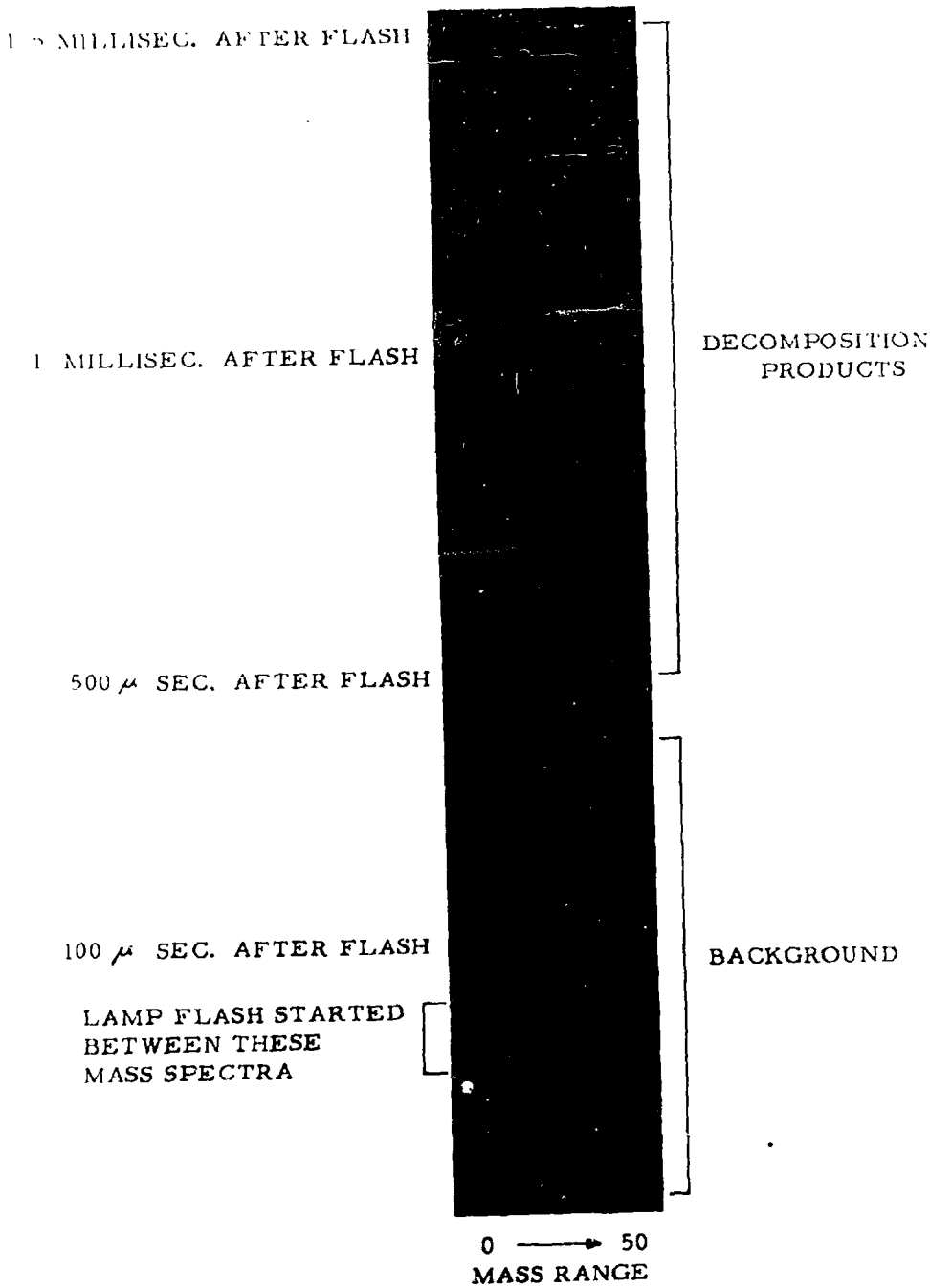

FIGURE 3. DRUM CAMERA PHOTOGRAPH OF MASS SPECTRA BEFORE AND DURING FLASH PHOTOLYSIS.

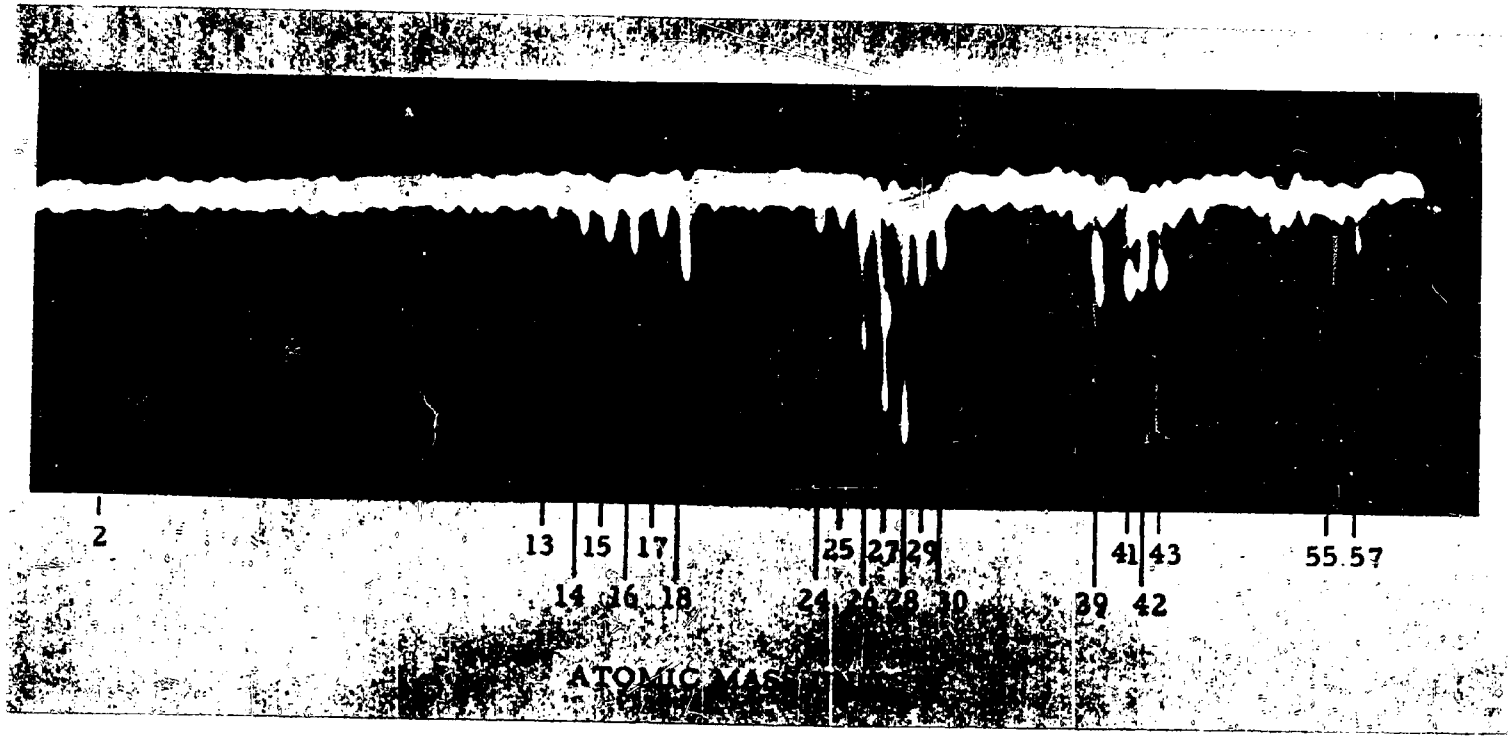

FIGURE 4. SINGLE MASS SPECTRUM RESULTING FROM FLASH PHOTOLYSIS OF PLASTIC SAMPLE 800 MICROSECONDS AFTER START OF FLASH.

choice of electron energies is very necessary, and the electrons must be highly monoenergetic.

5. Materials Preparation

For the most part, commercial materials of known composition have been studied. However, a modest amount of effort was devoted to synthesis of certain high carbon yield polymers which were not obtainable from any other source.

The phenolic resin, which has served as a standard, was made by condensing pure synthetic phenol and formaldehyde in aqueous medium with barium hydroxide as the catalyst. After removal of the catalyst, the resin was dehydrated, cured, and ground to a powder for fluid bed experimentation. Molded pieces for arc-image furnace experiments were made by blending four parts of cured powder with one part of uncured resin and molding at 160°C.

Meta-polyphenylene was made by the Wurtz reaction of m-dibromobenzene with sodium sand. Some isomerizaton to the para configuration and a little cross-linking occurred, but the reaction could be pushed to a polymer molecular weight of at least 15,000. The material could be molded into reasonably strong rods and disks at 275-315°C and 20,000 psi, and these samples have been used in arc image and TGA experiments. Polynaphthylene was similarly made from dibromonaphthalene and sodium.

Several attempts were made to prepare metapolyphenylene by Grignard synthesis so as to give more soluble, tractable material, expected to be more suitable for making laminated or fibrous filled samples. Meta-dibromobenzene was converted to the mono-Grignard and this was condensed with itself using cobaltous or ferric chloride as the catalyst. The reaction was clean in the sense of being free from branching or isomerization and gave a soluble, fusible product, but the molecular weight could be pushed only to about 3000. Molded pieces were glassy and brittle. Incorporation of 5-10 mole per cent of sym-tribromobenzene gave some improvement, but the Grignard synthesis cannot as yet be described as satisfactory.

6. Carbon-Filled Plastics

One way to achieve a more dense, stronger crust on the surface of carbonizing plastics might be to incorporate already formed carbon as a filler in the plastic matrix. Such filler would be expected to affect both the nature of the coke obtained on carbonizing the plastic and the carbonization process itself. Accordingly, a small study along these lines was initiated and has been in progress for about four months.

Two plastic matrices have been used: low density polyethylene cured with Varox peroxide, and Cincinnati Testing Lab's 91LD phenolic resin. The polyethylene compounds were blended in a Baker-Perkins dough mixer and molded at 200°C. The phenolic compounds were prepared by stirring the filler into the resin solution, heating in shallow trays until the solvent

had evaporated and the resin was converted to B-stage, and then grinding. Pieces were molded at 170°C.

An oxy-acetylene torch fitted with a No. 8 cutting tip was used for preliminary evaluation. The plastic sample, a one-half-inch thick disk, was clamped to a one-half-inch thick slab of foamed zirconia brick through which had been drilled a 5/8" diameter hole, and the whole assembly held in a horizontal position. A copper-constantan thermocouple with a flat weld junction was clamped against the top side of the plastic opposite the center of the hole in the zirconia.

In use, the torch was ignited, adjusted to give a maximum temperature, neutral flame, swung into position with the tip just below the hole in the zirconia, and the thermocouple recorder started. When the top side temperature reached 100°C, the torch was swung away, and any flames on the sample immediately put out with a CO_2 extinguisher. A new zirconia brick was used on each test so as to keep the hole size invariant.

Data obtained were the time-temperature plot of the thermocouple and sample weight loss. Visual observation was made of the depth of erosion and the strength and coherence of the char. In addition, thermal conductivity measurements were made on several of the polyethylene samples before testing to determine the effect of carbon type on this property.

C. Discussion of Results

1. Thermogravimetric Analysis

To study the effect of cross-linking on carbon yield, samples of polyethylene were exposed for various lengths of time to gamma radiation from a cobalt-60 source (maximum dosage - 3×10^8 rad), and then heated in the TGA apparatus to 900°C. In no case was any appreciable amount of residual carbon formed. This was also true of similarly cross-linked samples pyrolyzed in the arc-image furnace. One final sample was exposed to electron beam radiation (maximum dosage - 10^9 rad) from a resonant transformer until it became hard and brittle, indicating a very high degree of cross-linking. It also gave almost no carbon in either TGA or arc image tests.

It must be concluded, then, that a hydrogen-rich polymer like polyethylene will not form carbon under either slow or rapid thermal decomposition, no matter how high the degree of cross-linking.

For further comparison, a sample of sodium-polymerized polybutadiene, which had been thermally cured by heating for three days at 250°C, was heated in the TGA apparatus. Its thermogram, along with one for polyphenylene, is shown in Figure 5. It is to be noted that the polybutadiene, with a carbon/hydrogen ratio of 2/3, although very highly cross-linked, gives almost no residual coke. The polyphenylene, with a carbon/hydrogen ratio of 3/2, gives a very high coke yield, even though it is only lightly cross-linked.

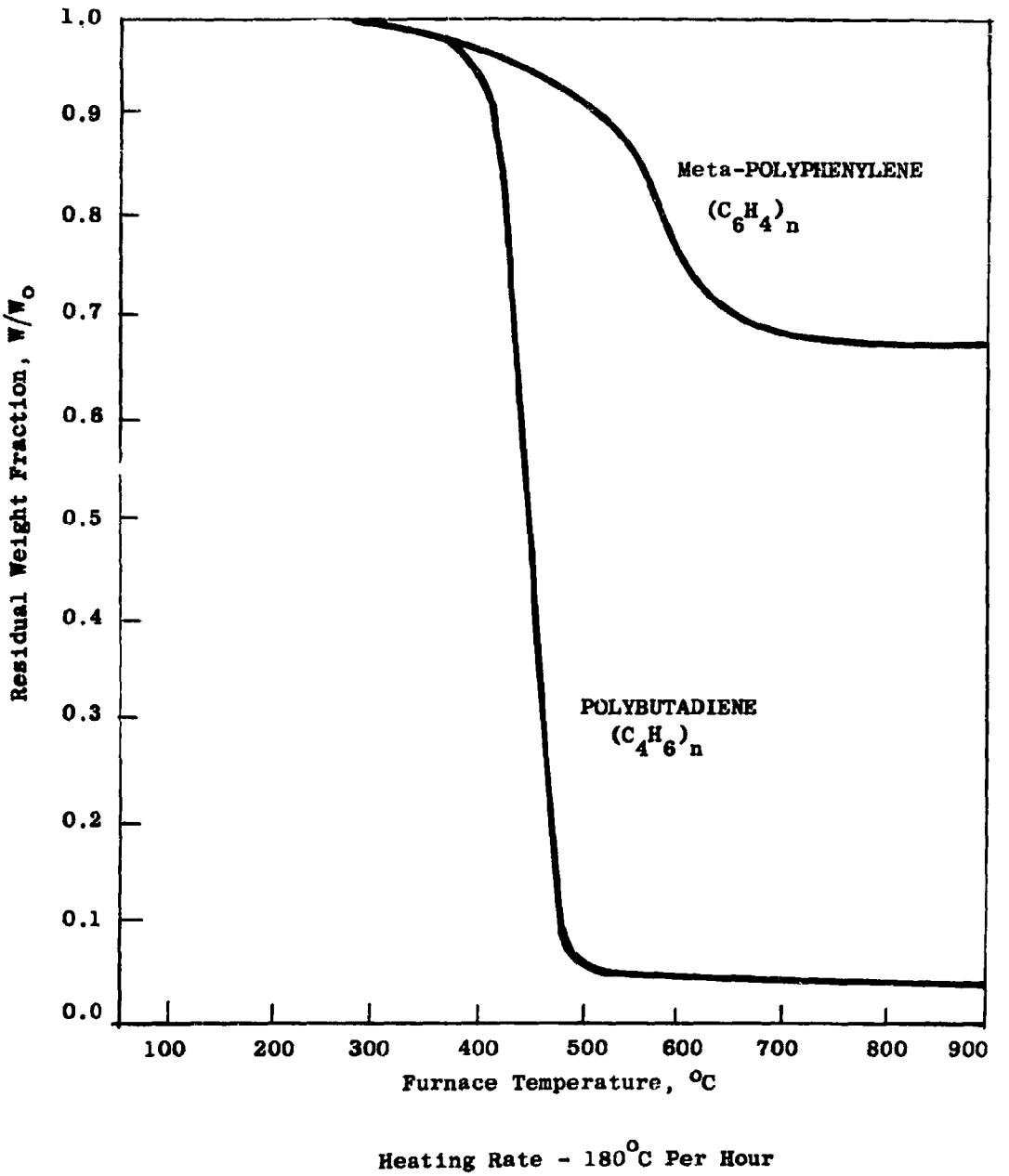

Figure 5 Thermogravimetric Analysis Of Two Polymers

The break in formation of carbon on pyrolysis occurs at a carbon/hydrogen ratio of about 1/1. Polystyrene, $(C_8H_8)_n$, gives very little coke; the polyene, $(C_2H_2)_n$, derived from polyvinyl chloride by dehydrohalogenation, gives about a 30% coke yield on pyrolysis [8]. Other polymer and pitches, with C/H ratios of 1/1, lie between these extremes.

As was stated in the Experimental Work section of the report, molded buttons of high carbon yield resins can be carbonized in the TGA apparatus without fracturing, and property measurements made on these buttons. The results on a series of phenolic samples are summarized in Table 1.

Table 1 - Properties of Phenolic Carbon-Residues

Top Temp. reached, °C	% of original wt.	Apparent density	Resistivity, ohm cm
As molded	100.0	1.275	1.5×10^{13}
500	83.5	1.147	1.2×10^{14}
600	70.8	1.140	2.4×10^{9}
700	67.0	1.208	3.5×10^{4}
800	65.5	1.212	3.9
900	65.0	1.335	2.1

It is of interest to note that most of the weight loss occurs by the time the material reaches 700°C. The density first drops a little and then slowly increases. The resistivity, after a slight increase, drops steadily with progressively higher temperature of carbonization, and, with the 700°C sample, is in the semi-conducting range.

In Table 2, a similar relationship between resistivity and temperature of carbonization is shown for polyphenylene.

Table 2 - Properties of Polyphenylene Carbon-Residues

Top Temp. reached, °C	Resistivity, ohm cm
As molded	8.4×10^{14}
500	1.7×10^{14}
600	4.6×10^{12}
700	2.9×10^{7}
900	0.45

It is probably significant that the resistivity of the 600° and 700°C polyphenylene samples is higher than in the corresponding phenolic samples, but that the 900°C sample is lower. The explanation would seem to be that the polyphenylene carbonizes at a higher temperature, but, when it does so, it gives a more graphitic, lower resistivity char.

To gain a little more insight into the nature of the semicarbonized samples, resistivity of the 600° phenolic sample was determined as a function of temperature of measurement. The data in Table 3 were taken on the cooling side of a thermal cycle in nitrogen.

Table 3 - Resistivity of Phenolic Carbon-Residue

Temperature, Degrees C	Resistivity, ohm cm
164	4.3×10^{8}
153	6.5×10^{8}
130	1.3×10^{9}
105	2.6×10^{9}
91	6.5×10^{9}
73	1.3×10^{10}
56	2.6×10^{10}
40	6.5×10^{10}

It will be noted that the resistivity is lower at higher temperatures of measurement as would be expected for an insulating material. However, the change with temperature is only about one-half as great as normal, indicating some degree of semiconducting character.

To further characterize the semi-carbonized molded samples, elemental analyses were obtained from a commercial analytical laboratory. The results are shown in Table 4.

The phenolic analyses were checked by submitting identical samples to another laboratory, and the results obtained were in substantial agreement with those shown.

The values for hydrogen percentage are reasonable; the carbon percentages seem low at the higher temperatures. This is particularly true of the polyphenylene results. The 500°C sample has a total carbon plus hydrogen of 99.6%, so there could have been no substantial quantity of other elements. Yet the 900°C carbon plus hydrogen totals only 94.9%.

There are perhaps two explanations for this anomaly. One may be difficulty in achieving complete combustion of the harder-baked samples to CO_2 in the

combustion train resulting in low carbon percentages. The other possibility is incorporation of nitrogen into the coking structure in the temperature range of 500-900°C. Neither explanation seems very likely to be correct, but both will be explored.

Table 4 - Chemical Analysis of Carbon-Residues

Top temp. reached, °C	% C	% H	% ash
Phenolic			
As molded	74.9	5.8	0.7
500	84.7	5.0	0.8
600	91.8	3.5	0.5
700	92.7	2.3	0.6
800	92.8	1.8	1.1
900	93.2	1.2	1.1
Polyphenylene			
As molded	92.1	5.1	---
500	94.7	4.9	---
600	94.8	4.1	---
700	94.2	2.9	---
900	93.6	1.3	---

2. Arc-Image Furnace

Although this equipment was primarily used for comparison of chars derived from various resins, some data were obtained with respect to the nature of the evolved gases. In Table 5 is shown a comparison of the gases from polyphenylene and polynaphthylene. The percentages are on a molar basis.

The polynaphthylene shows a somewhat greater degree of fragmentation, judging from the relatively higher yields of ethylene and water and lower yields of benzene and toluene. This is in line with the lower thermal stability of naphthalene as compared to benzene.

Table 5 - Vapor Degradation Products

Non-condensable gases	Polyphenylene	Polynaphthylene
Hydrogen	79	76
Methane	16	17
Carbon Monoxide	5	7
	100%	100%
Condensable gases		
Water	33	45
Benzene	33	11
Toluene	15	3
Ethylene	11	22
Carbon dioxide	5	17
Acetylene	1	2
Styrene	1	
Xylene	1	
	100%	100%

In order to provide comparison between the standard phenolic and other materials with regard to rate of weight loss under arc image exposure, several runs for varying periods of time were made with the phenolic. Conditions were heat flux of 43.5 cal/sec/cm^2 on the end of a 3/8" diameter rod in 0.1 atm. gently moving air (approximately 1/3 ft/sec at the specimen). The rate of weight loss during the first ten seconds was 13 mg/sec; from ten to sixty seconds the rate was 5.8 mg/sec. With strong pumping (pressure about 0.1 mm Hg), the weight loss, after the initial fast period, was only about one-half as great as in air, presumably because of the slower rate of oxidation of the carbon crust. The moving air data are more reproducible and hence will be used for comparison.

Several runs have been made with various polyphenylene samples. Meaningful rate of weight loss data from a quantitative standpoint were not obtained. Random scatter in rate measurements was high--possibly due to lack of uniformity from sample to sample--and no useful purpose would be served by their inclusion here. In no case was the rate of weight loss from any polyphenylene sample less than that of standard phenolic resin in spite of the higher polyphenylene coke yield in TGA experiments. The reason may be that the polyphenylene forms a slightly softer, more graphitic, probably more thermally conductive coke than phenolic, but this has not been firmly established.

Differences between the phenolic and polyphenylene chars were observed by X-ray diffraction examination. Evidence of crystallinity in these essentially amorphous chars is not overwhelming. The X-ray patterns are indistinct and diffuse; they acquire meaning only on very careful examination and measurement. Because of this, although their interpretation is valid, the inclusion of the diffractometer recorder traces does not appear warranted. Patterns corresponding to graphite were found in the char formed after 40 seconds of exposure of a polyphenylene rod to the arc image; phenolic samples required twice as long a heating period. The difference between the two materials was also evident by visual examination, the polyphenylene char being much more silvery gray in appearance. Only one graphite line appeared in the X-ray diffraction pattern - that corresponding to the 002 reflection. This indicates that parallel basal planes are formed, but that the temperature is not sufficiently high to provide the mobility necessary for orientation about the C-axis.

Molded phenolic samples were made containing, separately, finely powdered tungsten, niobium, tantalum, titanium, tungstic acid, titanium dioxide, tantalum oxide, and zirconium oxide, and the samples exposed to the arc image for sixty seconds. In all cases the powders were fine enough to pass a 200 mesh screen. The oxide samples did not differ markedly from unfilled phenolic; qualitatively, the metal-filled samples seemed to give denser cokes and a higher proportion of the evolved gas was hydrogen. In every case, X-ray diffraction gave substantial evidence (10 to 19 lines) of carbide formation. Some flaking or chipping of the char samples prevented attainment of quantitative rate of weight loss measurements, and characterization of chars is not complete.

One sample of phenolic containing chopped tantalum wool as a reinforcing agent was made and exposed to the arc image. The resulting coke was strong and coherent and X-ray diffraction gave evidence for tantalum carbide formation. Unfortunately, most of the tantalum fiber had been oriented along the axis of cylindrical sample, and, as might have been expected, the carbonized zone moved back through the sample about three times faster than normal. The experiment will be repeated with fiber orientation in the sample normal to the axis.

3. Fluid Bed

Four powdered resinous materials have been studied in detail. The phenolic was the standard synthetic phenol-formaldehyde resin. The epoxy resin in each of the epoxy samples was Dow's experimental epoxidized Novalac, #2638.1. Tonox, used as the curing agent in two samples, is mostly methylene dianiline with minor amounts of higher condensation products of aniline and formaldehyde. PMDA, used as the curing agent in one of the epoxies, is Du Pont's pyromellitic dianhydride. The anthracite was a typical low-ash Scranton coal, finely powdered, and added to the epoxy in approximately equal parts by weight before curing.

The results of fluid bed runs made with these materials are shown in the following tables (Tables 6 through 9) which indicate from mass spectrographic evidence the presence or absence of particular species in the vapor products of thermal degradation. Since all conceivable species are undoubtedly present in the evolving gas at all temperatures, a blank space does not indicate the absence of any species in a quantitative sense. It does indicate that its concentration is below the detectable threshold by mass spectrometry. An "X" means that the material was positively identified as being present most likely in substantial quantities; a "?" indicates faint evidence of its presence, probably in trace amounts. It is difficult to be more precisely quantitative about these terms in the highly complex, diverse collection of species present here. Detectability varies with the species and on the presence or absence of fragments or other stable species of similar mass. Some materials (such as acetone and propylene) are difficult to identify in concentrations below 1%. Certain compounds, such as hydrogen, methane and benzene can be positively identified down to 0.01%. It is estimated that on the average the dividing line between the symbols "X" and "?" may be about 0.1%.

The tables illustrate well the complexity of the carbonization process. It had been thought, when planning the fluid bed study, that at each temperature just a few species would be evolved, characteristic of that temperature. Experimentally, this has not proved to be the case, most species being found at most temperatures. Carbonization is a quite random, statistical sort of process in which all conceivable reactions occur. Only the proportions of the various products change with temperature, and even this change is not very rapid.

There are however, some discernible trends and differences among various materials. Carbon dioxide and water are always the most common species, then methane, benzene toluene, and ethylene. Two and three carbon fragments are more common in epoxy than in phenolic degradation. Less stable species like acetaldehyde, acrolein. phenols, and ethyl amine are found at the lower temperatures; at higher temperatures, species like carbon monoxide and hydrogen cyanide come in more strongly. Hydrogen itself is not common until temperatures of 500^{o}C and above. It is observed, too, that the epoxies give more tarry smoke on decomposition than do phenolics, and that this behavior is exhibited more by Tonox cured epoxy than one cured with PMDA.

All of the effects observed and the products identified are reasonable, understandable, and consistent with the findings of other investigators. It is unfortunate that the data are so blurred and indefinite, but this seems to be a function of the carbonization process itself rather than the fluid bed technique.

Table 6

Vapor Products from Fluid Bed Carbonization of Phenolic Resin

Material Evolved	Fluid Bed Temperature, °C							
	200	300	400	500	600	700	800	900
Hydrogen				X	X	X	X	
Methane		?	X	X	X	X	X	X
Water	X	X	X	X	X	X	X	X
Carbon Monoxide				?	X	X	X	X
Ethylene			?	X	X	X	X	X
Ethane				X	X	X	X	X
Methanol	X							X
Propylene				X				X
Carbon Dioxide	X	X	X	X	X	X	X	X
Formic Acid							X	X
Cyclopentadiene			?	?				
Benzene	?	X	X	X	X	X	X	X
Toluene		?	X	X	X	X	X	X
Phenol	X	X	X					
Xylene			?				?	
Cresol		X	X					
Xylenol		X	X					

Table 7

Vapor Products from Fluid Bed Carbonization of Epoxy-Tonox

Material Evolved	Fluid Bed Temperature, °C							
	200	300	400	500	600	700	800	900
Hydrogen				?	X	X	?	
Methane		?	?	X	X	X	X	X
Water	X	X	X	X	X	X	X	X
Hydrogen Cyanide						X	X	X
Carbon Monoxide				?	X	X	X	X
Ethylene		X	X	X	X	X	X	X
Ethane		X	X	X	X	X	X	X
Propylene		X	X	X	X	X	X	X
Propane or acetaldehyde	X	X	X	X	?			
Carbon Dioxide	X	X	X	X	X	X	X	X
Methyl Chloride	X	X	X	X				
Acrylonitrile				?	?			
Acrolein	X	X	X	X				
Acetone	X	X	X	?				
Benzene				X	X	X	X	X
Toluene	X			X	X	X	X	X
Phenol		?	X					
Cresol		?	X					
Xylene				X	X			

Table 8

Vapor Products from Fluid Bed Carbonization of Epoxy-PMDA

Material Evolved	Fluid Bed Temperature, °C							
	200	300	400	500	600	700	800	900
Hydrogen				?	X	X	X	X
Methane	?	X	X	X	X	X	X	X
Water	X	X	X	X	X	X	X	X
Carbon Monoxide		?	X	X	X	X	X	X
Ethylene		?	X	X	X	X	X	X
Ethane			?	X	X	?	X	X
Formaldehyde		?	X					
Propylene		X	X	X	?	?	?	
Carbon Dioxide	X	X	X	X	X	X	X	X
Propane		?	X	?	?	?		
Acrolein	X	X	X	?				?
Butene			X	?				
Acetone		?		?			?	
Butane			?					?
Benzene			?	X	X	X	X	X
Toluene	X		?	X	X	X	X	X

Table 9

Vapor Products from Fluid Bed Carbonization of Epoxy-Tonox-Anthracite

Material Evolved	Fluid Bed Temperature, °C							
	200	300	400	500	600	700	800	900
Hydrogen				?	X	X	X	X
Methane		X	X	X	X	X	X	X
Water	X	X	X	X	X	X	X	X
Hydrogen Cyanide					X	X	X	X
Carbon Monoxide	X	X	X	X	X	X	X	X
Ethylene		?	X	X	X	X	X	X
Ethyl Amine		X	X	X				
Ethane			X	X	X	X	X	X
Hydrogen Sulfide				?	X	X	X	X
Propylene		?	X	X	X	X	X	X
Propane		?	X	X	X	X	X	X
Acetaldehyde			X	X	X			
Carbon Dioxide	X	X	X	X	X	X	X	X
Methyl Chloride	X	X	?					
Acrolein	X	X	X	X				
Acetone	?	X	X	X	X	X	X	X
Benzene			?	X	X	X	X	X
Toluene	X	?	X	X	X	X	X	X
Epichlorohydrin	X	X	?					
Xylene				X	X	X	?	?

4. Time-of-Flight Mass Spectrometry

The data shown in Table 10 below show the extent of success in obtaining reproducible mass spectra and in providing accurate quantitative analysis of a known representative six-component gas mixture.

Table 10

Quantitative Analysis by Bendix Mass Spectrometer

Component	Volume Percent Actual Analysis	M.S. Analysis
H_2	13.6	13.6
N_2	18.5	17.5
CO	15.6	13.8
CH_4	17.5	17.3
C_2H_4	18.9	19.5
C_2H_6	16.0	18.3

It should be noted that this is not an easy mixture to handle, for N_2, CO, and C_2H_4 have their parent peaks at mass 28. C_2H_6 also has a large 28 contribution. It was therefore necessary to use the fragmentation patterns for complete and accurate analysis.

It is quite likely that further improvements will be achieved in analytical accuracy. Since performing the analysis, the cross-sectional area of the electron beam has been enlarged by installing Bendix parts for that purpose. The change produced a factor of ten increase in sensitivity with a very small decrease in resolution. This change could yield improvements in analytical accuracy.

Since the apparatus and instrumentation are just now approaching operability from the standpoint of needs, results of this mass-spectrographic study of plastics degradation have not been obtained. Of course, during the apparatus and methods development work accomplished, some data on degradation of two plastic formulations have been obtained. Figures 3 and 4 have previously been referred to as examples of such data, which confirm the merit of this approach and indicate the value of the information obtainable. The soundness of the flash photolysis method for plastics degradation studies was confirmed by the copious quantities of decomposition products formed when a fiber reinforced phenolic resin was flashed under the operating conditions established. Samples of this resin were observed to be well blackened after experiencing a number of flashes; the blackening

resulting from a single flash has not been investigated. Some problems remain to be solved to obtain satisfactory surface heating of other plastics, however. For example a polyformaldehyde resin also studied was found to be only slightly yellowed by repeated flashes and did not yield nearly so great a quantity of degradation products as did the phenolic.

In order to degrade plastics of this (polyformaldehyde) type, and others, it may be necessary to fill them with an inert substance, a procedure followed by Nelson with polyethylene.

Further work must be performed in the areas of obtaining more accurate quantitative analysis, preparing a catalog of time-of-flight mass spectra of pure compounds, improving drum camera pictures, and performing appearance potential studies as an aid in identification of initial degradation products. It is expected that quantitative analysis of degradation products will proceed in a semi-routine fashion during the coming year. The plastics to be studied will be selected from those that qualify as potentially good high temperature materials, as defined by the other parts of this program.

5. Carbon-Filled Plastics

Only a small amount of data have been obtained thus far on this phase of the project, but the results are interesting and indicate the directions which further work should take.

Thermal conductivity measurements were made on carbon-filled polyethylene. Unfilled, peroxide cured, polyethylene had a thermal conductivity of 6.1×10^{-4} in cgs units. When filled with equal parts by weight of various carbon blacks, activated charcoals, and bituminous and petroleum cokes, the conductivity increased to $9 - 11 \times 10^{-4}$, depending on the type of black.

Powdered graphite, at the same loading, effected nearly a fourfold increase, to 23×10^{-4}. For comparison, it might be noted that a typical glass cloth-phenolic laminate has a thermal conductivity of 10.5×10^{-4}, tested in a direction normal to the laminations. Thus, it is evident that substantial amounts of non-graphitic carbon can be included in plastic formulations without unduly increasing the thermal conductivity.

In torch tests on carbon-filled polyethylene samples, a great deal of variation was observed. Times for the top-side temperature to reach $100^{\circ}C$ on a 1/2" thick disk ranged from 30 sec. for coconut charcoal to 105 sec. for a bituminous coke. The factor most responsible for variation seemed to be particle size. Compositions containing larger particles seemed to spit and sputter more, resulting in faster rates of erosion and heat travel through the sample.

Some sintering of the carbon occurred, but it seemed to be independent of the thermal decomposition and volatilization of the polyethylene. Examination of the samples after test showed a center conical plug of sintered carbon surrounded by a layer of loose carbon black, which was in turn surrounded by the unaffected compound. Apparently, the thermal gradient traveling through the sample completed the decomposition of the polyethylene well ahead of the carbon black sintering process.

Only a few tests have been made with carbon-filled phenolic resins. The rate of heat travel through the samples is about the same as with polyethylene. But the coke formed is much stronger, and is tied solidly to the unaffected phenolic by a smoothly grading caramelized zone.

Figure 6 shows a petroleum coke-filled CTL91LD phenolic resin disk, 1/2" in thickness, after 100 sec. exposure to the torch. There are fissures in the coked structure, most of which probably developed on cooling, but there is little erosion or decrease in the original dimension. For comparison, Figure 7 shows a glass cloth laminate made with the same resin after approximately the same exposure.

These preliminary experiments indicate that study of the carbonization of carbon-filled plastics can profitably be made a major phase of the project. Future work will utilize the arc-image furnace and thermogravimetric analysis as well as torch testing.

FIGURE 6. CARBON POWDER FILLED PHENOLIC AFTER TORCH TEST.

FIGURE 7. GLASS CLOTH PHENOLIC AFTER TORCH TEST.

D. References

1. Franklin, R. E., Proc. Roy. Soc., London, 209A, 196 (1951).

2. Winslow, F. H., Baker, W. O., Pape, N. R., Matreyek, W., J. Polymer Sci., 16, 101, (1955).

3. Barry, W. T., Sutton, W. H., The Importance of Char Structures in the Ablative Performance of Organic Polymers, WADD Technical Report 60-101, (1960).

4. Marolo, S. A., Micro Structure of Ablative Plastic Chars, WADD Technical Report 60-856, (1961).

5. Doyle, C. D., Evaluation of Experimental Polymers, WADC Technical Report 59-136, (1959).

6. Coffman, J. A., Kibler, G. M., Riethof, T. R., Watts, A. A., Carbonization of Plastics and Refractory Materials Research, WADD Technical Report 60-646, Part I, (1961).

7. Nelson, L. S., Kuebler, N. A., Physical Chemistry in Aerodynamics and Space Flight, Pergamon Press, New York, (1961), p. 61.

8. Winslow, F. H., Matreyek, W. Yager, W. A., Industrial Carbon and Graphite, Society of the Chemical Industry, London, (1958), p. 190.

III. VAPOR PRESSURE OF REFRACTORY MATERIALS

A. Background

Because of the importance of vapor pressure and evaporation rate data in predicting the service life of refractory materials in high temperature rocket nozzles, and because of the utility of these data in deriving thermodynamic properties and the mechanism and energetics of processes occuring at high temperatures, a study of the vapor pressure of each of a number of refractories was undertaken in November, 1959.

By June, 1960, apparatus had been designed, built, and was in operation for the application of the Langmuir evaporation method to the measurement of vapor pressure data on TaC, ZrC and ThO_2. Work had been completed on TaC and started on ZrC (though the purity of the latter was not entirely satisfactory). Data had also been obtained on ThO_2 although it was clear that the method was not suited to this material. By the use of chemical analyses and X-ray diffraction analyses of the specimens and the condensed sublimates therefrom, information as to the stoichiometry of reactions being studied had been obtained. The application of resonance line absorption photometry and the matrix isolation techniques to the study of the atom species and the molecular species present in the vapors, respectively, had also been initiated and preliminary results had been obtained from the resonance line absorption effort. The details of the work up to that time (June 1960) were reported in the first Annual Report under this contract [1].

Since then, work has continued on each of these three experimental approaches. Langmuir studies on the evaporation of ZrC have been repeated, using specimens of satisfactory purity, and have been completed on HfC, TiC, and WC. Although it proved impossible to apply resonance line absorption methods to TaC and HfC, work has been satisfactorily completed on TiC and ZrC. Apparatus for matrix isolation studies on ThO_2 has been completed and is now operable.

Details of the effort during the period July, 1960 - June, 1961 follow.

B. Experimental Work

1. Langmuir Evaporation Studies

a. Procedure

The apparatus employed in the study of vapor pressure of refractory carbides by the Langmuir technique is essentially the same as that described in the previous annual report [1] on this contract. Recently, some modifications have been made in order to increase the pumping speed of the system. The main vacuum stopcock has been replaced by one having a one-inch bore and the mercury diffusion pump replaced by one having a pumping speed of 50 liters per sec

and an ultimate vacuum of 5×10^{-8} mm. Hg. With this improved system, overnight pumping usually produced a vacuum of about 3×10^{-7} mm. Hg.

In order to reduce adsorption of atmospheric gases on the specimen and on the walls of the vacuum system, argon was admitted to the system before the system was opened to remove the specimen.

All specimens were prepared by vacuum hot pressing appropriate powder (-325 mesh) in graphite dies. The pressed pieces were in the form of cylinders 1-1/4 inch diameter. The ring-shaped specimens were prepared from the pressed cylinders by cutting and grinding with diamond wheels and with a "Cavitron" machine. The finished specimens were 1-1/4-inch O.D., 1.0-inch I.D. and about 0.1-inch thick. Four black body holes .016-inch diam. and 0.75-inch deep were cut in the top surface of each specimen for temperature measurement with the optical pyrometer. To avoid temperature gradients circumferentially around the ring, it is necessary that the ring be uniform in cross-section. If the cross-section of the specimen is not uniform, then the smaller cross-section becomes hotter when the piece is heated inductively, more material is evaporated from the hotter section, making the area still smaller and so on until severe temperature gradients result. Considerable care was therefore taken to ensure that the outer and inner surfaces of the finished specimen were accurately concentric.

Radial temperature gradients were minimized by the choice of the small cross-sectional area of the ring. When a piece is inductively heated, heating occurs chiefly on the outer surface of the sample and the inner portion is heated mainly by conduction. The ratio ID to OD was kept as high as possible while still maintaining sufficient strength in the sample.

These steps were taken to ensure uniform temperature of the sample not only for accurate temperature measurements, but also to avoid destruction of the specimen by thermal shock during the rapid heating and cooling necessary for the rate of weight loss measurements.

Temperatures were measured during the course of each weight loss run on each of the four black body holes cut in the top surface of the specimen. The duration of the runs varies from three minutes at the highest temperature, for which one set of temperature readings (total of four) was made, to six hours at the lowest temperature for which readings were taken at approximately 45 minute intervals (total of 36 readings).

The transmission of the window and prism through which the pyrometer was sighted was checked periodically during the course of the measurements whenever it was judged that the window had become sufficiently fogged to affect the temperature measurements. The measured transmission was then used to correct the temperature readings by use of

Wien's law. The transmission was typically 75% which leads to a temperature correction of 82°C at an apparent temperature of 2200°C.

To account for the temperature variation of a black body hole during the course of a run and also for the circumferential variation, a procedure was adopted to calculate the "effective" temperature for each run. It should be noted that the effective temperature is higher than the average temperature since the rate of weight loss (and also vapor pressure) is approximately exponential with reciprocal temperature. It was assumed that the rate of weight loss, m, as a function of temperature, T, could be expressed by

$$\log m = A + B/T \tag{1}$$

where A and B are constants. To each measured temperature, T_i is assigned a time-at-temperature, t_i, an incremental weight loss W_i and area $x = \frac{1}{4}$ total area since there are four black body holes. Equation (1) also holds for each incremental weight loss so that

$$\log \left(W_i/xt_i\right) = A + B/T_i \tag{2}$$

or solving for W_i

$$W_i = xt_i\ 10 \exp\left(A + B/T_i\right) \tag{3}$$

If there are n temperature readings during a run then the measured total weight loss W is given by

$$W = \sum_1^n W_i = \sum_1^n x\ t_i\ 10 \exp\left(A + B/T_i\right) \tag{4}$$

The various t_i are determined from the time interval between temperature readings to that $\sum_1^n \frac{1}{4} t_i$ = total time of run A value for B is then estimated by plotting log n vs the average temperature for each run and obtaining the slope of the line.

This value for B was then used for each individual run in eq. (4) along with the other values obtained for each run and a value for A was calculated. A and B thus obtained were substituted in eq. (1) along with the measured weight loss rate to obtain the effective temperature.

Effective temperatures thus calculated were, under the most unfavorable conditions, ten degrees higher than the average temperature. Representative values are: for run Z-E-6 the standard deviation of all temperatures from the mean is 21 degrees and the effective temperature is 3 degrees higher than the average.

b. Zirconium Carbide Weight Loss Data

Evaporation rate measurements have been made on two specimens of zirconium carbide Specimen Z-E initially weighed 6.249 gm. and a total of 7.86% of this weight was lost in the course of 22 separate runs. Specimen Z-D, initial weight 5.273 gm., lost 13.67% of its initial weight in 20 runs.

These specimens were produced by hot pressing at about 2200°C under 4000 psi pressure for thirty minutes. Both pieces had a density of 6.35 gm. per cc. calculated from mass and dimensions which is 96% of the X-ray density computed from the lattice parameter, 4.6998 Å, determined here. Previously, measured densities had been reported (See Ref. 2, p. 577) which were actually higher than the X-ray density.

The zirconium carbide specimens were prepared from a sample of zirconium carbide (99% pure) obtained from A. D. Mackay Inc. The elemental analysis of the hot pressed piece is given in Table 11. The carbon analyses were obtained by combustion, the gas analyses by vacuum fusion and the remainder spectrographically.

TABLE 11

Analysis of Hot Pressed Zirconium Carbide

(Stoichiometric composition: 11.63% C, 88.37% Zr)

Element	% by wt.	Element	% by wt.
Total C (Combustion)	11.66	Mg	.0005
Free C (Appendix C)	1.09	B	.05
Combined C (diff.)	10.57	Fe	.05
O	.0013	Hf	.30
N	.0001	al	.005
H	.0008	Mo	.05
Si	.58	Zr (diff.)	87.30

Although the total impurity content as listed in Table 11 is rather high (approximately 1% excluding free carbon), it is obvious that on subsequent heating the impurities must either volatilize rapidly, leaving the specimen in a rather high state of purity or vaporize rather slowly in which case the weight-loss measurements are not expected to be affected by their presence.

During the course of the evaporation rate experiments, carbon analyses and a few spectrographic analyses of the condensed sublimate were made. Samples for analysis were obtained by carefully scraping the material from the evaporation chamber wall with a quartz rod. It was found by spectrographic analysis, that the more volatile impurities B, Fe and Si were evaporated during the early runs which gave rates of weight loss higher than subsequent heatings. After approximately 1% of the initial weight had evaporated, consistent weight loss measurements were obtained with both specimens.

Carbon analyses of the sublimate were made by weighing several milligrams of the sample in a tin capsule and heating the capsule and contents inductively, along with powdered iron catalyst, under flowing oxygen. The CO_2 evolved was measured conductometrically in barium hydroxide solution. The results of such analyses are shown in Figure 8A where the carbon content of the sublimate is plotted against accumulated weight loss expressed as percent of initial weight of the specimen. These analyses, of course, could only be made on the sublimates from runs in which rather large total weight losses occurred so that sufficient sample for analysis could be obtained. The results show that with increasing weight loss (or time at high temperature) the carbon content of the sublimate approaches a constant value which is approximately the carbon content of stoichiometric ZrC, that is 11.63% by weight.

The surfaces of the two specimens were examined by X-ray diffraction at various times throughout the course of the weight loss experiments. Zirconium carbide has the cubic NaCl-type structure (B1). The observed lattice parameter (a_o) is plotted against accumulated weight loss in Fig. 8B. Initially, a_o has the value 4.6942 Å and increases to 4.6998 Å after a weight loss of about 1% of the initial weight. With additional weight loss, a_o remains constant.

The average value of a_o measured after 1% of the initial weight had been evaporated is 4.6998 ± .0004 Å. This value is significantly higher than 4.69764 ± .00005 obtained [3] on a sample of zirconium carbide containing 11.14% total C and 0.26% free C (10.88% combined carbon). Since the lattice parameter increases with increasing combined carbon content, this indicates that the surface of the weight loss specimens had a combined content greater than 10.88%.

The value for a_o measured here on the specimens after 1% of the initial weight had been evaporated is in excellent agreement with the value 4.700 ± .001 Å obtained by Pollock[4] under similar conditions during his study of the vaporization of ZrC.

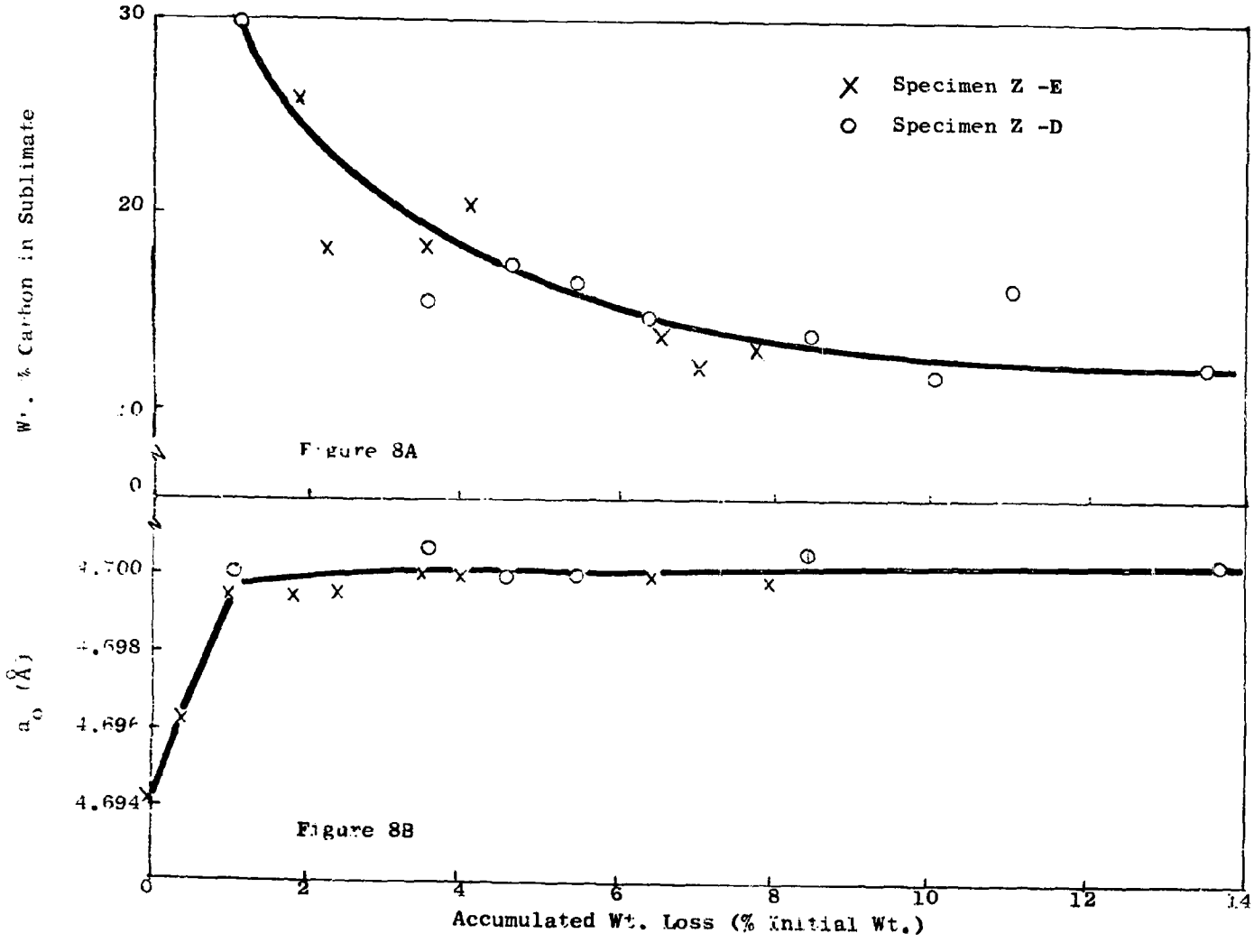

Figure 8 Lattice Constant and %C in Sublimate for ZrC

The above observations indicate that the vaporization of ZrC of stoichiometric combined carbon content is congruent, that is, no change of surface composition occurs as vaporization proceeds. This conclusion is supported by the constant value of a_o observed after vaporization of about 1% of sample (Fig. 8B). The observed rate of carbon evaporation higher than that expected for congruent evaporation seems to be due to the evaporation of free carbon near the surface. As this surface free carbon becomes depleted, the rate of carbon evaporation approaches that for congruent evaporation (Fig. 8A).

After the weight loss measurements were completed, total and free carbon analyses were performed on the specimens. The results showed 10.93% total carbon and .75% free carbon. Comparison with the starting material analysis given in Table 11, shows a decrease of 0.73% in total carbon, 0.34% in free carbon and 0.39% in combined carbon. These results are consistent with the observation that carbon evaporation is in excess of that for congruent evaporation as shown in Fig. 8A. However, the decrease in combined carbon is not consistent with congruent vaporization unless the carbon is removed in combined form during the course of the volatilization of impurities.

Pollock [4] concluded from his observations of the vaporization of ZrC that the amount of zirconium vaporized is in excess of the stoichiometric proportion and he based his vapor pressure calculations on a ten-to-one weight ratio of zirconium to carbon. However, he reports no analysis of the sublimate nor free carbon contents of the samples. His conclusion is based mainly on the increase of surface lattice parameter with vaporization and is inconsistent with his own data which show a decrease in total carbon content with increasing percent weight loss.

In view of the evidence from the present study, it is concluded that the vaporization of ZrC is congruent or nearly so and, if anything, the carbon content of the vapor is in excess of the stoichiometric proportion. The matter, of course, could be easily settled if pure stoichiometric ZrC with no free carbon were available.

A total of thirty-one reliable rate of weight loss measurements were made on the two ZrC specimens. These measurements extended from 2241°K to 2895°K over which range the rate of weight loss increased by a factor of nearly 10^4. In some of the earlier data the rate of weight loss was found to be unreasonably high for measurements made at the lowest temperatures. It was later found that if the sample was very carefully outgassed before the weight loss run, consistent data could be obtained even for total weight losses as low as one milligram. It was then concluded that the unreasonably high rates of weight loss were due to oxidation of the specimen either by adsorbed atmospheric gases or by residual oxygen in the system. The

TABLE 12

Rate of Weight Loss Data for ZrC

Run #	T_{avg} (°K)	T(°K)	(mgm) wt. loss	(cm^2) Area	(sec) heating time	$\left(\frac{gm}{cm^2 \text{ sec}}\right)$
Z-E-21	2241	2246	0.90	11.23	21,600	3.71×10^{-9}
Z-E-17	2251	2254	0.99	11.25	18,000	4.89×10^{-9}
Z-D-18	2285	2287	0.93	10.14	10,920	8.40×10^{-9}
Z-E-19	2310	2310	1.20	11.24	10,860	9.83×10^{-9}
Z-D-19	2315	2316	1.30	10.15	10,800	1.19×10^{-8}
Z-E-20	2348	2351	1.88	11.25	9,300	1.80×10^{-8}
Z-D-17	2353	2354	2.40	10.15	10,800	2.19×10^{-8}
Z-E-6	2381	2384	1.32	12.05	2,700	4.06×10^{-8}
Z-D-11	2396	2404	2.91	10.68	7,200	3.78×10^{-8}
Z-E-7	2435	2439	2.66	12.06	2,750	8.02×10^{-8}
Z-D-10	2466	2470	6.33	10.70	5[illegible],514	1.07×10^{-7}
Z-D-7	2490	2492	12.90	10.90	[illegible]7,260	1.63×10^{-7}
Z-E-12	2551	2553	34.77	11.56	[illegible]7,500	4.01×10^{-7}
Z-E-10	2554	2559	35.87	12.02	5[illegible],800	3.83×10^{-7}
Z-D-6	2591	2592	50.19	10.97	[illegible]7,200	8.35×10^{-7}
Z-E-14	2591	2593	33.85	11.37	[illegible]6,120	4.86×10^{-7}
Z-D-1	2614	2615	18.62	11.25	1,800	9.19×10^{-7}
Z-E-5	2619	2623	20.31	12.12	1,800	9.31×10^{-7}
Z-E-11	2616	2624	68.93	11.97	5,400	1.07×10^{-6}
Z-D-4	2624	2625	53.28	11.07	4,560	1.06×10^{-6}
Z-E-9	2625	2630	43.70	12.08	3,654	9.90×10^{-7}
Z-D-12	2672	2674	29.47	10.35	2,100	1.35×10^{-6}
Z-D-5	2684	2685	44.03	11.05	1,800	2.21×10^{-6}
Z-E-13	2697	2697	150.33	11.49	4,800	2.73×10^{-6}
Z-D-3	2716	2716	74.49	11.16	1,800	3.71×10^{-6}
Z-D-2	2726	2726	49.39	11.24	1,200	3.66×10^{-6}
Z-E-15	2763	2765	47.73	11.34	900	4.68×10^{-6}
Z-D-13	2789	2794	36.25	10.34	600	5.84×10^{-6}
Z-D-8	2795	2798	96.14	10.90	900	9.80×10^{-6}
Z-D-9	2814	2818	82.03	10.81	600	1.26×10^{-5}
Z-D-14	2895	2898	109.42	10.30	420	2.53×10^{-5}

procedure that was adopted for the rate of weight loss measurements was to first evacuate the system by overnight pumping and then to heat the specimen slowly to a temperature of about 2100°K while keeping the indicated pressure in the system less than 2×10^{-5} mm Hg. The specimen was then held at this temperature until the pressure in the system fell to about 1×10^{-6} mm Hg. The temperature was then increased to the desired value and the rate of weight loss measurement begun. It was found that only about .02 milligrams was lost during the preliminary treatment which for all practical purposes is negligible.

A summary of the rate of weight loss measurements on ZrC is given in Table 12. The first column is the run number, the second column the average of all temperature measurements for the particular run and the third column is the effective temperature calculated as described in the previous section. The fourth column is the weight loss and the fifth column is the true hot area which includes a correction for thermal expansion. The mean coefficient of linear thermal expansion between 25°C and the temperature of the measurement was estimated from the data of Ref. 5 to be 7.3×10^{-6} per °K. The sixth column is the heating time and the seventh column the rate of weight loss in gm. per $cm.^2$ per sec.

In Fig. 9 the logarithm of the rate of weight loss in gm per cm^2 per sec is plotted against reciprocal absolute temperature. Also plotted in Fig. 9 are the weight loss data from Ref. 4. The agreement between the two sets of data is rather remarkable and can be accounted for by a difference in measured temperature of about 8°K which is within the accuracy of the optical pyrometers at 2700°K. Pollock estimates his uncertainty in measured temperature to be about $\pm$ 15°K, which, it is felt, would be a fair estimate for the data obtained here also.

c. Hafnium Carbide Weight Loss Data

Evaporation rate measurements have been made on three different specimens of hafnium carbide. The starting material used was -200 mesh reactor grade powder obtained from the Varlacoid Chemical Company. The analysis of the as-received powder is given in Table 13.

TABLE 13

Analysis of Hafnium Carbide

(Stoichiometric composition: 6.30% C, 93.70% Hf)

Element	% by wt	Element	% by wt.
Total C (Combustion)	6.45	Zr	4.0
Free C (Appendix C)	.39	Fe	.01
Combined C (diff.)	6.06	Ti	.005
N	.005	Hf (diff.)	89.52
H	.011		
O	.000		

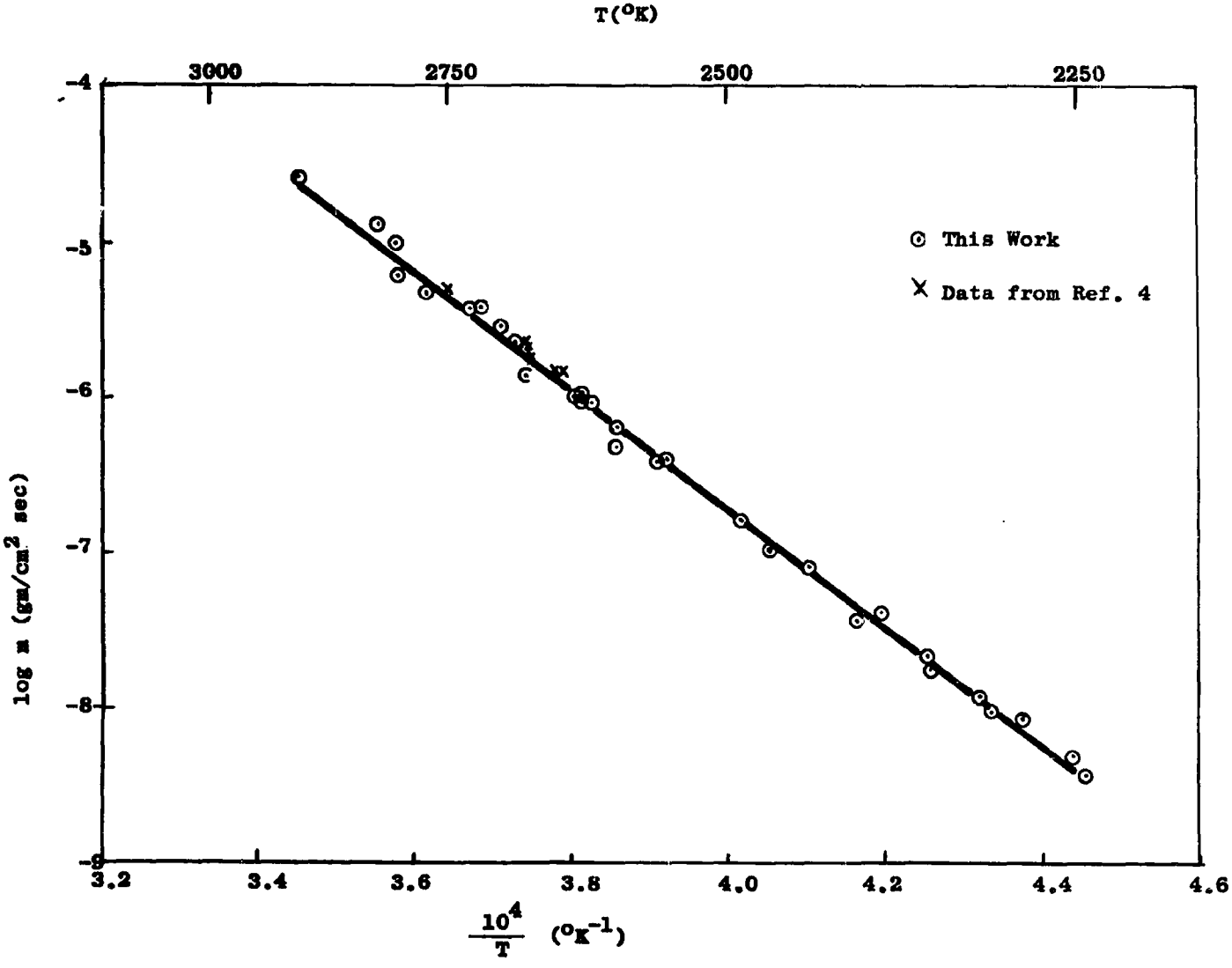

Figure 9 Rate of Weight Loss Data for ZrC

The first two specimens, H-A and H-B, were prepared by first grinding the powder to -325 mesh and then hot pressing in a graphite die at a pressure of 4000 psi, at 2250°C for 30 min. The resulting density was 8.7 gm per cc which is only 69% of the X-ray density 12.64 gm per cc, calculated from the lattice parameter, 4.6435 Å, determined here. It had been reported [6] that such conditions would yield specimens with densities greater than 95% of the theoretical value.

The relatively high porosity of these two samples caused considerable outgassing to occur when the specimens were heated. The inconsistent data at the lower temperatures, to be discussed in detail below, were also attributed to adsorbed atmospheric gases.

In order to eliminate these difficulties, an attempt was made to press a sample of higher density. To accomplish this, a portion of the powder, ground to -325 mesh, was intimately mixed with 1.5% by weight of hafnium hydride powder obtained from Metal Hydrides Inc. This mixture was hot pressed under the same conditions as the first two samples. The result was a piece, specimen H-D, with a density of 9.25 gm per cc or about 73% of the X-ray density, a rather minor improvement. No further attempts have been made to hot press high density specimens.

After hot pressing, specimens H-A and H-B had a total carbon content of 6.47% by weight of which 0.26% was free carbon giving a combined carbon content of 6.21%. Specimen H-D had a total carbon content of 6.43% of which 0.05% was free carbon and 6.39% was combined. The stoichiometric value for pure HfC is 6.30% carbon, and for HfC with 4.0% zirconium, the stoichiometric combined carbon content would be 6.55%.

All specimens were heated to about 2800°K in order to outgas them and volatilize impurities before the weight loss runs were begun. During this preliminary treatment the samples lost from 0.05 to 0.1 gm.

Carbon analyses of a number of samples of sublimates were made during the course of the weight loss runs as was done during the zirconium carbide measurements. Analyses of twelve separate samples gave an average value of 7.3% carbon and showed a slight trend to decreasing carbon content with increasing total weight loss. As with zirconium carbide, the carbon content of the sublimate being higher than that corresponding to stoichiometric HfC is attributed to the evaporation of free carbon from the specimen. Analysis of specimens H-A and H-B after completion of the weight loss runs showed that the free carbon content had been reduced to a very low value (0.05%) while the combined C was 6.19% which is essentially the same value as before the weight loss runs were begun.

Hafnium carbide has the cubic NaCl-type crystal structure (B1). Determination of the lattice parameter a_o, of the hot pressed samples before subsequent heating gave a_o = 4.6418 Å. Periodic measurements of a_o were made during the course of the weight loss determinations. An initial increase to a value of 4.6435 $\pm$ .0005 Å was observed after which a_o remained constant with increasing weight loss. This value is in good agreement with other recent determinations of 4.641 $\pm$ .001 Å [7], 4.63 Å [6] and 4.6365 Å [8].

From the carbon analyses of the sublimate, the constant value of a_o, and the constant combined carbon content of the specimens, it is concluded that HfC of stoichiometric combined carbon content vaporizes congruently.

A total of twenty-nine reliable weight loss measurements were obtained on the three specimens at temperatures ranging from 2313 to 3145°K. Initially, the measurements at the lower temperatures resulted in unreasonably high weight losses as mentioned previously. From the similar experience with zirconium carbide, an attempt was made to obtain good data at the lower temperatures by very carefully outgassing the specimen before the start of the run. Several trial heatings were made at a temperature of about 2200°K, at which temperature no appreciable weight loss should occur in 2 hours, as estimated from an extrapolation of the higher temperature data. Such runs, however, showed consistently a weight loss of about 0.3 mgm.

The following procedure was then used to correct the rate of weight loss data at temperatures less than 2500°K. First, a series of runs was made at the lower temperatures for a total heating time of one hour. From this series, a plot was made of weight loss occurring in one hour against temperature. For other runs for which longer heating times were used, the weight loss occurring during the one hour heating was subtracted from the measured weight loss and the actual heating time reduced by one hour. With this procedure, reproducible data were obtained for total weight losses as small as 0.9 mgm. The range of the measurements was thus extended to 2313 °K.

A summary of the rate of weight loss measurements on HfC is given in Table 14. All data at temperatures less than 2550°K have been corrected according to the procedure described above. The column headings are the same as for Table 12. In calculating the true hot area (column 5), the mean coefficient of linear thermal expansion was taken to be 7 x 10^{-6} per °K. This value was estimated from the data of Ref. 9.

In Fig. 10, the logarithm of the rate of weight loss is plotted against reciprocal absolute temperature. A comparison of Fig. 10 with Fig. 9 will show that the rate of weight loss for HfC is about one third that for ZrC at any temperature.

Rate of Weight Loss Data for HfC

Run #	T_{avg} (°K)	T(°K)	(mgm) wt. loss	(cm^2) Area	(sec) heating time	$\left(\frac{gm}{cm^2\ sec}\right)$ m
H-A-7	2310	2313	.50	9.14	18,000	3.04×10^{-9}
H-D-8	2364	2365	.39	9.26	7,200	5.85×10^{-9}
H-D-9	2368	2369	1.38	9.26	18,000	8.28×10^{-9}
H-D-10	2371	2372	1.78	9.26	18,000	1.07×10^{-8}
H-A-5	2384	2386	1.15	9.15	9,000	1.40×10^{-8}
H-A-6	2402	2404	1.61	9.15	14,400	1.22×10^{-8}
H-D-1	2426	2427	1.19	9.27	6,360	2.02×10^{-8}
H-D-7	2444	2446	4.35	9.27	18,000	2.61×10^{-8}
H-A-4	2448	2451	2.59	9.16	12,900	2.19×10^{-8}
H-D-5	2459	2463	2.29	9.27	7,200	3.43×10^{-8}
H-A-13	2486	2496	3.53	8.78	7,560	5.32×10^{-8}
H-D-3	2520	2520	4.83	9.28	7,200	7.23×10^{-8}
H-D-11	2521	2523	13.39	9.28	18,000	8.02×10^{-8}
H-A-3	2533	2535	6.71	9.18	9,120	8.02×10^{-8}
H-B-3	2567	2569	15.91	9.72	12,000	1.36×10^{-7}
H-B-9	2628	2634	27.42	9.28	9,600	3.08×10^{-7}
H-B-1	2648	2650	38.30	9.80	10,800	3.62×10^{-7}
H-A-1	2716	2720	28.96	9.31	3,600	8.64×10^{-7}
H-A-8	2720	2724	36.61	9.15	3,900	1.03×10^{-6}
H-A-2	2822	2824	53.00	9.26	1,800	3.18×10^{-6}
H-B-2	2865	2867	43.85	9.79	900	4.98×10^{-6}
H-B-8	2873	2881	49.01	9.36	900	5.82×10^{-6}
H-B-4	2932	2933	53.79	9.73	600	9.21×10^{-6}
H-B-5	2937	2942	65.39	9.66	600	1.13×10^{-5}
H-A-9	2958	2961	75.17	9.12	600	1.37×10^{-5}
H-B-6	3000	3003	102.23	9.59	600	1.78×10^{-5}
H-A-10	3041	3044	102.36	9.06	312	3.62×10^{-5}
H-B-7	3075	3085	169.32	9.48	318	5.84×10^{-5}
H-A-11	3138	3145	140.90	8.95	180	8.74×10^{-5}

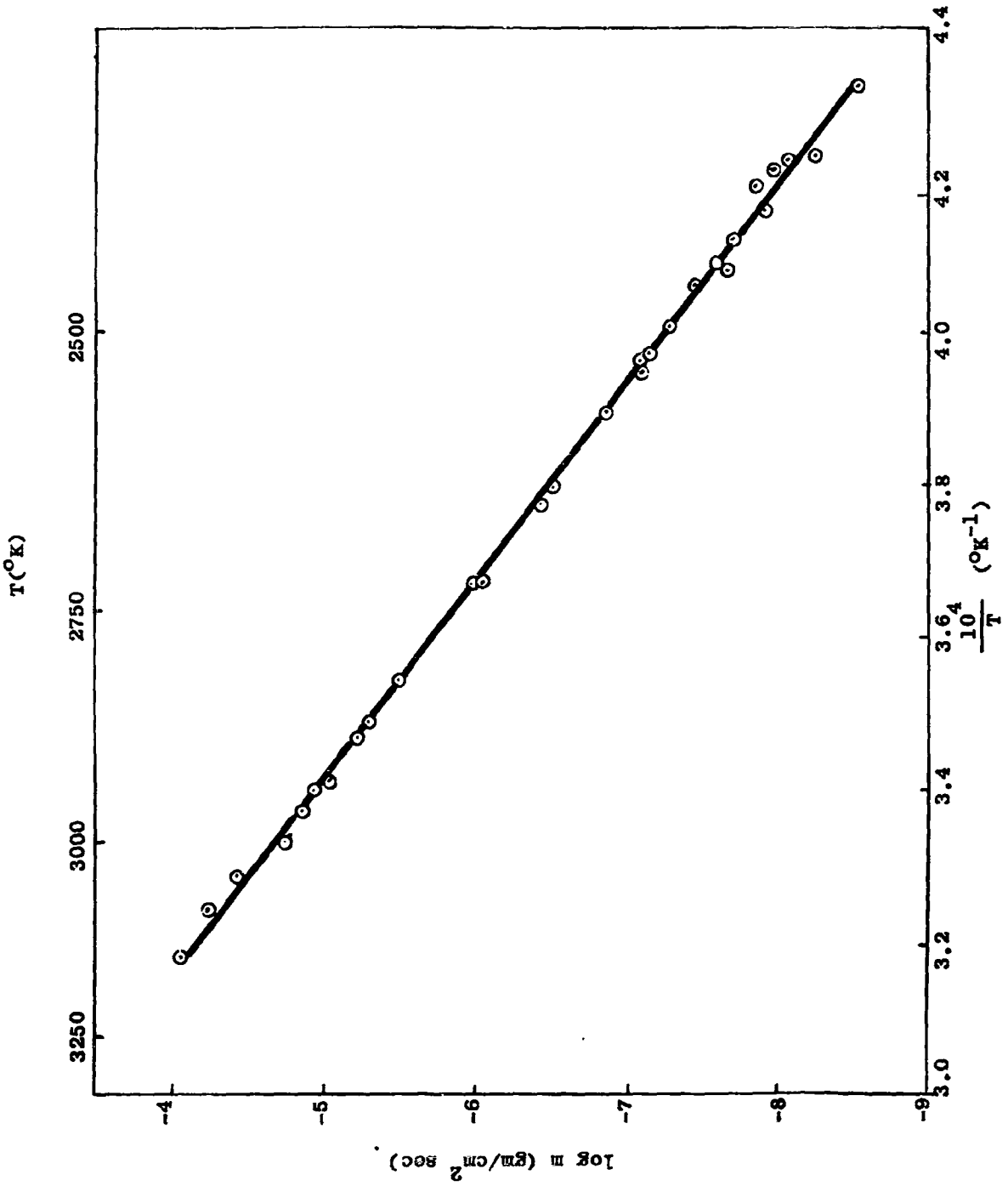

Figure 10 Rate of Weight Loss Data for HfC

d. Titanium Carbide Weight Loss Data

The two titanium carbide weight loss specimens were hot pressed from a sample of "Submicron Titanium Carbide" kindly furnished by the Union Carbide Metals Company. The density of the specimens was 4.364 gm. per cc. which is 89% of the X-ray density, 4.905 gm per cc, calculated from the lattice parameter 4.3284 Å, measured here. Like ZrC and HfC, titanium carbide has the face centered cubic (NaCl) type structure. The lattice parameter determined here is in excellent agreement with the most probable value for the stoichiometric composition given by Hansen [10] which is 4.329 ± .001 Å.

The material was from a lot which, according to Union Carbide, had the analysis given in Table 15. Analysis of the as-received powder performed here showed 19.3% total carbon and 0.064% free carbon.

TABLE 15

Analysis of Submicron Titanium Carbide

(Stoichiometric Composition: 20.05% C, 79.95% Ti)

Element	% by wt.
Total C	19.5
Free C	.01
Combined C (diff.)	19.5
O	.10
Ti	80.2

It was determined from thermodynamic calculations that the possibility exists for TiC to vaporize incongruently with Ti having a rate of weight loss higher than that corresponding to the stoichiometric composition (See Appendix A). If such were the case, since TiC cannot dissolve excess carbon, one would expect free carbon to form on the surface and possibly hinder further evaporation. From consideration of this fact, the total weight loss was kept small to minimize this effect if it did occur. For the first specimen, Ti-A, a total of 3.24% of the initial weight was evaporated and for Ti-B a total weight loss of 4.30% was obtained.

If congruent vaporization did occur and, for example, the weight loss of carbon were only 15% of the total weight loss instead of 20.05% (the stoichiometric value), then upon analysis of the specimens after the weight loss measurements, one would have found the total carbon content to have increased by about 0.2% over the initial value and a corresponding increase in free carbon. However, analysis of the

specimens after the weight loss runs were completed showed no change in either free or total carbon content from the initial analysis, within experimental error.

Some carbon analyses of the sublimate were also attempted, but so little material could be removed from the walls of the evaporation chamber that the results are very inaccurate. It might be mentioned that the highest value obtained was 23% and the lowest value 6% total carbon.

Determination of the lattice parameter at various times throughout the course of the weight loss determinations on both specimens gave a constant value of 4.3284 $\pm$ .0003 Å.

Thus, since there was apparently no change in total composition or in surface lattice parameter during the course of weight loss determinations, it is concluded that TiC vaporizes congruently or nearly congruently under the conditions employed here. However, it should be pointed out that the total weight loss on each specimen which occurred at temperatures below 2400°K is quite small in each case and any carbon formation under such conditions might have been too small to have been detected or even might have evaporated during subsequent runs at higher temperatures.

A total of ten evaporation rate measurements were made on the two specimens of TiC and a summary of the results is given in Table 16. Measurements were made at temperatures from 2110 to 2542°K. The column headings are the same as in Table 12. In calculating the true hot area (column 5), the mean coefficient of linear thermal expansion was estimated to be 7.7×10^{-6} per °K.

TABLE 16

Rate of Weight Loss Data for TiC

Run #	T_{avg} (°K)	T(°K)	(mgm) wt. loss	(cm^2) Area	(sec) heating time	$\left(\frac{gm}{cm^2\ sec}\right)$ m
Ti-B-5	2109	2110	3.03	9.95	12,600	2.42×10^{-8}
Ti-B-4	2173	2173	6.73	9.95	10,200	6.63×10^{-8}
Ti-A-2	2249	2251	5.20	9.95	2,400	2.18×10^{-7}
Ti-B-3	2272	2274	9.11	9.95	2,700	3.39×10^{-7}
Ti-A-3	2277	2279	5.95	9.95	1,800	3.32×10^{-7}
Ti-B-6	2288	2288	5.52	9.95	1,924	2.88×10^{-7}
Ti-B-2	2397	2401	17.94	9.95	900	2.00×10^{-6}
Ti-A-4	2450	2452	14.96	9.95	420	3.58×10^{-6}
Ti-A-5	2505	2507	21.11	9.95	300	7.07×10^{-6}
Ti-A-6	2540	2542	34.03	9.95	300	1.14×10^{-5}

In Fig. 11, the logarithm of the rate of weight loss is plotted against reciprocal absolute temperature. At 2500°K the rate of weight loss of TiC in vacuum is about 30 times that for ZrC and about 90 times that for HfC.

e. Tungsten Carbide Weight Loss Data

Rate of weight loss measurements were made on three specimens of tungsten carbide. The starting material was -325 mesh WC obtained from A. D. Mackay Inc. After vacuum hot pressing, the analysis given in Table 17 was obtained.

TABLE 17

Analysis of Hot Pressed Tungsten Carbide

(Stoichiometric composition: 6.13% C, 93.87% W)

Element	% by wt.
Total C (Combustion)	6.00
Free C (Appendix C)	.03
Combined C (diff.)	5.97
O	.033
N	.015
H	.001
Si	.005
Mg	.001
W (diff.)	93.92

X-ray diffraction patterns of the hot pressed material showed the simple hexagonal WC structure with a_o = 2.906 Å and c_o = 2.825 Å giving

$$\frac{c_o}{a_o} = .971.$$

Hansen[10] gives the most probable values as a_o = 2.906 Å, c_o = 2.837 Å and

$$\frac{c_o}{a_o} = .976.$$

The measured density was 15.6 gm per cc. which is 99% of the X-ray density (15.72 gm per cc) obtained from the measured lattice constants.

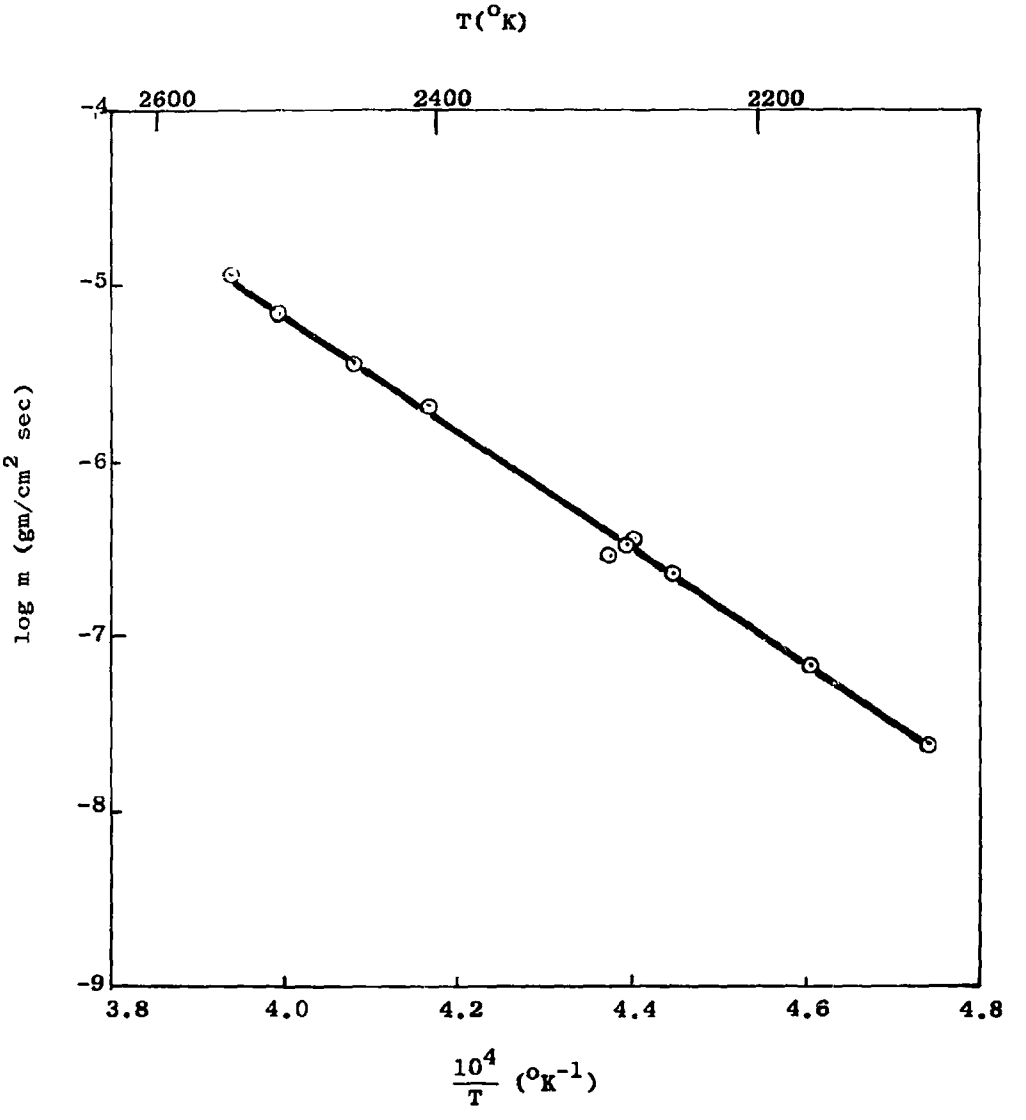

Figure 11 Rate of Weight Loss Data for TiC

When the first weight loss measurements were begun, specimen W-D was given a preliminary heating in order to outgas the specimen and volatilize trace impurities. The piece was slowly heated to about 2300°K. At this point rapid volatilization began and an increase of at least 100°K was noted at a constant induction heater power setting. The sample was then cooled and removed and found to have lost about 20 mgm. of weight. X-ray diffraction showed the surface had changed to the hexagonal close-packed structure of α-W_2C. Rate of weight loss measurements were then begun and continued until 1.30% of the initial weight had been evaporated. The specimen was then broken and microscopic examination made of the cross section. Fig. 12A is a photograph of the cross section as broken. This photo was made under polarized light with 50x magnification and shows the inner core of WC surrounded by the annular region of W_2C extending to the surface. The identity of the two phases was established by X-ray diffraction pattern on a section which had been powdered and mixed.

A second weight loss specimen (W-E) was then prepared. This specimen was slowly heated to 2000°K and held at this temperature for one hour. During this time the total weight loss was less than 0.1 mgm. Subsequent X-ray examination showed the α-W_2C structure even though the weight loss was small. Weight loss measurements were then made on this specimen. Initially, an increase in temperature was noted at a constant power setting of the induction heater and the specimen temperature was quite non-uniform. After a weight loss of about 50 mgm, a uniform and constant temperature was obtained. After 2.45% of the initial weight had been evaporated, this specimen was broken and the photograph of the broken cross section shown in Fig. 12B was obtained. In this photograph, the inner core of WC, smaller than in the previous photo, is obvious.

A third specimen (W-F) was prepared. During the early heatings, behavior similar to that of W-D and W-E was observed. Rate of weight loss measurements were made on W-F until a total of 3.54% of the initial weight had been lost. A subsequent X-ray diffraction pattern showed α-W_2C with five lines of the pattern of elemental tungsten visible. A photo of the broken cross section of W-F is shown in Fig. 12C. Only W_2C is visible in this photograph. In Fig. 12 some portions of the photos are out of focus due to the uneven surface of the fracture.

Some conclusions may be drawn from these observations. WC of near stoichiometric carbon content vaporizes by loss of carbon, the resulting phase being W_2C. With the specimens used here which contained 6.00% carbon, the loss of carbon results in immediate conversion to W_2C and hence the low carbon limit of the WC phase must be at or near 6.00% carbon. X-ray diffraction patterns of the W_2C surface showed the hexagonal structure with $a_o = 3.025$ and $c_o = 4.726$. These lattice constants were practically independent of the total carbon content of

FIGURE 12A. CROSS SECTION OF TUNGSTEN CARBIDE SPECIMEN W-D AFTER 1.30% WEIGHT LOSS. WC SURROUNDED BY W_2C. MAGNIFICATION 50X. POLARIZED LIGHT.

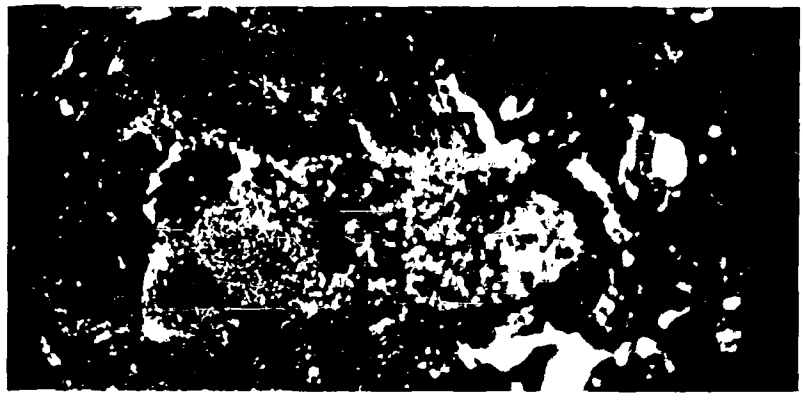

FIGURE 12B. CROSS SECTION OF TUNGSTEN CARBIDE SPECIMEN W-E AFTER 2.45% WEIGHT LOSS. WC SURROUNDED BY W_2C. MAGNIFICATION 50X. POLARIZED LIGHT.

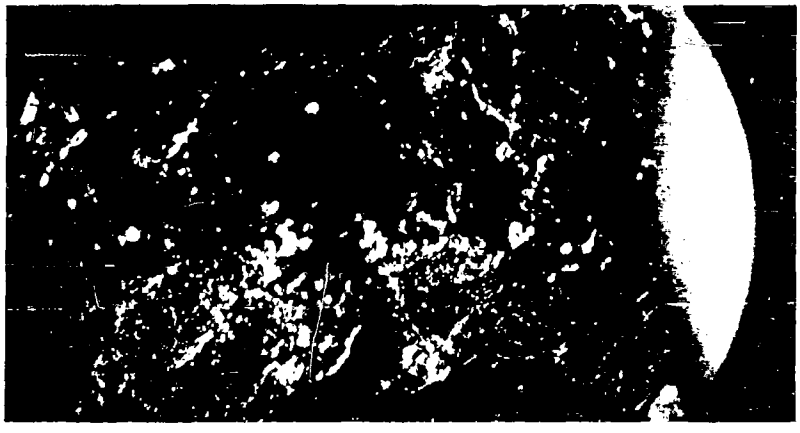

FIGURE 12C. CROSS SECTION OF TUNGSTEN CARBIDE SPECIMEN W-F AFTER 3.54% WEIGHT LOSS. NO WC VISIBLE. MAGNIFICATION 50X. POLARIZED LIGHT.

the specimen. This indicates that carbon diffuses quite readily through W_2C.

The absence of any tungsten containing species in the vapor can be shown in several ways. Samples of the sublimate were analyzed spectrographically and by X-ray emission. No tungsten was detected by either method. The final carbon content of the specimens may be calculated on the assumption that only carbon was lost in the evaporation process. That is, specimen W-D, which lost 1.30% of its initial weight, would have a final carbon content of 4.76% while carbon analysis showed 4.64%. For W-E, one calculates 3.64% carbon on the assumption that only carbon was lost while analysis showed 3.55% carbon. For W-F, the calculated value is 2.55% while carbon analysis showed 2.66%. This general agreement between the value calculated on the assumption that only carbon vaporizes and the measured value is further evidence that this assumption is correct. At least part of the discrepancy that does exist may be explained by inhomogeneities in the specimens after the weight loss measurements were completed.

The peculiar behavior of the temperature on initial heating of the WC piece is attributed to differences in electrical conductivity between WC and W_2C.

The fact that no elemental tungsten appeared on X-ray diffraction patterns until the total carbon content was reduced to about 2.6% is in agreement with the phase diagram of Ref. 10 which shows the W_2C field extending to about 2.5% carbon and also shows the field completely at carbon contents less than that for stoichiometric W_2C which is 3.16% carbon.

A summary of all rate of weight loss data for tungsten carbide is given in Table 18. The second column is the accumulated weight loss on the particular specimen at the completion of the run expressed as per cent of initial weight. The third column is the average temperature which is here taken as the true temperature since these data are not considered sufficiently meaningful to warrant the rather laborious calculation of the effective temperature, which amounts to a very small correction. The fourth column is the weight loss for the particular run and the fifth column is the area computed on the assumption of a mean coefficient of linear thermal expansion of 7×10^{-6} per ^{o}K. The sixth column is the heating time and the seventh column the rate of weight loss in gm. per cm^2 per sec.

The data of Table 18 are plotted in Fig. 13 as the logarithm of the rate of weight loss against reciprocal absolute temperature. Different symbols are used to denote the measurements made on samples with different accumulated weight loss. It is obvious from this plot that the rate of weight loss, at least at the

Run #	% Accum. wt. loss	T(°K)	(mgm) wt. loss	(cm^2) Area	(sec) heating time	$\left(\frac{gm}{cm^2\ sec}\right)$ m
W-D-1	.18	2319	2.71	11.11	3600	6.78×10^{-8}
W-D-2	.34	2443	19.61	11.11	3000	5.88×10^{-7}
W-D-3	.59	2652	31.03	11.11	300	9.31×10^{-6}
W-D-4	.61	2269	2.92	11.11	12000	2.19×10^{-8}
W-D-6	.88	2662	32.57	11.11	300	9.77×10^{-6}
W-D-7	.95	2385	8.68	11.11	4200	1.86×10^{-7}
W-D-8	1.24	2540	36.15	11.11	1800	1.81×10^{-6}
W-D-9	1.27	2282	4.58	11.11	13800	2.99×10^{-8}
W-D-10	1.29	2232	1.87	11.11	14520	1.16×10^{-8}
W-D-11	1.30	2198	1.06	11.11	17280	5.52×10^{-9}
W-E-4	.86	2558	19.05	8.66	1200	1.83×10^{-6}
W-E-5	1.23	2623	29.17	8.66	780	4.32×10^{-6}
W-E-6	1.69	2717	35.82	8.66	480	8.62×10^{-6}
W-E-7	1.85	2408	12.99	8.66	7200	2.08×10^{-7}
W-E-8	1.96	2353	8.90	8.66	10800	9.52×10^{-8}
W-E-9	1.98	2227	0.88	8.66	12000	8.47×10^{-9}
W-E-10	2.02	2299	3.30	8.66	10800	3.53×10^{-8}
W-E-11	2.38	2643	28.75	8.66	900	3.69×10^{-6}
W-F-2	1.07	2506	31.55	8.51	3600	1.02×10^{-6}
W-F-3	1.41	2562	25.47	8.51	1800	1.66×10^{-6}
W-F-4	1.56	2398	11.50	8.51	10860	1.24×10^{-7}
W-F-5	1.83	2654	19.81	8.51	600	3.88×10^{-6}
W-F-6	2.07	2472	18.10	8.51	5400	3.94×10^{-7}
W-F-7	2.31	2667	17.46	8.51	600	3.42×10^{-6}
W-F-8	2.41	2366	7.34	8.51	14400	5.99×10^{-8}
W-F-9	2.59	2471	13.48	8.51	5460	2.90×10^{-7}
W-F-10	2.86	2597	20.26	8.51	1800	1.31×10^{-6}
W-F-11	3.13	2659	20.25	8.51	1800	1.32×10^{-6}
W-F-12	3.35	2593	16.31	8.51	1800	1.06×10^{-6}
W-F-13	3.54	2501	14.44	8.51	7800	2.17×10^{-7}

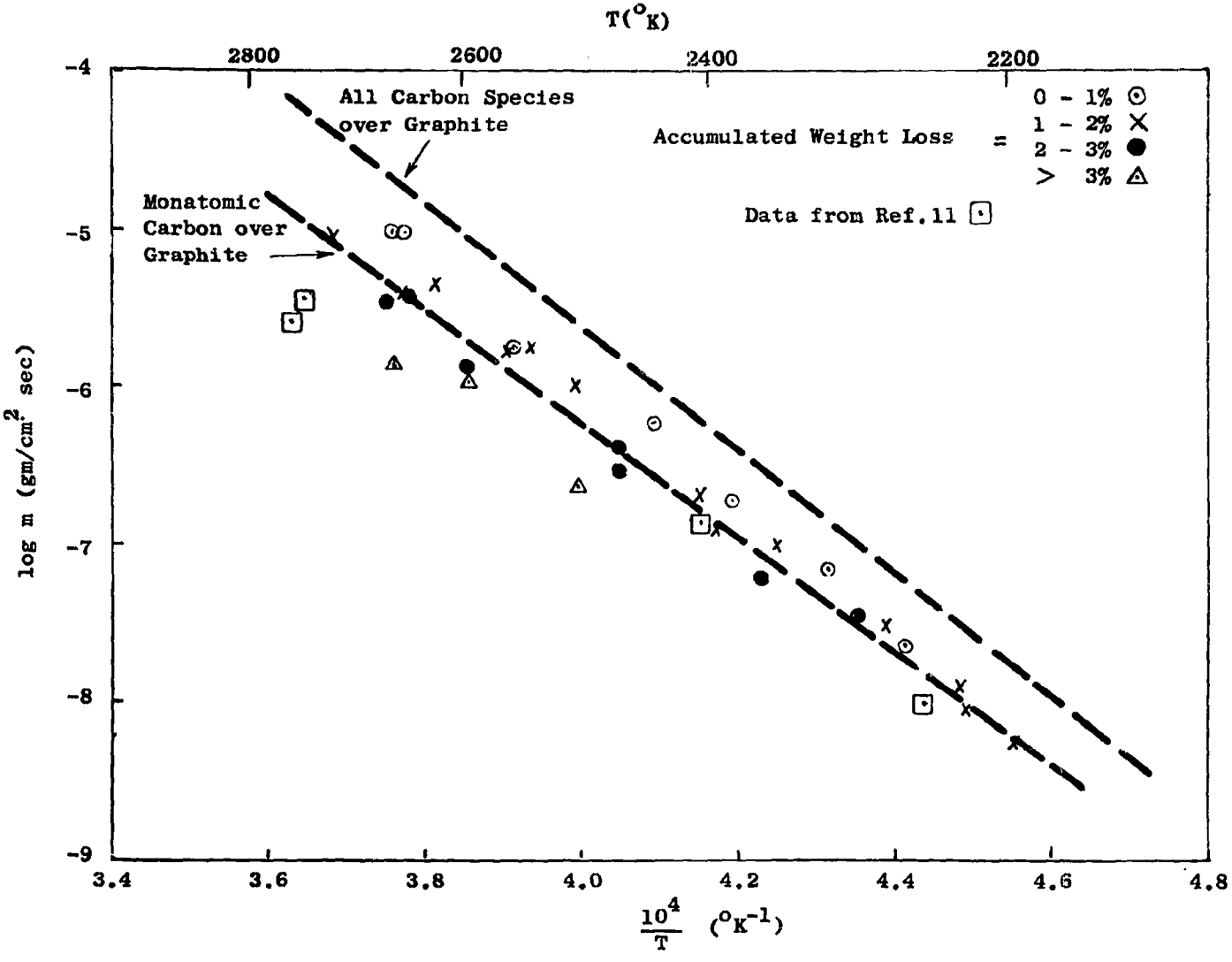

Figure 13 Rate of Weight Loss Data for Tungsten Carbide

higher temperatures, decreases with increasing accumulated weight loss or decreasing total carbon content. It should be remembered that as accumulated weight loss increases, the thickness of the W_2C layer surrounding the WC core increases. Also plotted for comparison are the data from Ref. 11 which are rates of weight loss on material corresponding approximately to the overall composition W_2C. These data are in agreement with the values reported here for the highest accumulated weight loss which specimens have, also the approximate overall composition W_2C.

Also plotted in Fig. 13 is the rate of weight loss of all carbon species from graphite. The rate of weight loss of monatomic carbon from graphite is calculated from the vapor pressure data in the JANAF tables [12] and the rate of weight loss of polyatomic species is calculated from the data of Ref. 13. These rates were calculated with the assumption of unit evaporation coefficient for all species. It may be noted from Fig. 13 that the rate of evaporation of tungsten carbide measured here is less than that of all carbon species over graphite and roughly equal to that of monatomic carbon over graphite. The significance of this comparison will be discussed in a later section.

2. Resonance Line Absorption Studies

The purpose of this investigation was to determine the standard molar free energy of formation of $TiC_{(g)}$ and $ZrC_{(g)}$. The method of measurement consisted, briefly, in generating a strong atomic resonance line from the appropriate metal, measuring the absorption of this line by the metal atoms in the equilibrium vapor over the metal carbide plus graphite at a selected temperature, determining the temperature at which an equivalent absorption is obtained from the equilibrium vapor over the pure metal. From the known vapor pressure of the pure metal, the pressure over the carbide system is available directly. The free energy of formation of the carbide is then calculated from the ratio of vapor pressure over the carbide system to the vapor pressure over the pure metal. Although vapor pressures of neither metal nor carbide are measured, comparison of results from this study with those of the Langmuir experiments permit evaluation of the validity of two assumptions critical to the interpretation of the Langmuir results. These are (1) the assumption of unit evaporation coefficient, and (2) the assumption that no significant molecular species are present in the vapor from ZrC or TiC.

a. Apparatus and Materials

The apparatus and techniques used were essentially the same as those described in the preceding annual report [1]. The description will not be repeated in detail; specifics of apparatus and its operation will be given only where changes have been made or insufficient information was presented earlier.

As previously described, the selected spectral line of titanium (and of zirconium) was obtained by slipping a cup made from a thin sheet of the appropriate metal in the bottom cup of the hollow cathode discharge tube. Obtaining a stable discharge presented no problem in the case of titanium, but was rather difficult for zirconium. Occasionally the discharge had to be run for several days before it would maintain itself in the zirconium cup under the usual current and gas pressure conditions. Once it started to operate properly, however, no further trouble was encountered for several days or weeks. This difficulty may have been due to the presence of an oxide coating on the metal, but this was never proved conclusively.

The current was held at 30 m.a. and the argon pressure was 5.0 to 0.7 mm of mercury in all the runs used.

The graphite absorption cell consisted of an 8" long graphite cylinder, having an outer diameter of 1-1/4" and a wall thickness of 1/8". At the two ends of the cell, tight fitting graphite diaphragms provided with an outside flange were slipped in and held in position with graphite pins.

When the absorption due to the vapor of the metal was being studied, a tube of this metal, machined to precisely the same outside diameter as the internal diameter of the graphite cell, was slipped into the cell. End caps for this tube liner were cut from sheet metal and slipped over the ends of the metal tube. The graphite diaphragms were then pinned in place.

Both the diaphragms and the metal liner end caps had 1/4" or 3/8" holes drilled through their centers. Thus, after assembly, the cell consisted of an area completely lined with the metal under investigation, and the only openings were the holes which defined the optical path.

To study the equilibrium vapor over the carbide phase, the loose, powdered carbide (approximately 5-10 gms), was placed directly in the graphite cell and the graphite diaphragms were placed at the ends. Here the presence of a pure graphite surface insured that the partial pressure of carbon over the carbide was the equilibrium vapor pressure of carbon.

The titanium metal liner end caps consisted of C.P. titanium sheet (Ti - 99.6% min.) provided by the American Titanium Corporation. The titanium metal tube was made of A-40, #1 temper tubing provided by the Frasse Co. The zirconium metal tube was furnished by the Carborundum Metal Co., and was their CP-3 seamless tube.

Impurity limits given by the vendors are as follows, specification checks only having been made here:

TABLE 19

Impurity Limits, Titanium and Zirconium Metal Tube and Sheet

Impurity Elements	Impurity Limits, Percent		
	Ti Sheet	Ti Tube	Zr Tube
Aluminum		0.10 max.	0.125 max.
Carbon	0.08 max.	0.10 max.	
Chromium			0.02 max.
Hydrogen	0.015 max.		
Iron	0.12 max.	0.25 max.	0.08 max.
Manganese		0.15 max.	
Nitrogen	0.05 max.		
Silicon		0.10 max.	
All other metals		0.60 max.	0.01 max.

Because of the danger of saturating the photomultiplier with a DC signal from the furnace at the high temperatures of interest, the monochromator was so placed, with relation to the furnace, that an image of the center of the furnace was made in free space before the light entered the monochromator slit. Masks were then placed at precisely the focal points of the image of the two hot graphite diaphragms at the ends of the cell, and all radiation from the diaphragms was thus eliminated from the beam. The masks were carefully positioned by means of multiple rack and pinion devices mounted rigidly to the monochromator table, and had apertures only slightly smaller than the size of the diaphragm image at its focal point.

All temperature measurements were made with a Pyro Micro Optical Pyrometer modified at this Laboratory by substituting a standard one ohm resistor and a portable Leeds and Northrop potentiometer for the calibrated ammeter. The dimensions of the three heater tubes used in obtaining the data presented here are shown in Figure 14.

Since the presence of sizeable temperature gradients within the cell could not be avoided, a rather arbitrary way of deciding what to call the cell temperature had to be established. In order to test the accuracy of the averaging technique used, the study of the vapor over both zirconium and zirconium carbide was carried out twice, using two tubes having widely different temperature gradients. The accuracy of the averaging technique used can then be established by examining the relation between I/I_o and T for the two cases.

b. Procedure

The resonance line chosen for measuring the absorption due to titanium atoms is the 3371.45 Å line due to an $a^3F_4 - y^3G_5$ resonance transition which promotes an electron from the 4s state to 4 p. This line is known to have a relatively high oscillator strength, and it proved to be quite satisfactory for these studies.

Zirconium has the same outer electron configuration, and its spectrum bears a close resemblance to that of titanium atoms because both obey the L-S coupling rules to a high degree of approximation. The analogous zirconium line 3601.19 Å line was used. It has the same term designation and results from the promotion of a 5s electron to 5p.

These lines also have the advantage of being far enough in the violet to be well removed from the peak of the black body curve for the temperature of the furnace, where difficulties due to photomultiplier saturation are most serious. Also, they are not so far in the violet to present problems due to loss of intensity or difficulties in obtaining transparent materials for windows.

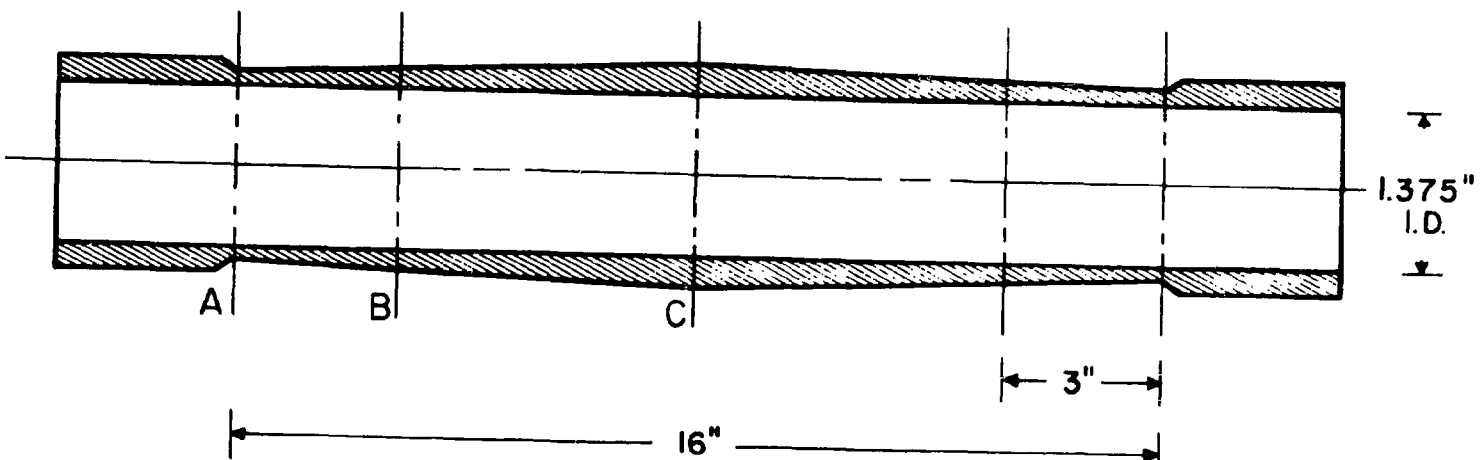

	WALL THICKNESS AT: (in inches)			HEATER TUBE O.D. AT: (in inches)		
	A	B	C	A	B	C
Ti C	.040	.062	.100	1.455	1.499	1.575
Zr C #1	.040	.062	.100	1.455	1.499	1.575
Zr C #2	.048	.059	.100	1.471	1.493	1.575

FIGURE 14. HEATER TUBE DIMENSIONS AS USED IN TiC and ZrC.

The intensity and stability of both lines in the hollow cathode discharge was quite adequate at the relatively low value of the current of 30 m.a.

After starting the hollow cathode source, the carbon resistor furnace, containing a new AUC graphite heater tube and an empty graphite cell at the center of the tube, was heated to approximately 2000°C in a good vacuum. This initial heating was carried out in order to distill the volatile impurities from the graphite. The temperature was then raised to a value 100° to 200° higher than the final temperatures at which measurements would be made, and 10 to 20 cm of mercury pressure of argon was introduced into the furnace.

After turning on the chopper and phasing the amplifier, blank values of I/I_o were obtained by comparing the strength of the desired line after passing through the hot cell (I), with the strength after passing it through the rapidly cooled cell (I_o). Initially, an increase in the strength of the signal was often observed which was attributed to residual amounts of zirconium and titanium in the graphite. Further prolonged heating in a vacuum, however, did not eliminate this apparent absorption. Some argon lines from the discharge then also appeared to be absorbed, so that the low value of I could not be attributed to absorption by the atomic species in question. Investigation revealed that this apparent absorption could be eliminated by carefully masking the radiation from the hot furnace walls; this masking was described on a preceding page.

When the I/I_o ratio became unity, the furnace was turned off and the cell was carefully removed from the furnace and loaded. The cell was then replaced in the heater tube without changing the optical alignment. The furnace was evacuated, a known pressure of argon gas was added, the power was turned on, and the measurement of I/I_o was repeated, this time with the metal or the carbide present in the cell.

Measurements were made over a 10° to 50° temperature range, and at several argon pressures in order to establish the effect of pressure broadening. The temperatures were chosen so as to yield I/I_o values of approximately 0.5.

Two different samples of zirconium carbide were used in this work. Initial experiments were performed using a sample manufactured by Kennametal Inc. The reported analysis was:

10.56%	total carbon
0.22%	free carbon
1.0%	Titanium
0.5%	Tungsten
0.5%	Hafnium
0.25%	Niobium
0.10%	Tantalum
0.1%	other elements

This material was re-analyzed before use and the values of 11.65% total carbon, 0.45% free carbon were obtained. Subsequent work was carried out on a sample of the same material used for the Langmuir measurements. This latter sample was obtained from A.D. Mackay and its analysis is given in a preceding section of this report.

The titanium carbide sample, provided by Union Carbide, was identical to the material used in Langmuir evaporation studies. Its analysis is also presented earlier in Section III.B.1.d.

The preparation of samples presented some problems. General observation showed that initially the density of the metal vapor species under investigation tended to be low and erratic. Prolonged heating of the samples tended to increase the absorption and greatly improved their reproducibility. This effect is attributed to the presence of a layer of oxide or of some other compound on the surface, which slows the rate of vaporization of the material and so tends to keep the atom density below the equilibrium value.

In the case of titanium metal and titanium carbide, this effect gave rise to no major difficulties, because heating in a vacuum at a temperature only one or two hundred degrees higher than the measurement temperature resulted in a rapid cleaning of the surface well beforethe melting point was reached. The considerable volatility of TiO_2 is probably responsible for this.

More difficulty was encountered in the case of zirconium metal and zirconium carbide. The zirconium carbide samples gave erratic results even after prolonged heating at 2700°C, and improvement was obtained only when the carbide sample was mixed intimately with a large excess of powdered pure graphite (National Graphite purest grade). Thus, physical contact with carbon appeared to be necessary in order to accomplish the removal of the surface film. The higher zirconium atom density shows that the change in density could not have been due to a change in the composition of the carbide phase, since addition of carbon should have resulted in a lowering of the zirconium atom vapor pressure. When the graphite was added, the I/I_o measurements readily settled to a reproducible value, and the excessive scatter disappeared. The data obtained are therefore considered reliable.

A different problem was encountered in the case of zirconium metal. Its low melting point (1857°C) was the maximum temperature to which the cell could be heated, and at this temperature rather long (1-3 hrs.) heating and pumping was necessary in order to clean the surface sufficiently. The melting of the zirconium had to be avoided, because the liquid tended to seep through the porous graphite cell walls and into the graphite heater tube. When this happened, large temperature gradients invariably were observed, due to the partial shorting of sections of the heater tube.

Since the value of I/I_o was approximately 0.60 at the melting point, care had to be taken to obtain sufficiently high absorption for good accuracy, while avoiding melting the metal.

Establishing the temperature of the cell with sufficient accuracy turned out to be the most difficult problem encountered. After trying several methods of obtaining the temperature inside the cell, the following one was chosen. The cross section of the cell is shown in Figure 15. The temperature was measured at four places, indicated by the letters A, B, C and D. No other points could be viewed adequately with an optical pyrometer, in view of the requirement that the pyrometer lens be uniformly filled with light emanating from the point being sighted. The difference in the size of the two holes through the diaphragms was necessary in order to obtain a reading on the inside of the other diaphragm.

The object indicated as (B) consisted of a piece of material projecting sufficiently far into the optical path to be clearly visible in the pyrometer, but not so far that it blocked a large fraction of the light beam. When TiC and ZrC were under investigation, this object was a piece of graphite. When the vapor over the metal was being studied, (B) consisted of a bent piece of sheet of the metal used to line the cell.

Temperature measurements were made at the four indicated points both before and after each measurement of I. Preliminary work had shown that the temperature difference across the two diaphragms was almost identical. The temperature on the inside of the diaphragm shown on the left was therefore taken to be A + C - D. The average temperature of the two ends of the cell was then $(A + 2C - D)/2$, while the temperature of the center was B. The effective cell temperature was again assumed to be given by the average of $(A + 2C - D)/2$ and of B. Thus

$$T_{eff} = \frac{A + 2C - D + 2B}{4} \qquad (5)$$

The difference between the center temperature B and the average temperature of the inside of the diaphragm is taken as a measure of the lack of uniformity of temperature of the cell, and is later listed as Δ.

$$\Delta = B - \frac{A}{2} - C + \frac{D}{2} \qquad (6)$$

All of the listed values of A, B, C, and D are the average of the measurements taken before and after the measurement of the beam intensity I.

All recorded temperature readings were corrected for effects due to losses at the window and mirror.

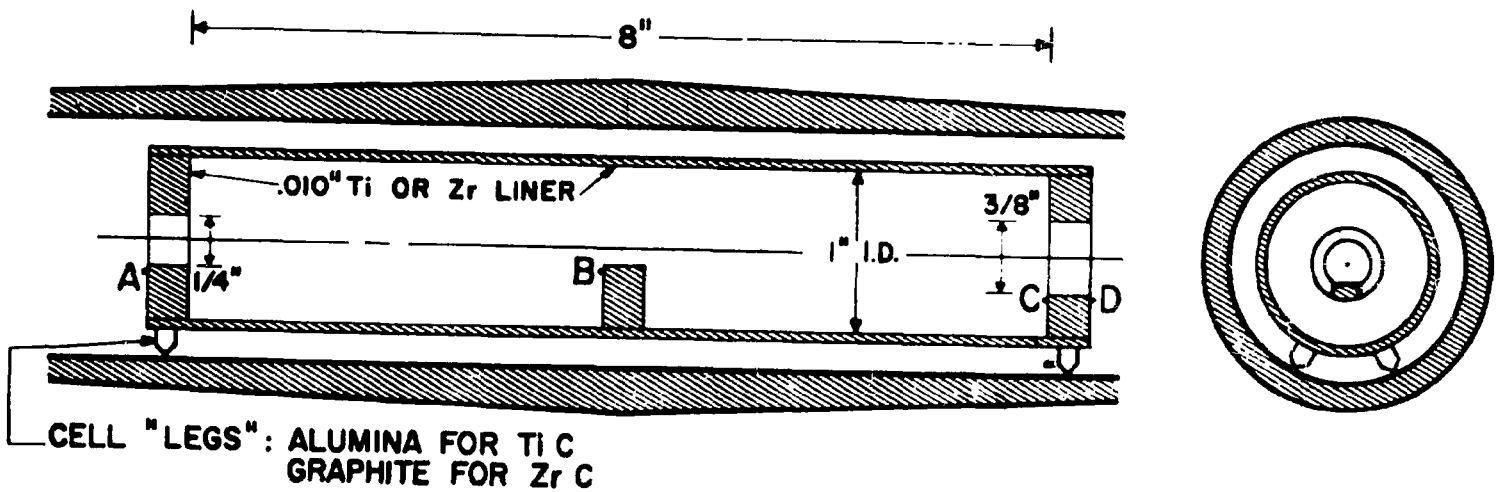

FIGURE 15. GRAPHITE CELL WITH LINER.

c. Experimental Data and Methods of Computation

The results obtained in the final sets of runs, after earlier difficulties were eliminated, are given in Tables 20 and 21.

TABLE 20

Resonance Line Absorption Data - T_i and T_iC

Run No.	Temperature (^oK) A	B	C	D	T_{eff}	Δ	I/I_o	P_{Argon} (cm)
Material - T_iC								
1	2164	2229	2207	2170	2217	25	.536	18.2
2	2182	2247	2221	2188	2233	29	.426	18.9
3	2170	2236	2210	2179	2221	30	.486	18.0
4	2165	2231	2204	2173	2216	31	.509	18.3
5	2166	2235	2206	2176	2218	34	.513	18.5
Material - T_i								
1	1625	1657	1652	1628	1654	6	.392	15.7
2	1611	1645	1645	1611	1644	1	.541	15.5
3	1614	1647	1647	1618	1646	2	.497	15.5
4	1612	1645	1645	1616	1644	2	.561	15.3
5	1613	1645	1645	1616	1644	2	.507	15.5
6	1618	1651	1651	1621	1650	1	.449	15.1

The measured absorption data must be converted to metal atom pressures in order to produce the desired thermodynamic information. In order to do this it is necessary to know the vapor pressure-temperature relationship for the pure metals, the temperature and pressure variations of the absorption coefficient, and the fraction of the metal atoms which absorb the resonance line radiation. None of these were measured directly in this work. Vapor pressure data for the pure metals are available in the literature; relative population of metal atoms in the electronic state capable of absorbing the radiation line used can be obtained by evaluating the appropriate electronic partition functions. Since measurement of the resonance line width, shape, structure, broadening, etc. involves high resolution spectroscopy beyond the capabilities of the instrumentation used, these effects must be eliminated or allowed for in the treatment of the data.

TABLE 21

Resonance Line Absorption Data - Zr And ZrC

Material and Tube	Run No.	Temperature (^{o}K) A	B	C	D	T_{eff}	Δ	I/I_o	P_{Argon} (cm)
ZrC	1	2642	2801	2709	2659	2751	100	.582	17.6
heater	2	2642	2791	2706	2646	2748	87	.571	17.8
tube (1)	3	2647	2796	2705	2651	2750	93	.572	17.9
	4	2644	2787	2697	2644	2742	90	.591	17.9
ZrC	5	2682	2746	2711	2685	2728	36	.649	19.3
heater	6	2684	2752	2725	2694	2736	32	.646	18.0
tube (2)	7	2707	2773	2747	2718	2757	32	.599	18.1
	8	2700	2763	2740	2724	2746	35	.628	18.0
Zr	1	2067	2114	2108	2099	2100	22	.647	14.6
heater	2	2066	2112	2106	2100	2101	23	.678	15.2
tube (1)	3	2055	2100	2100	2091	2091	18	.733	15.1
	4	2048	2091	2091	2083	2089	17	.772	14.9
	5	2076	2116	2110	2100	2107	18	.652	14.8
Zr	6	2082	2062	2100	2106	2075	-26	.796	14.4
heater	7	2100	2074	2113	2119	2089	-28	.742	14.6
tube (2)	8	2096	2086	2126	2130	2098	-23	.728	14.9

(1) Vapor Pressures of Pure Zr, Ti

Reliable vapor pressure data for zirconium have been measured between 1949 and 2054^{o}K. Reference to these data appear in Stull and Sinke[17].

From these, the temperature dependence of the vapor pressure can be calculated from 1800^{o}K up to the melting point of zirconium (2125^{o}K) through use of the Clapeyron-Clausius relationship.

$$\frac{d \ln P}{dT} = \frac{143,600}{RT^2} \qquad (7)$$

Above 2125°K, the slope of the ln P vs 1/T curve is changed by the heat of melting of the metal. Although no experimental value of the latter is available, it has been estimated to be 4000 cal/mole. From 2125° to 2700°K the following equation was therefore used:

$$\frac{d \ln P}{dT} = \frac{139,600}{RT^2} \tag{8}$$

Similarly, the corresponding expression for the vapor pressure of titanium is:

$$\frac{d \ln P}{dT} = \frac{108,400}{RT^2} \tag{9}$$

up to the melting point (1950°); and at higher temperatues becomes

$$\frac{d \ln P}{dT} = \frac{103,800}{RT^2} \tag{10}$$

(2) Line Width, Structure, Doppler and Pressure Broadening

While the effect of Doppler broadening is easily evaluated, correcting for pressure broadening and hyperfine structure of the line requires independent knowledge of the optical collision cross section and of the line structure. These three effects interact in a complex manner. While the available data are insufficient to compute an oscillator strength from the present absorption measurements, the calculation of the free energy of formation requires only an estimate of how the absorption coefficient varies over a short pressure and temperature interval. As shown here this estimate may be made with sufficient accuracy for our purposes.

In lieu of measurement of the line width, the assumption was made that the line from the hollow cathode source is thin compared to the line contour of the hot gas in the furnace, Appendix B gives evidence, collected during the course of these studies, which supports this assumption.

In order to assess the effect of hyperfine structure, the isotopic compositions of naturally occurring titanium and zirconium must be known. These are given in Table 22.

TABLE 22

Isotopic Composition Of Natural Ti And Zr

Element	Mass No.	Relative Abundance	Nuclear Spin
Ti	46	7.95%	0
	47	7.75	5/2
	48	73.45	0
	49	5.51	7/2
	50	5.34	0
Zr	90	51.46	0
	91	11.23	5/2
	92	17.11	0
	94	17.40	0
	96	2.80	0

TABLE 23

Isotope Splitting, Selected Zirconium Spectral Lines

Line (Å)	Lower State	Upper State	= 91	= 92	= 94	= 96
6143	$^3F_2$	$^3F_2^o$		-8.5	-14.7	
6135	$^3F_3$	$^3F_3^o$		-8.7	-15.4	
6127	$^3F_4$	$^3F_4^o$		-8.8	-16.5	
5935	$^3F_2$	$^3F_3^o$		-11.1	-17.5	
5798	$^3F_3$	$^3D_2^o$	-3.7	-7.3	-14.4	-20.7
5736	$^3F_2$	$^3D_2^o$		-9.5	-16.3	
4688	$^3F_4$	$^3F_5^o$		-11.6	-21.0	
4635	$^3F_3$	$^3G_4^o$		-10.5	-18.5	
4576	$^3F_2$	$^3G_3^o$		-12.2	-16.2	

No information is available on the isotopic splitting or the hyperfine structure of the Ti 3371 Å line. Notice however that almost 75% of the titanium consists of a single isotope having zero nuclear spin, and consequently this line has no spectral hyperfine structure. Since the various isotopes may be assumed to have identical values of oscillator strengths, ignoring the existence of the other isotopes cannot lead to a change in the effective absorption coefficient of more than 25%. The effect on the measured I/I_o is indeed probably considerably less than this, since the splitting may well be smaller than the Doppler and pressure broadened width of the spectral line. Here, however, we are only concerned with the variation in the effective absorption coefficient on changing the temperature by approximately 500°. The probable effect of hyperfine structure will therefore be quite small.

Zirconium also has five normally occurring isotopes. The most abundant has a mass number of 90, zero nuclear spin, and it makes up about half of naturally occurring zirconium. No hyperfine structure data is available for the 3601 Å line, but the magnitude of the isotope splitting of a large number of other lines has been measured, including many having the same lower state. These are listed in Table 23. Notice that all the isotopes except one have zero nuclear spin, and so have no hyperfine structure.

Since the Doppler halfwidth of the zirconium 3601 Å line is about 100 x 10^{-3} cm^{-1} at 2000°K, the hyperfine structure will not appreciably affect the shape of the line.

Ignoring the hyperfine structure in both cases, as was done, appears justified based on the above reasoning.

In order to estimate the effect of pressure broadening, the optical collision cross section for the transitions in question, with respect to collision with argon gas, must be known. They are not known, however, and as a consequence the dependence of I/I_o on pressure was measured directly while the cell temperature was kept constant. Table 24 shows the results of these measurements. No apparent change is seen in I/I_o for titanium on varying the argon pressure from 9 to 36 cm of mercury. An appreciable effect is seen in the case of zirconium, however, as might be expected in view of the greater size and polarizability of zirconium, but even in this case the Doppler broadening is greater than pressure broadening.

TABLE 24

Effect Of Argon Pressure On Absorption Measurements

Compound	Argon Pressure (cm of Hg)	I/I_o	$-\log I/I_o$
TiC	18.5	.555	.256
	18.1	.531	.275
	18.5	.555	.256
	9.3	.549	.260
	9.3	.544	.264
	36.6	.555	.256
	36.5	.563	.250
ZrC	18.8	.482	.317
	9.4	.419	.378
	9.2	.419	.378
	9.3	.402	.396
	37.5	.513	.290
	19.9	.484	.315
	36.5	.562	.280
	36.5	.517	.287
TiC (Avg.)	9.3		.262
	18.5		.262
	36.6		.253
ZrC (Avg.)	9.3		.384
	19.4		.316
	36.8	.286	

The data given in Table 24 are not sufficiently precise to enable one to calculate an optical collision cross section, particularly in view of possible changes in effective path length with inert gas pressure. Since, however, the number of collisions is proportional to both the atom density (and thus to P/T) and to the average velocity (and thus to $T^{1/2}$), comparative values of I/I_o measured at constant $PT^{-1/2}$ will have been obtained under conditions of equal collision rates with inert gas molecules, thus largely eliminating the effect of pressure broadening. Accordingly, the experimental program was so conducted that the absorption over zirconium was compared to that over zirconium carbide, and the absorption over titanium to that over its carbide, under conditions of constant $PT^{-1/2}$.

If, indeed, the hyperfine structure, which is ignored, is truly negligible, and the pressure broadening effects are cancelled by the equal $PT^{1/2}$ provision, then Doppler broadening is the only source of broadening to be considered. In the case of titanium, these conditions are met because both hyperfine structure and pressure broadening are negligible, and the line can thus be assumed to be Doppler shaped. For zirconium, pressure broadening is not negligible, and the line is not Doppler shaped. It can, however, be treated as if it were, since only comparative measurements are involved and the constant $PT^{-1/2}$ provision should cause equivalent broadening effects which then cancel. Doppler broadening, being due to the effects of velocity of the absorber is dependent on temperature, and its effect on absorption can be expressed in terms of changes in the absorption coefficient at the center of the line (k_o). From such an expression as

$$k_o = \left(\frac{\pi M}{2RT}\right)^{1/2} \frac{e^2}{m v_o} Nf \qquad (11a)$$

(where M is the molecular weight of the gaseous absorber atom, R is the gas constant, T is the temperature, e is the charge of an electron, m is the mass of an electron, v_o is the frequency of the center of the absorption line, N is the density of the gaseous absorber species, and f is the oscillator strength of the line), it can can be seen that for constant N, k_o is inversely proportioned to the square root of the temperature. Using the ideal gas law and introducing the appropriate values of various constants, this becomes

$$k_o = 8.512 \times 10^{15} \frac{P'f}{v_o} \frac{M^{1/2}}{T^{3/2}} \qquad (11b)$$

where P' is the partial pressure of the absorber atoms in the lower electronic state of the transition in question.

The absorption of a parallel beam of light of frequency ν_o and intensity I_o, on passing through a homogeneous gas of thickness l, is

$$\ln I/I_o = -k_o l \qquad (11c)$$

where I is the intensity of the emerging beam, provided other than Doppler broadening phenomena are absent.

Now if the value of k_o from 11b is inserted in 11c and all constant terms are combined, the resulting expression

$$T^{3/2} \log I/I_o = A P' \qquad (11d)$$

permits conversion of the measured absorptivities to relative pressure functions, which are to a good degree of approximation independent of inert gas pressure as long as $P_{argon}\, T^{-1/2}$ is held constant. The values of $A P'$, calculated for all the runs listed in Tables 20 and 21 are shown in the following Table 25.

All the $- A P'$ values for the various runs performed on a particular material must now be reduced to a common temperature, so that these relative pressures can be averaged and compared. The integrated form of the Clapeyron-Clausius equation (equations 7 - 10) is used for this calculation:

$$\log \frac{P_1}{P_2} = \frac{\Delta H\,(T_1 - T_2)}{2.303 \times R T_1 T_2} \qquad (12)$$

The values of $\Delta H/2.303\ R$ and of the common reference temperature T_2 for the four vaporization reactions are:

	$\frac{\Delta H}{2.303R}$	T_2
Ti	23,790	1650
TiC	34,480	2220
Zr	31,350	2100
ZrC	41,140	2740

TABLE 25

Atom Partial Pressure Functions From Absorption Measurements

Material	Run No.	T	$-\log I/I_o$	$-AP' \times 10^{-4}$
ZrC	1	2751	.2351	3.39
	2	2748	.2434	3.51
	3	2750	.2426	3.50
	4	2742	.2284	3.82
	5	2728	.1878	2.68
	6	2736	.1904	2.72
	7	2757	.2226	3.22
	8	2746	.2020	2.91
Zr	1	2100	.1891	1.820
	2	2101	.1688	1.626
	3	2091	.1349	1.290
	4	2089	.1124	1.073
	5	2107	.1858	1.797
	6	2075	.0991	.937
	7	2089	.1296	1.238
	8	2098	.1379	1.325
TiC	1	2217	.2708	2.83
	2	2233	.3706	3.91
	3	2221	.3134	3.28
	4	2216	.2933	3.06
	5	2218	.2899	3.03
Ti	1	1654	.4067	2.74
	2	1644	.2668	1.78
	3	1646	.3036	2.03
	4	1644	.2916	1.94
	5	1644	.2950	1.97
	6	1650	.3478	2.33

TABLE 26

Absorber Atom Partial Pressure Functions Reduced To Common Temperatures

Material	Run No.	T_1	$\frac{(T_1 - T_2)\ \Delta H}{T_1 \times T_2 \times 2.303R}$	$-(AP')_{T_2} \times 10^{-4}$
Zrc	1	2751	.060	3.00
	2	2748	.044	3.16
	3	2750	.055	3.07
	4	2742	.011	3.18
	5	2728	-.066	3.11
	6	2736	-.022	2.86
	7	2757	.093	2.60
	8	2746	.033	2.98
Zr	1	2100	-	1.82
	2	2101	.007	1.59
	3	2091	-.064	1.50
	4	2089	-.079	1.29
	5	2107	.050	1.59
	6	2075	-.180	1.41
	7	2089	-.079	1.49
	8	2098	-.014	1.36
TiC	1	2217	-.021	2.97
	2	2233	.090	3.18
	3	2221	.007	3.22
	4	2216	-.028	3.27
	5	2218	-.014	3.12
Ti	1	1654	.035	2.54
	2	1644	-.053	2.01
	3	1646	-.035	2.19
	4	1644	-.053	2.19
	5	1644	-.053	2.23
	6	1650	-	2.33

The heats of vaporization of the carbides are estimated from data in Stull and Sinke [17] and from Krikorian [18].

In view of the shortness of the extrapolation, any uncertainty in the value of ΔH does not lead to errors worth mentioning.

The values of $-AP'$ reduced to these common temperatures are given in Table 26.

These AP' values are then averaged, and the root mean squares and root mean square deviations are given in Table 27.

TABLE 27

Mean And Deviations Of Absorber Atom Partial Pressures

Material	$(-AP')_{Ave} \times 10^{-4}$	T_2	rms dev. ($\times 10^{-4}$)	rms dev. %
Ti	2.25	1650	0.13	5.8
TiC	3.15	2220	0.10	3.2
Zr	1.51	2100	0.15	9.9
ZrC	3.00	2740	0.18	6.0

Finally, AP' must be converted to AP, where P is the total pressure of the metal atom under investigation rather than the partial pressure of atoms in the particular state capable of absorbing the radiation from the source. This is done by evaluating

$$N_1(T) = \frac{(2J_1 + 1)\, e^{-E_1/kT}}{\sum_i (2J_i + 1)\, e^{-E_i/kT}} = \frac{P'}{P} \qquad (13)$$

where the summation over i is the summation over all the states listed in reference 14 for the atomic species, and where the subscript 1 stands for the lowest $^3F_4$ level, which is the lower state of transitions in question. Values of $N_1(T)$ are given for both titanium and for zirconium at the temperatures where measurements were carried out. These appear in Table 28. Now since $P' = N_1 P$, the quantity AP is easily calculated; these values are also tabulated in Table 28.

TABLE 28

Conversion Of Partial Pressure Functions To Total Atom Pressures

Atomic Species	Material	T°K	N_1	$-(AP)_{Ave}$
Ti	Ti	1650	.365	6.16×10^4
Ti	TiC	2220	.372	8.47×10^4
Zr	Zr	2100	.254	5.94×10^4
Zr	ZrC	2740	.255	11.76×10^4

Using the expression for the temperature dependence of the vapor pressure of the appropriate pure metal, it can be shown that the pressure of $Zr_{(g)}$, in equilibrium with ZrC in the presence of excess graphite at 2740°K is equal to the pressure of $Zr_{(g)}$ over pure zirconium at 2144°K. Similarly, the pressure of $Ti_{(g)}$ over $TiC_{(s)} + C_{(s)}$ at 2220°K is equal to the pressure over $Ti_{(s)}$ at 1666°K.

These conclusions are the direct experimental information obtained by these experiments. No thermodynamic data have been used to this point except for the expressions for the temperature dependence of the vapor pressure over the metal. No detectable error could have been introduced by their use because of the shortness of the temperature extrapolations.

Other thermodynamic quantities are calculated in a succeeding section. Since these are obtained by making use of other thermodynamic data available in the literature, they are derived thermodynamic quantities.

d. Borides and Boron Carbide

Utilizing the equipment and techniques described in a, b, and c above, the resonance line absorption studies are now being applied to boron carbide and to refractory borides.

In the case of B_4C and boron metal, the absorption of the 2497.73 Å boron resonance line is being measured photometrically. I/I_o values for this line have been measured over B_4C at approximately 2150°K. The B_4C was obtained both in powdered and tubular form from the Norton Company. This material had an analysis of 76% boron indicating that the material was approximately 97% pure B_4C. Values of I/I_o were determined using (1) a B_4C cell with B_4C end pieces, (2) powdered B_4C contained in a carbon cell with carbon end pieces and intimately mixed with an equal amount of pure graphite and (3) a B_4C cell with carbon end pieces. The resulting I/I_o values obtained in each of these cases were compared and a slight variation in absorption was noted going from one cell to another. However, it is felt that the

more reliable measurements were obtained in the case of the powdered B_4C and graphite mixture contained in the carbon cell, since the presence of the graphite phase insures that the vapor pressure of the boron atoms is at an invariant point. Nevertheless, the presence of excess graphite might alter the composition of the B_4C sufficiently to lower the boron vapor pressure. Therefore, further measurements on B_4C are continuing under different environmental conditions.

In order to determine the thermodynamic properties of B_4C and other borides, it is necessary to measure the absorption of 2497.73 Å boron resonance line over pure boron metal. This has presented somewhat of a problem since the containment of boron at high temperatures is especially difficult. Both B_4C and graphite were tried unsuccessfully as container materials for the pure metal. Here the absorption continually decreased at constant temperature indicating that boron atoms were being removed through reaction with the container. However, boron nitride has been found to be a suitable material for the containment of the hot metal. Initial measurements indicate that reproducible results are obtainable. It must be mentioned, however, that boron nitride is suitable as a container only when the small amount of boric oxide (which is added as a binder) is removed from the BN by heating in hydrogen.

Samples of powdered titanium boride, TiB_2, and zirconium boride, ZrB_2, have been obtained from the Cooper Metallurgical Company and self-bonded tubes of these materials are available from the National Carbon Company. Several of these tubes are on order. In the case of these materials, absorption measurements of both the boron atoms and titanium or zirconium atoms are possible since all three atoms have been or are under investigation.

3. Matrix Isolation Studies

In the preceding Annual Report [1] on this project, the apparatus and method were generally -- and briefly -- described. The apparatus necessary to the study was largely in existence, having been used in other investigations [15].

However, the existing apparatus could be used only to temperatures of about 1500°C. This limitation was due to its design and construction characteristics, namely: 1) the coupling between the effusion cell and the induction coil was weak since the coils were wrapped around the outside of the apparatus and hence were relatively far from the susceptor, and 2) the Dewar surrounding the heated source was made of Pyrex and it was felt that operation of the source at temperatures higher than 1500°C might be dangerous.

In order to overcome these limitations, the new source required that the induction coils be as close to the susceptor as possible and that the Dewar surrounding it be made of quartz.

In order to bring the induction coils closer to the susceptor, the coils could no longer surround the outside of the Dewar but instead must be brought inside the Dewar itself. By so doing, a 3/4" diameter susceptor could be surrounded by a 1 1/4" diameter coil, thus bringing the coils 1/4" away from the susceptor at any point. Under these conditions, the coupling between the 15 k.w. induction heater and the susceptor was sufficiently great to easily heat the susceptor to temperatures approaching 3000°K. Introducing the coils inside the vacuum system creates several severe problems of electrical insulation and vacuum tightness. These problems were overcome by bringing the induction coil leads into the vacuum area coaxially. By grounding the outside conductor, it could be welded directly to the base plate and vacuum tightness and electrical insulation were achieved by a Teflon gasket and "O" ring seals. In order to prevent arcing inside the vacuum system and also to increase the coupling efficiency, a high current, low voltage transformer was added to the output of the induction heater. The Pyrex container in which the source is mounted was replaced by a quartz envelope. This envelope was made to be compatible with the Pyrex pipe (which forms the lower end of the liquid helium Dewar) and the ends were ground flat so that "O" rings could be used to complete the seal between both the Pyrex pipe of the remainder of the Dewar and the brass supporting plate. A detailed drawing of this high temperature vaporization source is shown in Figure 16.

In order to limit unnecessary radiation into the liquid helium cooled cold finger, two molybdenum radiation shields were placed above the susceptor with openings whose diameter allowed molecules from the hot cell to pass but prevented radiation from the rest of the susceptor from reaching the cold finger. These shields were sufficiently far from the r.f. field so that they were not appreciably inductively heated. Without the radiation shields it became impossible to keep the cold window sufficiently cool so as to effect matrix isolation. Initial experiments with this source made use of a tungsten/tungsten-rhenium thermocouple to measure the temperature of the cell. However, it was found that the temperatures measured with this couple became quite erratic and also disagreed as much as 200°C with a corresponding optical pyrometric measurement of the temperature. Therefore, the use of the thermocouple for temperature measurements was abandoned in favor of the optical pyrometer. The sighting window and black body hole for use with the pyrometer are also shown in Figure 16.

With this new source, it has now become possible to heat specimens to temperatures approaching 3000°K. A second Dewar has also been constructed, similar to the one described in reference 15, except that the new source is compatible with it and the infrared frequency range has been extended to 34 microns.

Samples of 3/8" diam. thoria rods of better than 99% purity were obtained from the Norton Company. A sample of rod, approximately 1/8" long, was placed in a tungsten cell lined with iridium sheet. A disc of 2 mil iridium, having a 1/8" opening, served as a lid for the cell. This cell is shown schematically in Figure 17.

A	Molybdenum Shields	F	Tungsten Cell	L	Induction Coil Leads
B	Quartz Envelope	G	Black Body Hole	M	Tungsten Support Rod
C	Quartz Window	H	Alumina Rod	N	Teflon Spacer
D	Induction Coil	J	Quartz Tube	O	Water Jacketed Coaxial Lead
E	Iridium Liner	K	Brass Plate	P	Teflon Plug with "O" Rings

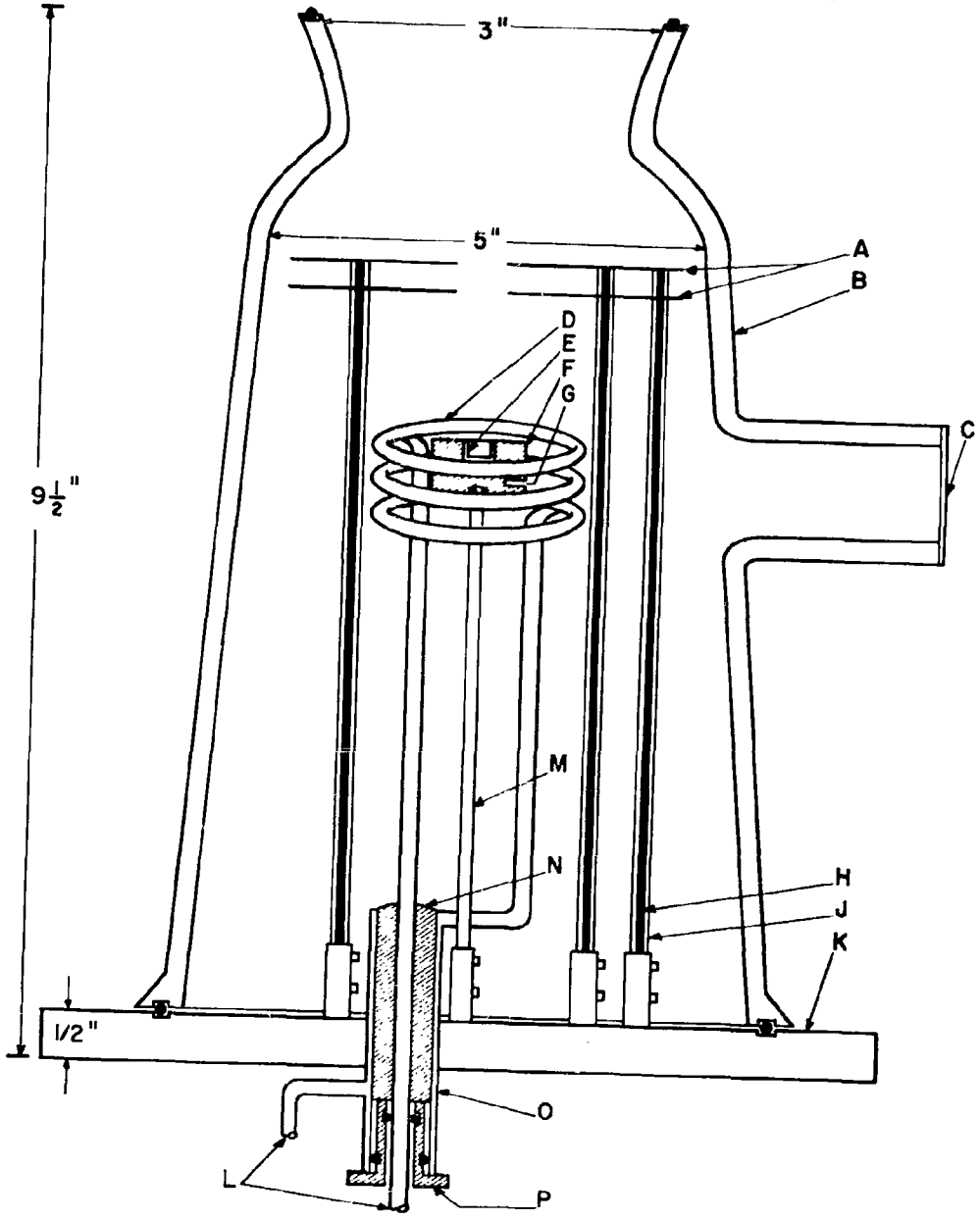

FIGURE 16. HIGH TEMPERATURE SOURCE FOR MATRIX ISOLATION.

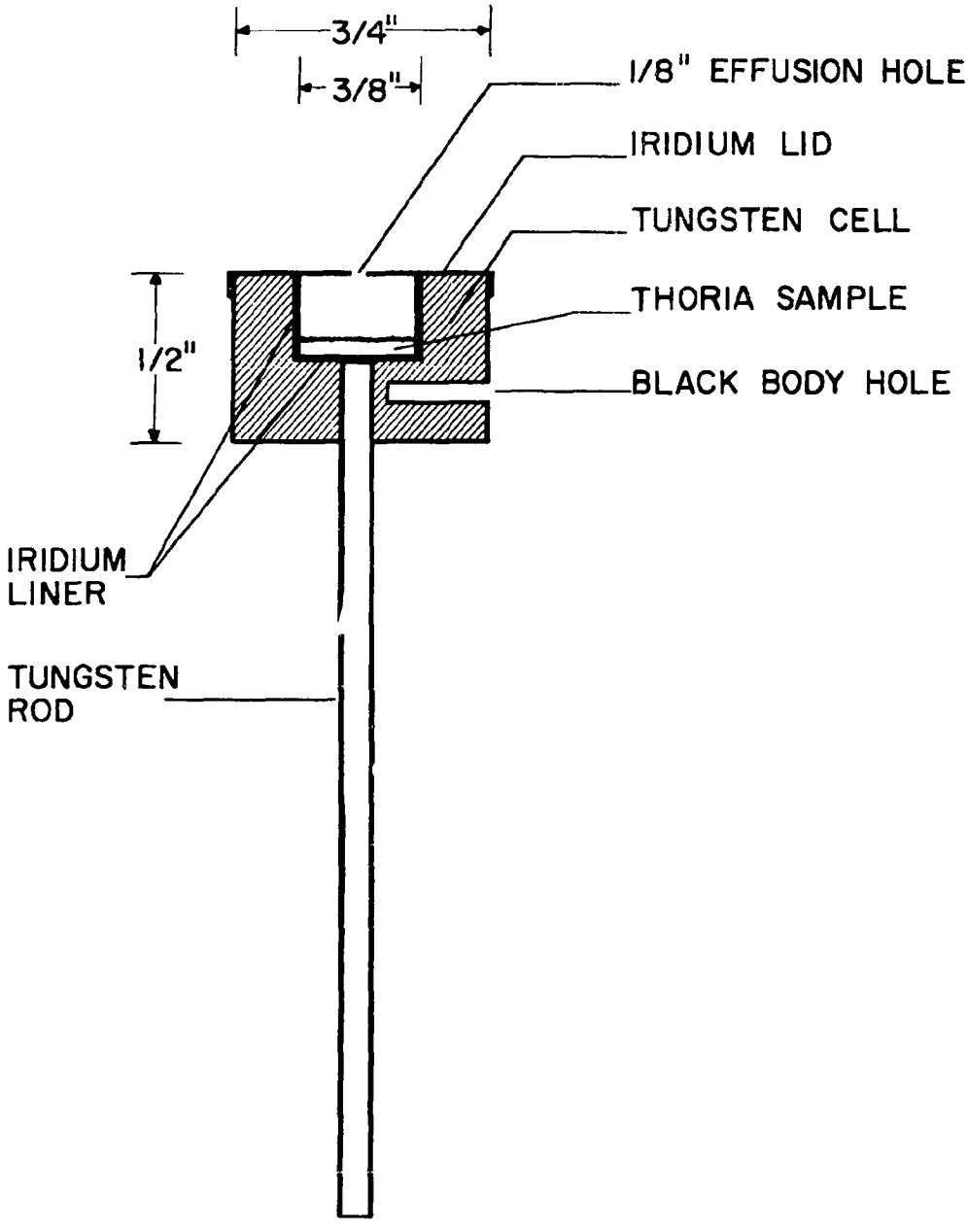

Figure 17. Tungsten Cell With Thoria Sample

The cell was placed in the new high temperature source and carefully aligned with the helium cooled cold window. The cell was heated to 2620°K and matrix isolation of the vaporization products of the thoria sample was attempted for 90 minutes using argon as the matrix material. The spectrum was scanned from 2 μ to 34 μ and two very weak lines were observed around 760 cm^{-1} using the double pass infrared spectrometer. However, these results should be taken as extremely tentative until several more runs can be performed. During the isolation, the new source functioned perfectly and the consumption of liquid helium was comparable to runs with the older apparatus.

A second run on thoria is being set up using a powder sample having an analysis of better than 99.9%. This run will be carried out at approximately 2800°K.

C. Results and Discussion

1. Langmuir Evaporation Studies

a. General Treatment of Vapor Pressure Data

The objectives of the Langmuir measurements are to obtain: a) the rate of weight loss in vacuum, b) the mechanism of vaporization and c) the equilibrium vapor pressures from which basic thermochemical data may be obtained. The rate of weight loss in vacuum is of obvious importance for any application involving prolonged exposure of the material to high temperatures and low pressures. The mechanism of vaporization may also be important since, if incongruent vaporization occurs, then appreciable vaporization could lead to a change in structure of the solid and a resulting change in physical and mechanical properties. Such a change occurs with tungsten carbide as was shown in the previous section.

If rates of weight loss in vacuum and the mechanism of evaporation are known, then, under certain conditions, equilibrium vapor pressures and other basic thermochemical data may be obtained. From such data may be computed the interaction of a material with its enviroment.

We will consider the equilibrium

$$MC_{(s)} \rightleftharpoons M_{(g)} + C_{1(g)} \qquad (14)$$

where MC represents any solid metal carbide and M and C are monatomic vapors of the metal and carbon respectively. If the rates of weight loss of the metal and carbon in vacuum are known then the equilibrium vapor pressure of each may be computed from the usual Langmuir equation.

$$P = \frac{m}{\alpha}\sqrt{\frac{2\pi RT}{M}} \qquad (15)$$

where P is the equilibrium vapor pressure, m the corresponding rate of weight loss, α the evaporation coefficient, R the gas constant, T the absolute temperature and M the atomic weight of the vapor. The standard free energy change, ΔF^{o}_{T}, of reaction (14) may then be computed from the thermodynamic relation

$$\Delta F^{o}_{T} = -RT \ln K_p \tag{16}$$

where $K_p = (P_{M_{vap}})\ (P_{C_1})$ is the equilibrium constant.

Equation (16) may be conveniently expressed in terms of free energy functions thus,

$$\left(\frac{F^{o}_{T} - H^{o}_{298}}{T}\right)_{M_{(g)}} + \left(\frac{F^{o}_{T} - H^{o}_{298}}{T}\right)_{C_{1(g)}} - \left(\frac{F^{o}_{T} - H^{o}_{298}}{T}\right)_{MC_{(s)}} + \frac{\Delta H^{o}_{298}}{T} = -R \ln K_p \tag{17}$$

where H^{o}_{298} is the standard enthalpy of the substance at 298.15°K and ΔH^{o}_{298} is the standard enthalpy change of reaction (14). That is

$$\Delta H^{o}_{298} = (\Delta H^{o}_{f})_{C_{1(g)}} + (\Delta H^{o}_{f})_{M_{(g)}} - (\Delta H^{o}_{f})_{MC_{(s)}} \tag{18}$$

where ΔH^{o}_{f} is the heat of formation of the substance at 298.15°K. The usual method of treating vapor pressure would be to use eq. (17) to calculate ΔH^{o}_{298} for each measured vapor pressure and $(\Delta H^{o}_{f})_{MC}$ from eq. (18). This is the so called "third law" method, which is applicable where thermochemical data other than $(\Delta H^{o}_{f})_{MC}$ for all species, both solid and vapor, are available.

However, such is generally not the case for the metal carbides considered here. For these substances, only incomplete or inaccurate data are available except in the case of titanium carbide. It is therefore convenient to expand the free energy function of the metal carbide in terms of specific heat and entropy. Thus, eq. (17) may be written,

$$\left(\frac{F^{o}_{T} - H^{o}_{298}}{T}\right)_{M_{(g)}} + \left(\frac{F^{o}_{T} - H^{o}_{298}}{T}\right)_{C_{1(g)}} - \left(\frac{1}{T}\int_{298}^{T} C_p dT - \int_{298}^{T} \frac{C_p}{T} dT\right)_{MC_{(s)}} +$$

$$\left(S^{o}_{298}\right)_{MC_{(s)}} + \frac{\Delta H^{o}_{298}}{T} = -R \ln K_p \tag{19}$$

where C_p is the specific heat at constant pressure of the metal carbide, and S^{o}_{298} the standard entropy at 298.15°K. This equation along with eq. 18 shows the relation between the various thermodynamic

quantities of all species involved in reaction (14). Where sufficient information is available to reduce eq. (19) to one unknown and K_p, then each measured K_p point may be used to independently calculate the unknown. If two unknowns are present, for example $(S^o_{298})_{MC(s)}$ and ΔH^o_{298}, and if measurements of K_p are available over a sufficiently large temperature range, then the "second law" method may be applied. With this method, eq. (19) is plotted as a linear equation and the two unknowns calculated from the slope and intercept values.

b. Zirconium Carbide Evaporation

In a previous section discussing the rate of weight loss measurements on zirconium carbide, it was concluded that this material of stoichiometric carbon content vaporizes congruently. For the purpose of calculating vapor pressure, it is assumed that congruent vaporization applies to each weight loss measurement. It might appear that congruent evaporation indicates that the molecule ZrC is of importance in the vapor phase. However, there is no evidence for the existence of such a molecule. In fact, it is believed that none of the slowly volatile metallic carbides can exist undissociated in the gaseous state (16). Thus, it is assumed that ZrC vaporizes only by decomposition to the elements. The excellent agreement with the resonance line absorption results, to be shown later, strongly supports this assumption.

It is further assumed, at this point, that the vapor is composed of monatomic elements only. Thus, the vaporization process is taken to be as in eq. (14),

$$ZrC_{(s)} \rightleftarrows Zr_{(g)} + C_{1(g)} \qquad (20)$$

With the evaporation coefficient taken as unity, eq. (15) may be written in logarithmic form thus,

$$\log P = -1.6467 - \log m + 1\ 2 \log T - 1/2 \log M \qquad (21)$$

where P is the vapor pressure in atmospheres and m is the rate of weight loss in gm per cm^2 per sec. To calculate the vapor pressure of carbon, $M_c = 12.01$ and $m_c = .1163\ m$ (where m is the total weight loss rate from Table 12) are substituted in eq. 21 to obtain

$$\log P_c = -3.1209 + \log m + \log T \qquad (22)$$

and since $m_{Zr} = m - .1163$ and $M_{Zr} = 91.22$, the expression for the vapor pressure of zirconium is

$$\log P_{Zr} = 0.4405 + \log P_c \qquad (23)$$

The values of $\log P_c$ and $\log P_{Zr}$ thus calculated along with $\log K_p = \log P_c - \log P_{Zr}$ are tabulated in Table 29.

TABLE 29

Vapor Pressure Over ZrC

Run #	T (°K)	-log P_c	-log P_{zr}	-log K_p
Z-E-21	2246	9.876	9.436	19.312
Z-E-17	2254	9.755	9.315	19.070
Z-D-18	2287	9.517	9.077	18.594
Z-E-19	2310	9.446	9.006	18.452
Z-D-19	2316	9.365	8.925	18.290
Z-E-20	2351	9.181	8.741	17.922
Z-D-17	2354	9.095	8.655	17.750
Z-E-6	2384	8.823	8.383	17.206
Z-D-11	2404	8.854	8.414	17.268
Z-E-7	2439	8.523	8.083	16.606
Z-D-10	2470	8.396	7.956	16.352
Z-D-7	2492	8.211	7.771	15.982
Z-E-12	2553	7.814	7.374	15.188
Z-E-10	2559	7.834	7.394	15.228
Z-D-6	2592	7.611	7.171	14.782
Z-E-14	2593	7.727	7.287	15.014
Z-D-1	2615	7.449	7.009	14.458
Z-E-5	2623	7.442	7.002	14.444
Z-E-11	2624	7.383	6.943	14.326
Z-D-4	2625	7.388	6.948	14.336
Z-E-9	2630	7.415	6.975	14.390
Z-D-12	2674	7.273	6.833	14.106
Z-D-5	2685	7.062	6.622	13.684
Z-E-13	2697	6.970	6.530	13.500
Z-D-3	2716	6.835	6.395	13.230
Z-D-2	2726	6.840	6.400	13.240
Z-E-15	2765	6.733	6.293	13.026
Z-D-13	2794	6.632	6.192	12.824
Z-D-8	2798	6.406	5.966	12.372
Z-D-9	2818	6.296	5.856	12.152
Z-D-14	2898	5.987	5.547	11.534

A linear fit of the data by the method of least squares gives

$$\log P_c = 7.288 - \frac{3.8586 \times 10^4}{T} \quad (24)$$

$$\log P_{Zr} = 7.728 - \frac{3.8586 \times 10^4}{T} \quad (25)$$

$$\log K_p = 15.016 - \frac{7.7173 \times 10^4}{T} \quad (26)$$

and $\Delta F_T^\circ = -RT \ln K_p = 35.313 \times 10^4 - 68.710\ T$ (27)

where ΔF_T° is the standard free energy change for reaction 20.

It can now be shown that the equilibrium pressure of polyatomic carbon species in equilibrium with the measured monatomic carbon (eq. 24) is negligibly small. The equilibrium constants for the two reactions:

$$2C_{(g)} \rightleftharpoons C_2\ (g) \qquad K_2 = \frac{P_{C_2}}{P_C^2} \quad (28)$$

and

$$3C_{(g)} \rightleftharpoons C_3\ (g) \qquad K_3 = \frac{P_{C_3}}{P_C^3} \quad (29)$$

can be calculated from the mass spectrometric measurements[13] of the equilibrium vapor pressures of C_2 and C_3 on graphite. The results of these calculations are given in Table 30 at 2000°K, 2500°K and 3000°K. As can be seen from this table, the ratio of the pressures of monatomic carbon to diatomic carbon is 36.8 at 3000°K and is greater at all lower temperatures. The ratio of monatomic to triatomic carbon is 154 at 3000°K and greater at all lower temperatures. If one performs the same calculation for C_4 and C_5, it is found that the ratio of monatomic carbon pressure to C_4 or C_5 is greater than 10^5 at all temperatures below 3000°K. On the basis of these calculations, all polyatomic carbon species have been neglected.

TABLE 30

Ratios of C_1 to C_2 and C_3 in Carbon Vapor at Equilibrium

T (°K)	log K_2	log $\frac{Pc}{Pc_2}$	$\frac{Pc}{Pc_2}$	log K_3	log $\frac{Pc}{Pc_3}$	$\frac{Pc}{Pc_3}$
2000	9.295	2.712	515.0	20.866	3.148	1406
2500	6.135	2.013	103.0	13.736	2.560	363
3000	4.009	1.566	36.8	8.963	2.187	154

The expression for ΔF_T° (eq. 27) yields a value of 164.7 kcal per mole at 2740°K. If this is combined with the free energy of formation of monatomic carbon and of zirconium vapor [17] the value for the free energy of formation of ZrC at this temperature may be obtained. The value thus calculated is $\Delta F_{f2740}^\circ = -39.2$ kcal per mole. This may be compared with -38.8 + 1 kcal per mole obtained by the resonance line absorption technique and -38.9 + 1.5 kcal per mole obtained by Pollock [4] in the same temperature range. These values were all computed using the same thermal data for the elements. The agreement between the three completely independent sets of measurements is quite remarkable. The excellent agreement between the value obtained by the Langmuir method and by the resonance line absorption technique is strong evidence that the assumptions made in the Langmuir calculations are correct, that is, that the evaporation coefficients for both C_1 and Zr on ZrC are unity and that only Zr and C_1 exist in the vapor. These same conclusions were reached by Pollock by a comparison of Langmuir measurements with Knudsen measurements.

Due to the methods of calculation it may be shown that the agreement between the free energy of formation calculated from resonance line absorption measurements and that calculated from the Langmuir measurements is good evidence that the heat of vaporization of elemental zirconium (146 kcal per mole at 298.15°K) is substantially correct.

The vapor pressure of ZrC may be considered to be firmly established from the agreement between the three independent sets of measurements described above. Two measurements of the standard heat of formation at 298.15°K have been reported, both values having been obtained by combustion calorimetry. Krikorian [18] gives a value -44.4 $\pm$ 1.1 kcal per mole in agreement with -44.1 $\pm$ 1.5 kcal per mole reported by Mah and Boyle [19], although the later authors note that "the purity of the substance leaves much to be desired". Krikorian [18] has also estimated the specific heat of ZrC at high temperatures. Some recent measurements [20] are in essential agreement with this estimate. Combining the estimated specific heat values and the measured heat of formation of ZrC with the thermal properties of the elements and the vapor pressure data (eq. 18 and 19) one finds a value of 9.2 cal per mol per °K for the entropy of ZrC at 298.15°K. This is in good agreement with several estimates which have been made: 8.5 $\pm$ 1.5 [21] and 9.0 [22] cal per mole per °K.

c. Hafnium Carbide Evaporation

It has been shown that the vaporization of hafnium carbide of stoichiometric carbon content is congruent. As in the case of ZrC it is assumed that HfC vaporizes only to monatomic elements and that the evaporation coefficients are unity. The vaporization process is, then

$$HfC_{(s)} \rightleftarrows Hf_{(g)} + C_{1(g)} \qquad (30)$$

Substituting $M_C = 12.01$ and $m_c = .063$ m into eq. 21 one finds the expression for the vapor pressure of monatomic carbon,

$$\log P_c = -3.3872 + \log m + \tfrac{1}{2} \log T \qquad (31)$$

where m is the total rate of weight loss on HfC given in Table 14. Since $m_{Hf} = m - .063$ m and $M_{Hf} = 178.6$, the expression for the vapor pressure of hafnium is

$$\log P_{Hf} = \log P_c + 0.5863 \qquad (32)$$

The values of log Pc and log P_{Hf} thus calculated along with log K_p = log P_c + log P_{Hf} are given in Table 31. It may be shown by a calculation analogous to that performed for ZrC, that the equilibrium pressure of any carbon polymer is less than 1% of the total carbon pressure over the entire temperature range investigated here so that these species are neglected in the calculations.

In order to proceed further it is necessary to have additional thermodynamic data. Such data for hafnium and its compounds are extremely sparse. Recently, however, some enthalpy data for HfC to high temperatures have been reported [20]. In order to verify these measurements and to extend them to room temperature, enthalpy measurements on HfC to 1367°K have been made here. The same material used for the rate of weight loss determinations was employed. A commercial (Parr Instrument Co.) adiabatic calorimeter, modified to accept a drop tube, was used for the measurements. The sample was heated in a resistively heated tube furnace mounted above the calorimeter and temperature measured with a Pt-Pt Rh thermocouple. The sample was encapsulated in Hastelloy R-235.

The results of these measurements are given in Table 32. From the chemical analysis of the HfC used, the enthalpy measurements were corrected for impurities. This correction amounted to about 3.5% in the enthalpy. The analysis of the material used to obtain the data of Ref. 20 was not given. It was quite arbitrarily assumed to have the same chemical composition as the material used here. The reported enthalpy was hence reduced by 3.5%. These corrected values are also given in Table 32.

All data were then fit to the usual high temperature enthalpy expression containing four constants. Additional stipulations were imposed, namely, that the specific heat is 7.25 cal per gm atom at the melting point (4160°K) and that $H_T - H_{298} = 0$ at 298.15°K. The resulting expressions for the enthalpy and specific heat are

$$H_T - H_{298} = 12.70\ T + 2.20 \times 10^{-4} T^2 + 5.4 \times 10^5 T^{-1} - 5616 \text{ cal/mole} \qquad (33)$$

and

$$C_p = 12.70 + 4.40 \times 10^{-4} T - 5.4 \times 10^5 T^{-2} \text{ cal/mole } ^\circ K \qquad (34)$$

TABLE 31

Vapor Pressure of HfC

Run #	T(^{o}K)	-log P_c	-log P_{Hf}	-log K_p	$-\left(\frac{F^{o}_{T} - H^{o}_{298}}{T}\right)_{HfC}$	ΔH^{o}_{298} (kcal/mole)
H-A-7	2313	10.22	9.64	19.86	23.95	374.3
H-D-8	2365	9.93	9.35	19.28	24.19	376.4
H-D-9	2369	9.78	9.20	18.98	24.21	373.8
H-D-10	2372	9.67	9.08	18.75	24.23	371.8
H-A-5	2386	9.55	8.97	18.52	24.29	371.4
H-A-6	2404	9.61	9.03	18.64	24.38	375.5
H-D-1	2427	9.39	8.80	18.19	24.48	376.1
H-D-7	2446	9.28	8.69	17.97	24.56	374.5
H-A-4	2451	9.35	8.77	18.12	24.59	377.0
H-D-5	2463	9.16	8.57	17.73	24.64	374.4
H-A-13	2496	8.96	8.38	17.34	24.79	374.9
H-D-3	2529	8.83	8.24	17.07	24.90	375.4
H-D-11	2523	8.78	8.20	16.98	24.91	374.8
H-A-3	2535	8.78	8.20	16.98	24.96	376.6
H-B-3	2569	8.55	7.96	16.51	25.11	376.1
H-B-9	2634	8.20	7.61	15.81	25.39	377.1
H-B-1	2650	8.12	7.53	15.65	25.46	377.4
H-A-1	2720	7.73	7.15	14.88	25.75	377.8
H-A-8	2724	7.66	7.07	14.73	25.77	376.4
H-A-2	2824	7.16	6.57	13.73	26.18	377.3
H-B-2	2867	6.96	6.38	13.34	26.35	377.8
H-B-8	2881	6.89	6.31	13.20	26.41	377.8
H-B-4	2933	6.69	6.10	12.79	26.61	379.1
H-B-5	2942	6.60	6.01	12.61	26.65	377.8
H-A-9	2961	6.51	5.93	12.44	26.72	377.9
H-B-6	3003	6.40	5.81	12.21	26.88	380.0
H-A-10	3044	6.09	5.50	11.59	27.04	376.5
H-B-7	3085	5.88	5.29	11.17	27.19	375.6
H-A-11	3145	5.70	5.11	10.81	27.42	376.5
						Avg. 375.9 $\pm$ 1.9

TABLE 32

Enthalpy of HfC

This Work		Data from Ref 20 (corrected)	
T(°K)	(cal/mole) $H_T - H_{298}$	T(°K)	(cal/mole) $H_T - H_{298}$
440	1014	540	2200
518	2217	826	6130
554	2503	1089	8300
582	3269	1362	12410
627	3463	1625	16400
644	3530	1955	20580
678	3720	2216	24060
738	4630	2505	27730
784	5250	2722	32540
840	5840	3016	32430
888	6380		
896	6320		
947	7270		
992	7680		
1038	8230		
1085	8830		
1143	9760		
1187	10150		
1239	10860		
1246	11020		
1328	11800		
1367	12840		

The enthalpy values from Table 32 and the enthalpy expression (eq. 33) are shown in Fig. 18. Eq. (33) yields a value for the enthalpy about 8% higher than the estimate of Kelley [23] at 1000°K and about 3% higher at 2000°K.

The specific heat thus determined (eq. 34) has been combined with the entropy at 298°K estimated by Kelley [23], S^{o}_{298} = 10.91 cal per mole °K, to give the free energy function at the various temperatures. These values are given in column six of Table 31. The heat of reaction (30), ΔH^{o}_{298}, at 298°K has been calculated using eq. (17) and the free energy functions for the elements taken from Ref. 17. ΔH^{o}_{298} thus obtained is given in column 7 of Table 31. The average value is ΔH^{o}_{298} = 375.9 ± 1.9 kcal per mole. This may be compared with the value calculated from the heats for formation of HfC, C_1 and Hf vapor according to eq (18). Using $(\Delta H^{o}_{f})_{C_1}$ = 170.9 [17], $(\Delta H^{o}_{f})_{Hf_{(g)}}$ = 168.0 [17] and $(\Delta H^{o}_{f})_{HfC_{(s)}}$ = -44.7 [23] one obtains ΔH^{o}_{298} = 383.6 kcal per mole which is 7.7 kcal per mole higher than that obtained from the vapor pressure measurements.

If one uses a "second law" treatment of the vapor pressure data as described previously using eq. 19, one obtains the values ΔH^{o}_{298} = 361.3 kcal per mole and S^{o}_{298} = 16.5 cal per mole °K. Thus ΔH^{o}_{298} obtained in this manner is 22.3 kcal lower than that calculated from the various heats of formation. The conclusion reached is that the vapor pressure measurements are not consistent with the best estimates of other related thermal data. In looking for the source of this discrepancy, it should be pointed out that the entropy and heat of formation of HfC and the heat of formation of Hf vapor are all estimated values.

It is difficult to assign meaningful tolerances to any of the reported estimates. For what it is worth, a considered opinion here is that the estimated heat of formation of hafnium vapor is too high by roughly ten kcal per mole. It should be obvious at this point that much more experimental work is needed to firmly establish the thermodynamic data for hafnium and its compounds. An accurate measurement of the heat of formation of hafnium vapor and the entropy of hafnium carbide would be especially useful.

d. Titanium Carbide

In a previous section it was concluded that titanium carbide of near stoichiometric carbon content vaporizes congruently. However, the possibility was not excluded that, at the lower temperature, the rate of evaporation of carbon was less than that corresponding to congruent evaporation. A mass spectrometric investigation [24] of the vapor from a graphite cell containing titanium showed the absence of any appreciable TiC vapor.

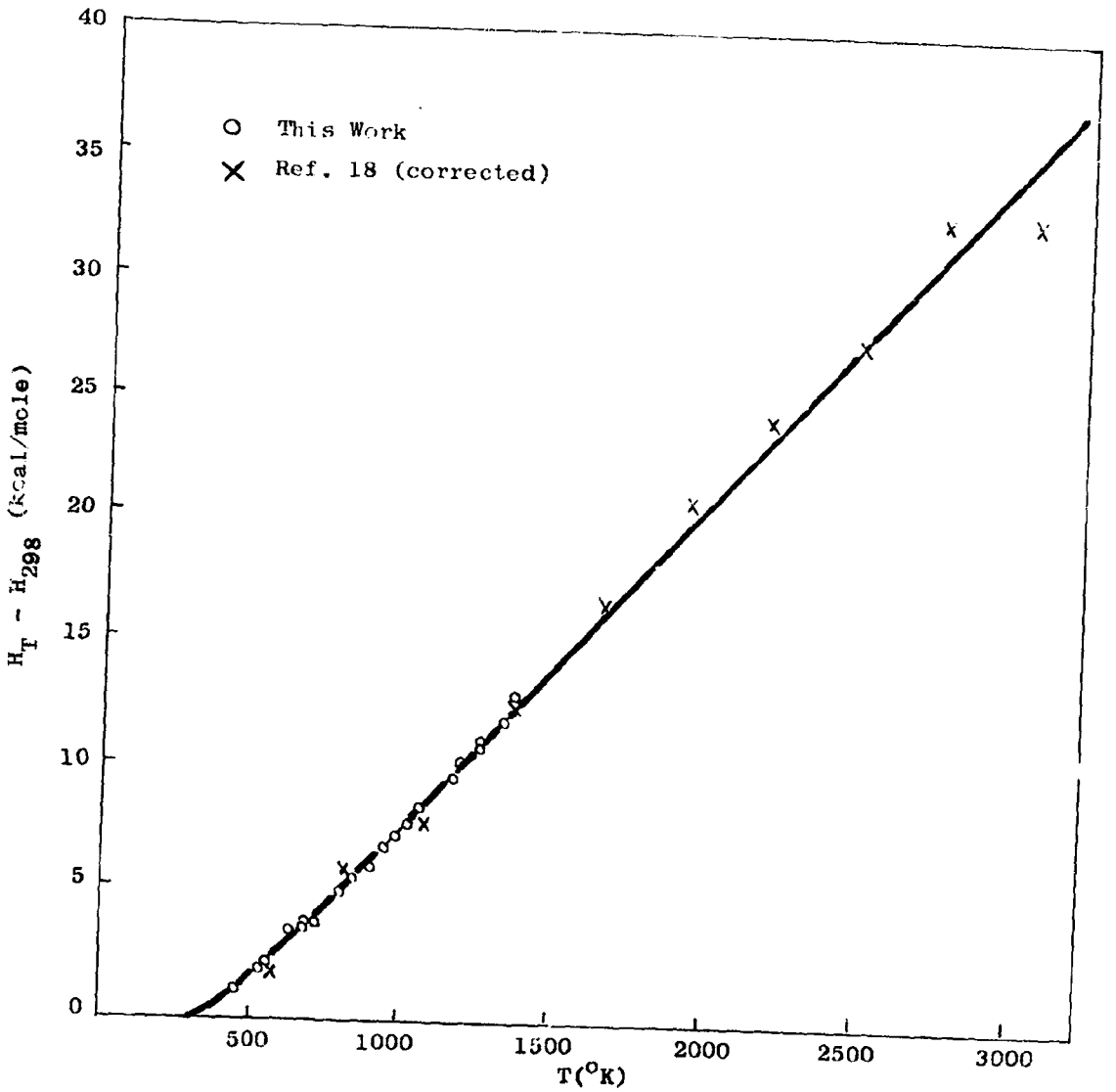

Figure 18 Enthalpy of Hafnium Carbide

The rate of evaporation of carbon from TiC is so high that, in a true equilibrium system, appreciable polyatomic carbon species would be present. For the purposes of calculating vapor pressures we assume, however, that all polyatomic carbon species have evaporation coefficients so low that the weight loss of such species from the TiC surface is completely negligible. Some justification for this assumption is the fact that the condensation coefficient (and presumably also the evaporation coefficient) is usually small for instances where the vapor species are structurally difficult to fit into the surface geometry of the condensed phase, as should be the case for polyatomic carbon species on TiC.

Thus it is assumed that the vaporization of TiC is congruent and that the species evaporating are monatomic elements only with evaporation coefficients unity. We consider the equilibrium

$$TiC_{(s)} \rightleftarrows Ti_{(g)} + C_{1(g)} \tag{35}$$

so that, making appropriate substitutions in eq. 21 we obtain

$$\log P_c = -2.884 + \log m + \tfrac{1}{2} \log T \tag{36}$$

$$\text{and } \log P_{Ti} = -2.584 + \log m + \tfrac{1}{2} \log T \tag{37}$$

The values thus calculated along with $\log K_p$, where $K_p = P_{Ti}P_c$, are given in Table 33. The standard enthalpy change of reaction (35), ΔH^o_{298}, calculated from equation (17) using free energy functions from Ref. 12 is given in the sixth column of Table 33. The average value thus obtained is 326.2 $\pm$ 1.2 kcal per mole. Using $(\Delta H^o_f)_{Ti(g)}$ = 112.5 kcal per mole [12] and $(\Delta H^o_f)_{C_{1(g)}}$ = 170.9 kcal per mole [12] one obtains $(\Delta H^o_f)_{TiC_{(s)}}$ = -42.8 $\pm$ 1.2 kcal per mole. This agrees very favorably with the value -43.8 $\pm$ 2.0 kcal per mole [12] obtained from heat of combustion measurements and -42.7 $\pm$ 0.5 kcal per mole obtained from resonance line absorption studies. This is in complete disagreement with the value, -31.3, recently obtained [25] by Knudsen effusion measurements.

It may be noted from Table 33 that the calculated value for ΔH^o_{298} has a slight trend toward higher values with increasing temperature. Such a trend is sometimes indicative of a non unit evaporation coefficient. However, in this case it may also be due to the fact that the vaporization process may not be exactly congruent at the lower temperatures.

One could treat the data presented here under assumptions other than those chosen, which are, it is admitted, not completely justified. Other reasonable assumptions would, in general, make the computed heat of formation of TiC more negative. For example, the data have also been treated on the assumption of congruent vaporization and equilibration of polyatomic carbon species. The details of this calculation are not

presented here. It is sufficient to note that the average value obtained for the heat of formation of TiC under such assumptions is -48.3 kcal per mole.

TABLE 33

Vapor Pressure of TiC

Run #	T(°K)	-log P_c	-log P_{Ti}	-log K_p	ΔH^o_{298} (kcal/mole)
Ti-B-5	2110	8.84	8.54	17.38	324.4
Ti-B-4	2173	8.39	8.09	16.48	325.1
Ti-A-2	2251	7.87	7.57	15.44	325.9
Ti-B-3	2274	7.68	7.38	15.06	325.1
Ti-A-3	2279	7.68	7.38	15.06	326.0
Ti-B-6	2288	7.75	7.45	15 20	328.6
Ti-B-2	2401	6.89	6.59	13.48	325.8
Ti-A-4	2452	6.64	6.34	12.98	326.9
Ti-A-5	2507	6.34	6.04	12.38	327.2
Ti-A-6	2542	6.12	5.82	11.94	326.9
					avg. 326.2 $\pm$ 1.2 kcal/mole

e. Tungsten Carbide Evaporation

It has been shown in a previous section that the evaporation of mono-tungsten carbide, WC, proceeds in a vacuum according to the reaction

$$2\ WC_{(s)} \rightarrow W_2C_{(s)} + C_{(g)} \qquad (38)$$

and that the annular core of WC in the ring shaped specimens used here diminishes in size as evaporation of carbon proceeds. However, the apparent vapor presssure of carbon one might calculate from the rate of weight loss measurements could not be the true equilibrium pressure of equation (38) since the rate of weight loss at constant temperature decreases with decreasing total carbon content or increasing thickness of the surface W_2C as shown in Fig. 13. Such behavior is entirely inconsistent with the concept of equilibrium and is thought to be due to the rate of evaporation of carbon from the surface being at least partially dependent on the rate of diffusion of carbon through the W_2C.

An additional complicating factor is that, since the rate of weight loss of carbon is so high, as in the case of TiC, the equilibrium pressure of polyatomic carbon species is quite appreciable. From a comparison of the rate of weight loss of carbon on tungsten carbide with the rate of weight loss of carbon on graphite as shown in Fig. 13, it is clear that, if one assumes that only monatomic carbon evaporates from the tungsten carbide, the calculated vapor pressure would be about equal to the equilibrium pressure of monatomic carbon over graphite. If on the other hand, one assumes the equilibration of all carbon species in the vapor pressure calculations, the result would be that the calculated pressure of any carbon species would be less than the equilibrium pressure over graphite.

There seems to be little use in carrying the calculations further. The heat of formation of WC has been measured by combustion calorimetry with the result [26] $\Delta H^{o}_{f} = -8.4 \pm 0.2$ kcal per mole. The heat formation of W_2C has been estimated [18] to be $\Delta H^{o}_{f} = -11 \pm 4$ kcal per mole. The results of the Langmuir experiments here lend general confirmation to these results in that it is concluded from the relatively high weight loss of carbon, that the tungsten carbides have rather low thermodynamic stability in comparison to the other carbides investigated.

2. Resonance Line Absorption Studies

a. Calculation of Derived Thermodynamic Quantities

The data directly obtained and appropriately reduced from resonance line absorption studies have been summarized (IIIB above) in these statements:

1) The vapor pressure of zirconium atoms over zirconium carbide at 2740°K is equal to the vapor pressure of zirconium atoms over pure zirconium at 2144°K.

2) The vapor pressure of titanium atoms over titanium carbide at 2220°K is equal to the vapor pressure of titanium atoms over pure titanium at 1666°K.

Since the vapor pressures of the pure metals are known (reference 17) and can be expressed as

$$\log P_{Zr/Zr,\ 2144^{o}K} = -7.660$$

and $$\log P_{Ti/Ti\ \ 1666^{o}\ K} = -7.296\ .$$

the following values are thus obtained:

$$\log P_{Zr/ZrC,\ 2740^{o}K} = -7.660$$

$$\log P_{Ti/TiC,\ 2220^{o}K} = -7.296$$

In order to derive the desired thermodynamic quantities, let us consider the reaction

$$MC_{(s)} \rightleftarrows M_{(g)} + C_{(s)} \qquad (39)$$

The standard molar free energy change at any temperature may be calculated from

$$\Delta F^{o}_{T} = - R\ T\ \ln\ P_{M/MC} \qquad (40)$$

where $P_{M/MC}$ is the equilibrium pressure of the appropriate metal atom over its carbide plus graphite. Since these pressures were those experimentally determined for ZrC and TiC, the standard molar free energy change may be evaluated. Thus, for

$$ZrC_{(s)} \rightleftarrows Zr_{(g)} + C_{(s)}$$

$$\Delta F^{o}_{2740} = 96060 \text{ cal/mole}$$

and $$TiC_{(s)} \rightleftarrows Ti_{(g)} + C_{(s)}$$

$$\Delta F^{o}_{2220} = 74130 \text{ cal/mole}$$

The standard molar free energy of formation of the carbides in question is, by definition, the free energy change of the reaction

$$M(s) + C(s) \rightleftarrows MC(s) \qquad (41)$$

where M(s) is the standard state, either liquid or solid, depending on the temperature.

This reaction may be considered to be the result of subtracting reaction (39) from (42).

$$M(s) \rightleftarrows M(g) \qquad (42)$$

$$MC\ (s) \rightleftarrows M(g) + C(s) \qquad (39)$$

Values of ΔF^{o}_{T} for reaction (39) have just been obtained above, while those for reaction (42) are given in reference 17.

$$\Delta F^{o}_{2220}\ (Ti)\ (\ell) = 38{,}660 \text{ cal/mole}$$

$$\Delta F^{o}_{2740}\ (Zr)\ (\ell) = 57{,}300 \text{ cal/mole}$$

Then

$$\Delta F^{o}_{f_{2220}} \text{ (TiC)} = -35.470 \text{ kcal/mole}$$

$$\Delta F^{o}_{f_{2740}} \text{ (ZrC)} = -38.760 \text{ kcal/mole}$$

These free energy values depend on the magnitude of the heat of melting of the pure metal, and on the heat capacity of the liquid at temperatures as much as 600° above the melting point. No reliable experimental data are available for these quantities, so that the value of $\Delta F^{o}_{T}(M)$ in reference 17 is based in part on their estimated value in both metals. While no reliable quantitative estimate can be made of the resulting error, our opinion is that it is smaller than the uncertainty due to experimental errors.

It is interesting to compare literature values of the above quantities with the free energy of formation of TiC given above. In this case sufficient data are available for a complete comparison of the compatibility. The heat of formation at 0°K of TiC is given by

$$\Delta H^{o}_{f_0} = \Delta F^{o}_{f_{2220}} \text{ (TiC)} + (F^{o}_{2200} - H^{o}_{0})_{Ti(s)} + (F^{o}_{2200} - H^{o}_{0})_{C(s)} - (F^{o}_{2200} - H^{o}_{0})_{TiC}$$

The following values of the various quantities may be substituted:

	Kcal/mole	Reference
$(\Delta F^{o}_{f_{2220}})_{TiC_{(s)}}$	-35.470	this report
$(F^{o}_{2220} - H^{o}_{0})_{Ti(s),\ (\ell)}$	-33.920	6
$(F^{o}_{2220} - H^{o}_{0})_{C(s)}$	-12.970	6
$(F^{o}_{2220} - H^{o}_{0})_{TiC(s)}$	-39.930	6

when this is done it is found that for $TiC_{(s)}$

$$\Delta H^{o}_{f_0} = -42.430 \text{ kcal/mole}$$

$$\Delta H^{o}_{f_{298}} = -42.730 \text{ kcal/mole}$$

which is in good agreement with the most reliable value available [27].

$$\Delta H^{\circ}_{f_{298}} = -43.8 \pm 2.0 \text{ kcal/mole}$$

This agreement is further evidence that TiC does not tend to dissolve appreciable excess carbon even at 2220°K.

A completely analogous computation could be carried out for ZrC; however, sufficient thermodynamic data are lacking in order to do this. An approximation has been made for the heat capacity of ZrC from 298° to 1700°K by Krikorian [8] as follows:

$$Cp = 11.06 + 1.52 \times 10^{-3}T - \frac{2.43 \times 10^{5}}{T^{2}}$$

From this expression and the enthalpy and entropy values for Zr(s) and C(s) given in reference 17, the change in the entropy and enthalpy of formation from 298° to 1700° can be calculated. For lack of further information at temperatures above 1700°K, the assumption is made that ΔH°_{f} and ΔS°_{f} are constant using the value of $\Delta S^{\circ}_{f_{298}} = -2.7 \pm 1$ e.u. [18]. The free energy of formation of ZrC at 2740°K can be written in terms of $\Delta H^{\circ}_{f_{298}}$ as follows:

$$\Delta F^{\circ}_{f_{2740}} = \Delta H^{\circ}_{f_{298}} + (H^{\circ}_{1700} - H^{\circ}_{298})_{ZrC} - (H^{\circ}_{1700} - H^{\circ}_{298})_{Zr(s)}$$

$$-(H^{\circ}_{1700} - H^{\circ}_{298})_{C(s)} - H_{Zr_{fusion}} - T\left[\Delta S_{f_{298}} + (S^{\circ}_{1700} - S^{\circ}_{298})_{ZrC}\right.$$

$$\left.-(S^{\circ}_{1700} - S^{\circ}_{298})_{Zr(s)} - (S^{\circ}_{1700} - S^{\circ}_{298})_{C(s)} - \frac{H_{Zr_{fusion}}}{2125^{\circ}}\right]$$

Therefore, for $ZrC_{(s)}$

$$\Delta H^{\circ}_{f_{298}} = -38.76 + .83 + 4.0 + 2.740\left(-2.7 - .41 - \frac{4000}{2125}\right)$$

$$\Delta H^{\circ}_{f_{298}} = -47.6 \pm 3 \text{ kcal/mole}$$

The error of ± 3 kcal/mole is assigned on the basis of the estimated error of ± 1 e.u. in the entropy of formation. This value of the heat of formation of ZrC is in agreement with the value given by Krikorian [18] of -44.4 ± 1.1 kcal/mole. When a more reliable entropy and specific heat values becomes available, $\Delta H^{\circ}_{f_{298}}$ of ZrC can be calculated to a precision inherent in the $\Delta F^{\circ}_{f_{2740}}$, namely ± 1 kcal/mole.

b. Estimate of Experimental Error

The principal source of error is the experimental scatter of the measured values of I/I_o. The standard deviation of log I/I_o, and thus of the pressure, was less than 6% for titanium and less than 10% for zirconium. This leads to an uncertainty of 0.3 kcal/mole in the calculated heats and free energies of TiC, and of 0.6 kcal/mole in the case of ZrC.

Uncertainties in the temperature readings and errors due to the temperature gradients are not important. This can be demonstrated by comparing the values of $(-AP')_{T2}$ (which are corrected to a common temperature) obtained for Zr and ZrC using the two different heater tubes.

	Tube	Zr	ZrC
rms value of $-(AP')_{T_2} \times 10^{-4}$	1	1.57	3.10
	2	1.42	2.89
rms deviation on separate sets	1	.17	.07
	2	.05	.19
difference in rms values of $-(AP')_{T_2} \times 10^{-4}$		.15	.21

From this it is seen that the difference between rms values obtained from the two tubes is approximately the same as the rms deviation of values obtained on a single tube. Notice that the gradient is quite different for the two tubes used (Δ differs by 50^o), and that Δ is strongly dependent on the temperature.

In view of these findings the decision was made to use the averaged data from both tubes rather than trying to select data obtained in runs where the temperature gradient is smaller. The probable error of the reported results is felt to be of the order of the root mean square deviations reported in the preceding paragraph.

The claimed accuracy is somewhat more conservative, and is $\pm$ 0.5 kcal for TiC and $\pm$ 1 kcal for ZrC for free energy and enthalpy values.

c. Matrix Isolation Studies

The major effort involved in the application of this technique to refractory oxides has been directed toward modification of apparatus to permit operation at temperatures required by the materials ThO_2 and ZrO_2. While several experiments with ThO_2 have been performed at 2600°K and weak bands near 760 cm^{-1} have been observed, these results are very tentative. Further discussion at this time is not warranted.

D. References

1. Coffman, J. A. et al., Carbonization of Plastics and Refractory Materials Research, WADD Technical Report 60-646 Part 1 (Feb. 1961).

2. Lustman, B. and Kerze, F., The Metallurgy of Zirconium, McGraw-Hill, New York (1955).

3. Kempter, C. P. and Fries, R. J., Anal. Chem. 32, 570 (1960).

4. Pollock, B. D., J. Phys. Chem. 65, 731 (1961).

5. Elliott, R. D. and Kempter, C. P., J. Phys. Chem. 62, 630 (1958).

6. Sanders, W. A. and Grisaffe, S. J., NASA TN D-303 (Aug. 1958).

7. Cotter, P. G. and Kohn, J. A., J. Amer. Ceram. Soc. 37, 415 (1954).

8. Curtis, C. E. et al, J. Amer. Ceram. Soc. 37, 415 (1954).

9. Grisaffe, S. J., J. Am. Ceram. Soc. 43, 494 (1954).

10. Hansen, M., Constitution of Binary Alloys, McGraw Hill, New York (1958).

11. Hoch, M. et al., J. Phys. Chem. 59, 97 (1955).

12. JANAF Thermochemical Tables, The Dow Chemical Co., Midland, Mich. (March 1961).

13. Drowart, J. et al., J. Chem. Phys. 31, 1131 (1959).

14. Moore, C. E., Atomic Energy Levels, 1949 National Bureau of Standards Circular 467 (1949)

15. Linevsky, M. J., J. Chem. Phys. 34, 587 (1961).

16. Brewer, L. et al., Paper #4. Chemistry and Metallurgy of Miscellaneous Materials, McGraw Hill, New York (1950). Edited by L. L. Quill.

17. Stull, D. R. and Sinke, G. C., Thermodynamic Properties of the Elements, American Chemical Society, Washington (1956).

18. Krikorian, O. H., High Temperature Studies, II. Thermodynamic Properties of Carbides, University of California, UCRL-2888 (1955).

19. Mah, A. D. and Boyle, B. J., J. Amer. Chem. Soc. 77, 6512 (1955).

20. Neel, D. S. et al., The Thermal Properties of Thirteen Solid Materials to 5000°F or Their Destruction Temperatures, WADD Technical Report 60-924 (Nov. 1960).

21. Kubaschewski, O. and Evans, E., Metallurgical Thermochemistry, Pergamon Press, New York (1958).

22. Blumenthal, W., The Chemical Behavior of Zirconium, Van Nostrand Co. Inc., Princeton (1958).

23. Thomas, D. E. and Hayes, E. T. Ed., The Metallugy of Hafnium, U. S. Gov. Printing Office, Washington (1960).

24. Chupka, W. A. et al., J. Phys. Chem. 62, 611 (1958).

25. Fujishiro, S. and Gokcen, N. A., J. Phys. Chem. 65, 161 (1961).

26. Huff, G. et al, J. Am. Chem. Soc. 70, 3380 (1948).

27. Preliminary Report on the Thermodynamic Properties of Selected Light-Element Compounds, Report #6645, National Bureau of Standards, January 1960.

IV. SPECTRAL EMISSIVITIES OF REFRACTORY MATERIALS

A. Background

A discussion of the thermal radiation laws and the experimental techniques for measuring spectral emissivity, including pictures of the equipment as well as circuit and block diagrams, are contained in WADD TR 60-646, Part I (1).

Briefly summarized, emissivity is defined as a dimensionless ratio which compares the radiation from the material under consideration with that from an ideal radiator (blackbody) at the same temperature. Emissivity may be total or spectral depending on whether it is considered over the entire wavelength region or just a narrow portion of the entire spectral region. Geometrically, the emissivity may be either normal or hemispherical. This work is concerned with normal emissivity only.

In an opaque solid, light penetrates only a very short distance into the surface. As a result, the thermal radiation characteristics are strongly influenced by surface inhomogeneities which are large compared to the wavelength being viewed. Worthing [2] defines emissivity as the emittance of a material that has an optically smooth surface and a thickness sufficient to be opaque.

In the direct measurement of emissivity, two methods may be used depending on whether absolute energy is measured, or whether the radiation of the specimen is compared with that from a blackbody radiator or some other specimen of known emissivity. In the former, use is made of Planck's radiation law

$$J(\lambda, T) = c_1 \lambda^{-5} \left(e^{\frac{c_2}{\lambda T}} - 1\right)^{-1} d\lambda$$

where c_1 and c_2 are the first and second radiation constants. This requires that both the temperature and the radiating area of the specimen must be known, and that the radiated power must be measured accurately. [3]

In the second method, use is made of a radiator (usually a blackbody) which must be at the same temperature as the specimen, or else the temperatures of the radiator and the specimen must be known accurately. It is possible to incorporate the reference cavity directly into the specimen [4-7], or to use an external blackbody standard. [3, 8] This second method with integral reference cavity, was used in the present studies.

B. Experimental Work

1. Equipment

The apparatus designed, built and utilized for the measurement here reported included the following:

1) Heating Unit - Sylvania high intensity induction light source

2) Specimen - containing a blackbody cavity

3) Specimen Chamber - for controlling the environment

4) Transfer Optics - for transferring the radiation to the monochromator

5) Monochromator - for dispersing the radiation into the desired narrow spectral region

6) Radiation Detector - including amplifiers and recorder

7) Temperature Measuring Device - Optical Pyrometer

Detailed explanations and photographs of this equipment were given in an earlier report. [1]

Some slight modifications have been made in this equipment. In the transfer optics, the oscillating mirror M_1 was changed from a solenoid - permanent magnet affair to two solenoids alternatively activated. The mount for the first spherical mirror M_2 was redesigned to permit minute adjustments without disturbing the alignment. The double pass monochromator used earlier was also replaced by a single pass instrument. The resolution was decreased thereby but, as desired, an increase in signal resulted.

2. Procedure

Unless a specimen has its surface prepared or coated, it is polished to give it an optically smooth surface. The polishing procedure starts with carbide paper of #240 grit, then going to #400 and eventually to #600 grit. Afterward the specimen is polished on a silk cloth using a Linde A grinding compound. Final polishing is done on a felt cloth using Linde A compound.

After the specimen is polished using the procedure described, photomicrographs and X-ray diffraction patterns are taken of the surface.

Prior to insertion into the chamber, the specimen is washed in acetone and then in alcohol, after which it is dried with dry nitrogen. When the specimen is in the chamber, a suitable environment is chosen (vacuum or argon). The specimen is then brought to temperature gradually while being monitored with the optical pyrometer. Final adjustments are made to ascertain that the blackbody cavity is focused exactly on the entrance hole to the monochromator. Emissivity versus wavelength is recorded directly with the scan lasting about 30 minutes.

These scans are continued at increasing temperatures until the specimen shows signs of surface damage or until desired data have been obtained. The following materials have been studied; the source of each is as indicated:

1) Molybdenum + 1/2% Titanium with Chromalloy W2 coating obtained from Chromalloy Corporation, White Plans, New York.

2) Siliconized ATJ Graphite, National Carbon Co., New York, New York.

3) Tantalum 99.9% purity, Bram Chemical Co., Philadelphia 26, Pa.

4) Molybdenum 99.9%, General Electric Co., Cleveland, Ohio

5) Tungsten 99.9%, Carbide Specialty Co., McKeesport, Pa.

6) Tungsten Carbide, A. D. Mackay

7) Zirconium 99.9%, Carborundum Metals Co., Akron, New York.

C. Results and Discussion

1. W-2 Coated Molybdenum Alloy

Specimens of the alloy containing molybdenum plus 0.5% titanium and surfaced with Chromalloy W-2 coating were heated both in air at normal atmospheric pressure and in argon at 0.33 atmosphere pressure. During the heating process, surface changes in the specimen were observed to occur as evidenced by changes in appearance under visual observation or observation through the pyrometer, by changes in X-ray diffraction patterns and by irreversible changes in emissivity after prolonged heating or upon heating above some critical temperature region.

For example, while viewing these specimens (heated in argon) through the optical pyrometer, it has been noticed that the specimens develop bright spots on the surface when heated to about 1600°K. Furthermore, all specimens developed cracks in their surface when heated to 1800°K. The period of time before these cracks appear seems to depend on the previous heating history of the specimen.

The surface change observed in the case of W-2 coatings heated in air has been the formation of a white crystalline coating which completely covers the surface. The X-ray diffraction patterns taken routinely before and after heating indicate that the W-2 coating underwent changes of the following type:

1) Transformation of $Mo\ Si_2$ to $Mo_5\ Si_3$. Two samples (3 and 4) have been observed to undergo such changes when heated in argon.

2) Oxidation. Specimens heated in air increase in newly formed $Mo\ O_2$ content.

Surface melting of one specimen at a temperature slightly above 2000°K was also observed. Figure 19 shows a photomicrograph of the W-2 surface before heating. This may be contrasted with the appearance of the piece which experienced surface melting as shown in Figure 20. Figure 21 shows a W-2 specimen after being heated in air where the cracks which form on heating, and the white coating can be seen forming.

Figure 22 shows the emissivity of a W-2 specimen, heated in argon as a function of wavelength and temperature. The emissivity decreases with increasing wavelength and increasing temperature. There is a small but definite negative temperature coefficient of emissivity at all wavelengths. The wavelength dependence may be somewhat influenced by the relatively rough surface of the coated specimen, which would tend to raise the emissivity at wavelengths smaller than the size of the surface inhomogeneities. The results from another sample shown in Figure 23, are similar to those in Figure 22, but it can be seen that there is some random variation between different specimens. This is again characteristic of rough inhomogeneous surfaces.

Figure 24 shows the change in emissivity of a W-2 coated specimen heated in air at 1400°K for six hours. Figures 25 and 26 show the changed emissivity of the specimen after it has been heated in air over a varied temperature sequence. The effect is not too noticeable unless the specimen is heated above 1600°K. Figure 27 shows the change in emissivity at several wavelengths, as a function of time of heating at 1600°K in air.

2. Siliconized ATJ Graphite

Siliconized ATJ graphite also undergoes surface changes on heating. During prolonged heating at temperature sequences from 1400°K to 2200°K, crystals were observed to form on the surface of these specimens (Figures 33 and 34). These crystals cause erratic results and emissivity measurements must be discontinued. It is suspected that the crystals are silicon carbide, although attempts to analyze the crystals failed due to the insufficient amount of material which is available from a specimen.

Figures 28, 29 and 30 show plots of emissivity vs. wavelength of siliconized ATJ graphite. As can be seen from all "typical" curves, emissivity increases with increasing wavelength and decreases with increasing temperature. While there may be some random variation due to differences among specimens, it is clear that there is little metallic character to the material and that the emissivity is high and remains high at all wavelengths as long as the surface remains unchanged. In Figure 29 the results of measurements made at 1435°K, 1830°K and 2040°K are characteristic of the original surface. So are the curves at 2077°K and 2241°K in Figure 30. In the latter figure the change during the experiment at 2360°K is quite evident. Similar changes also occurred during runs at 2236°K and 2270°K as shown in Figure 29.

Figure 19. Chromalloy W-2 Coated Mo + 1/2% Ti Before Heating

Figure 20. Chromalloy W-2 Coated Mo + 1/2% Ti Showing Surface Melting

Figure 21. Chromalloy W-2 Coated Mo + 1/2% Ti After Heating In Air

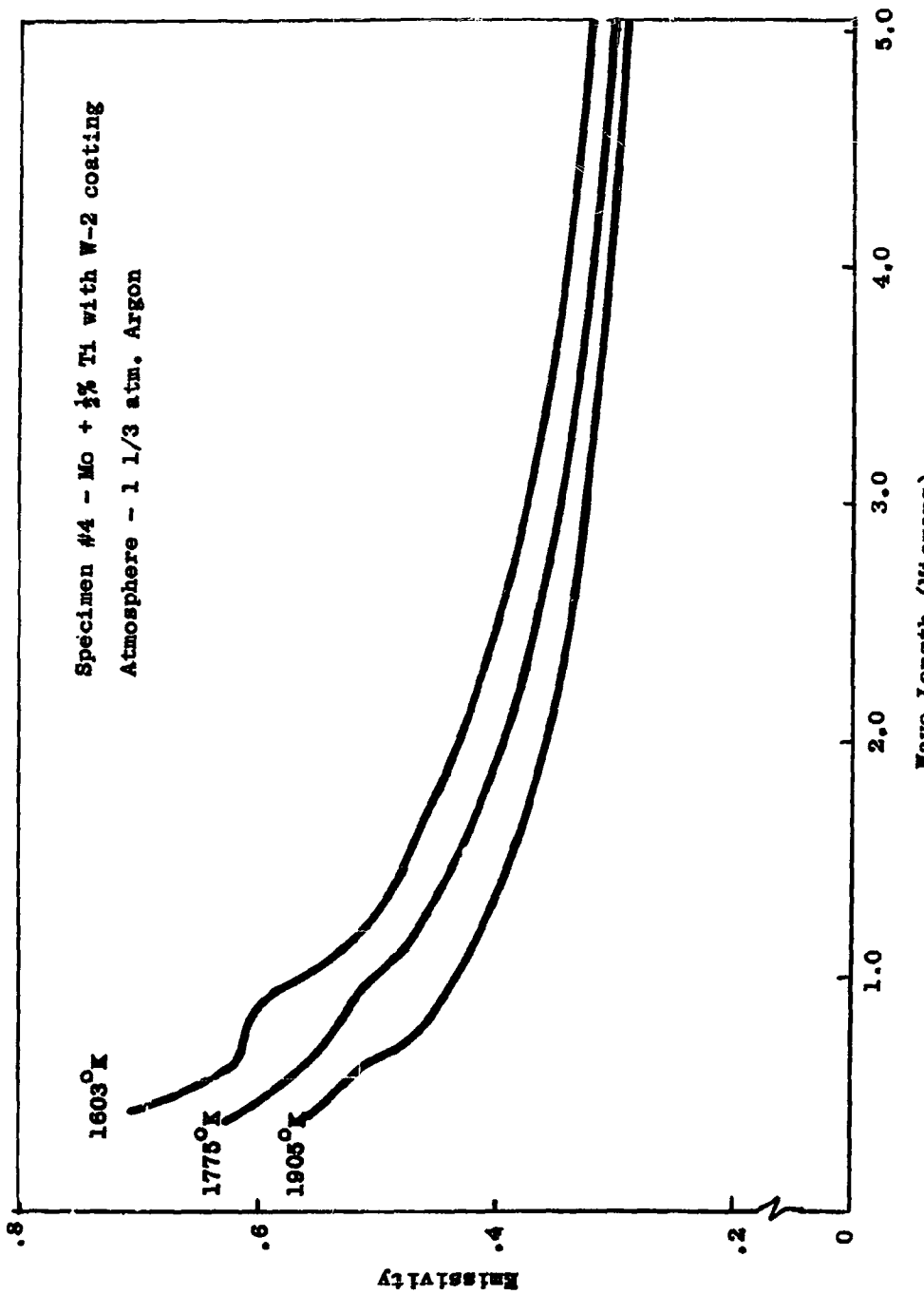

Figure 22 Normal Spectral Emissivity of W-2 Coating in Argon, Specimen #4

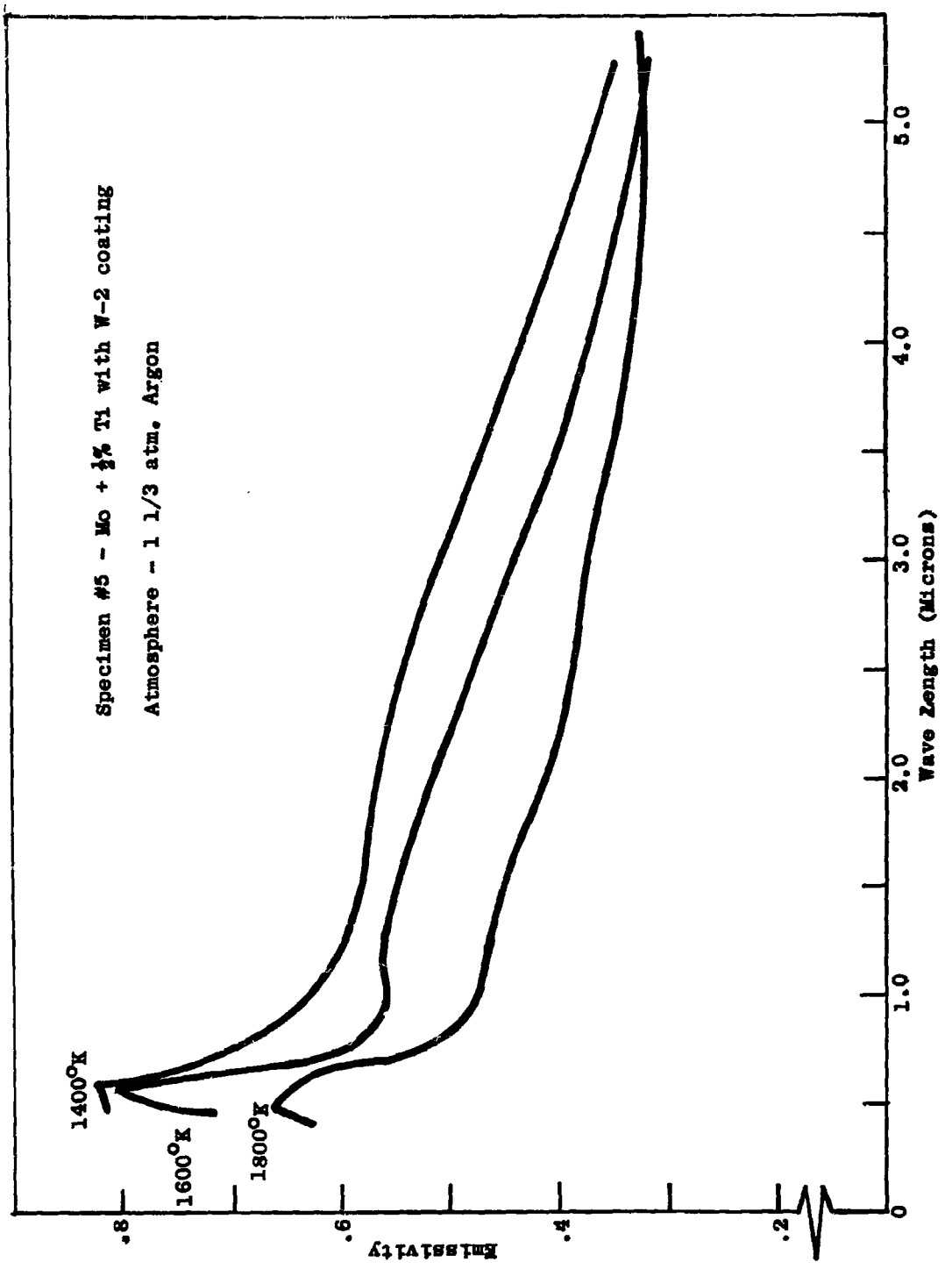

Figure 23 Normal Spectral Emissivity of W-2 Coating in Argon, Specimen #5

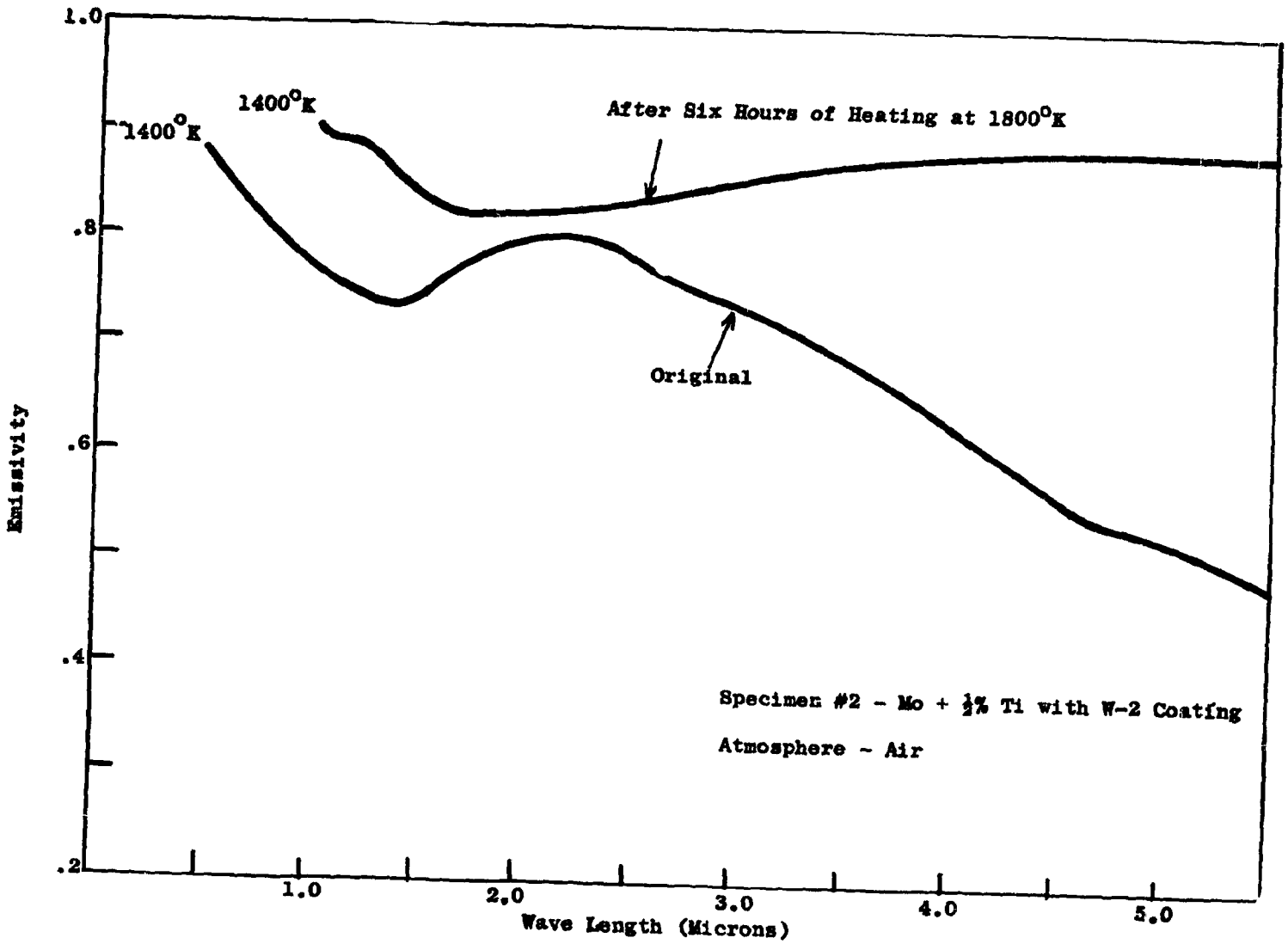

Figure 24 Normal Spectral Emissivity of W-2 Coating in Air, Specimen #2

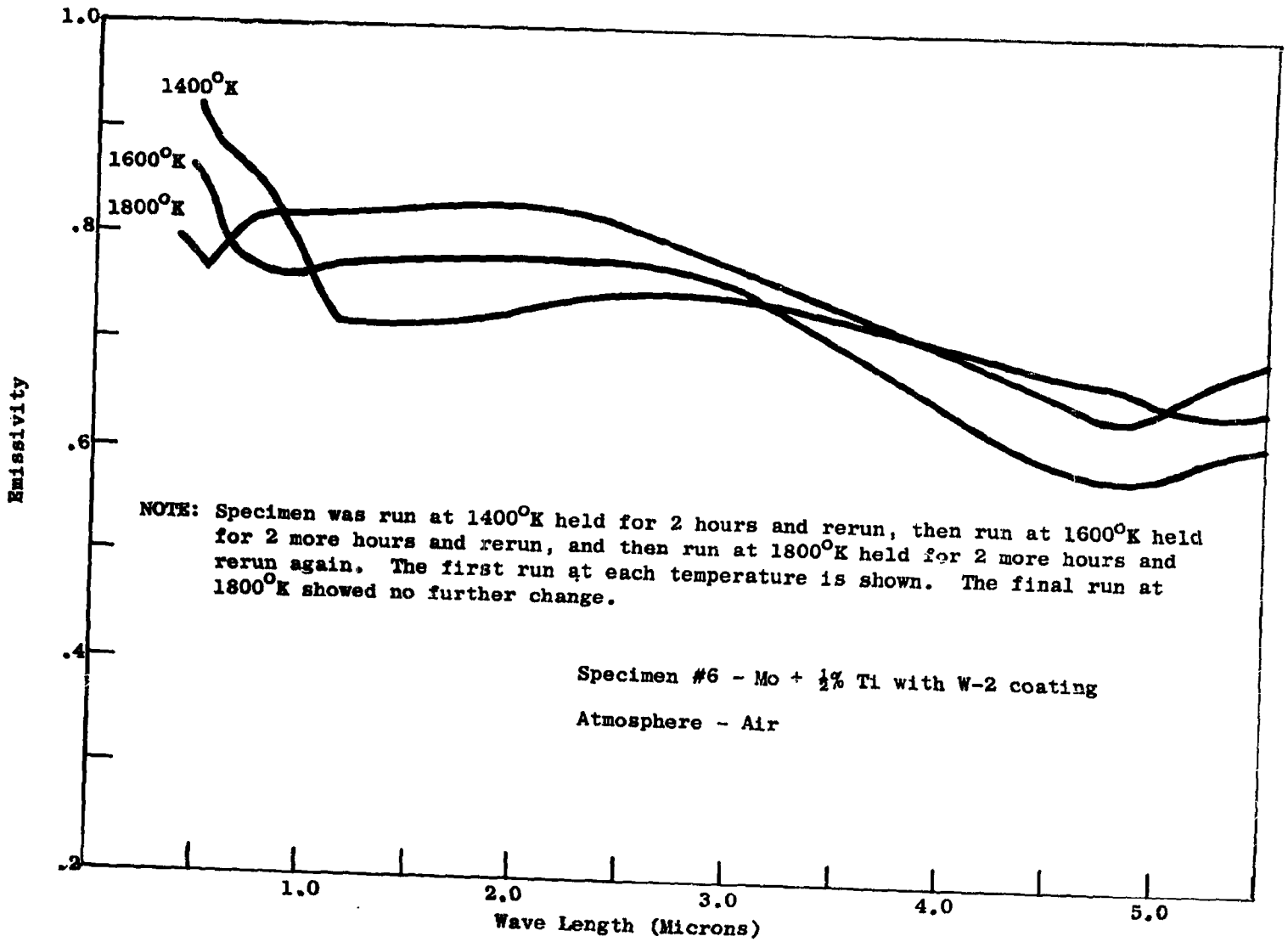

Figure 25 Normal Spectral Emissivity of W-2 Coating in Air, Specimen #6

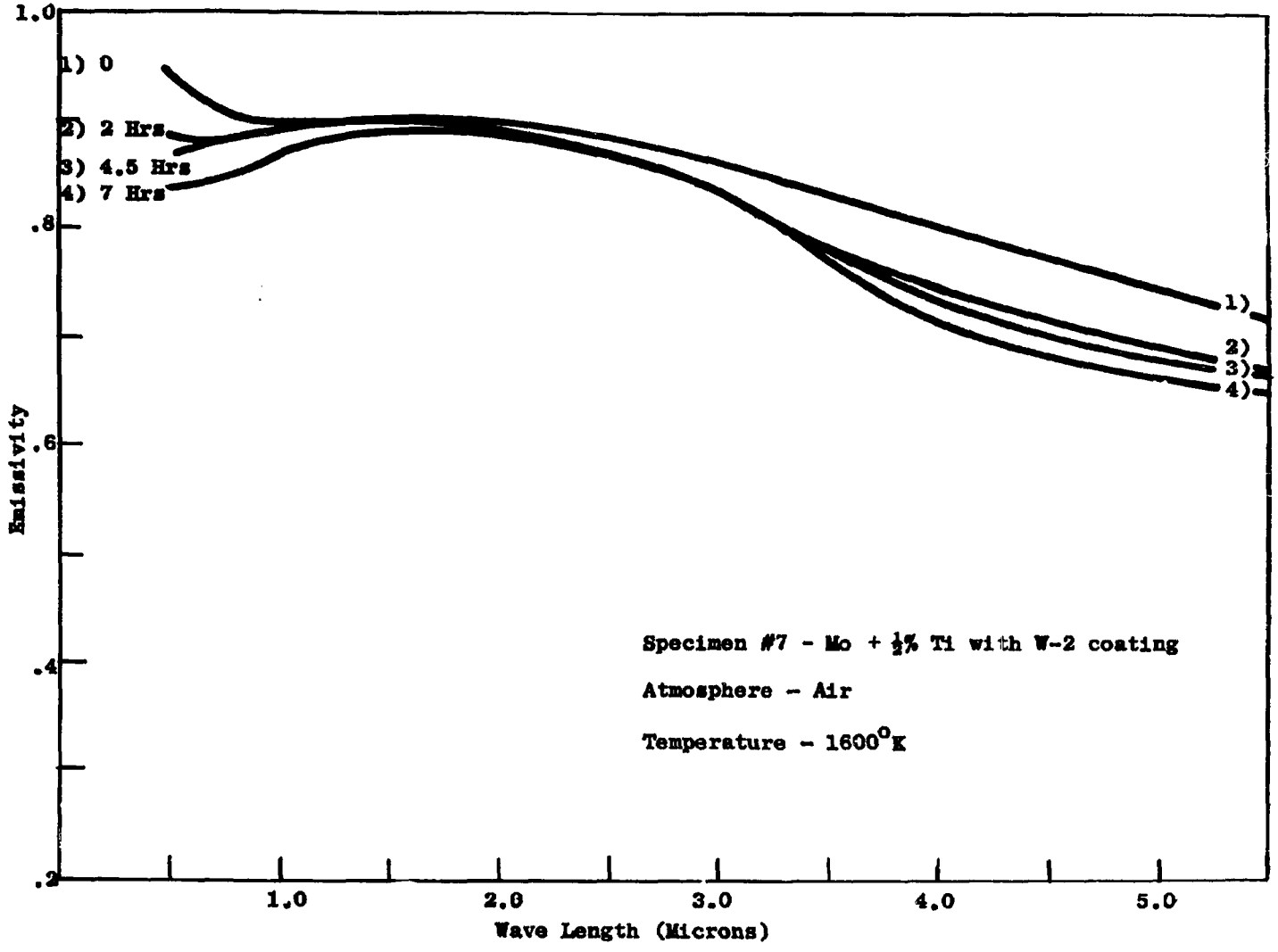

Figure 26 Normal Spectral Emissivity of W-2 Coating in Air, Specimen #7

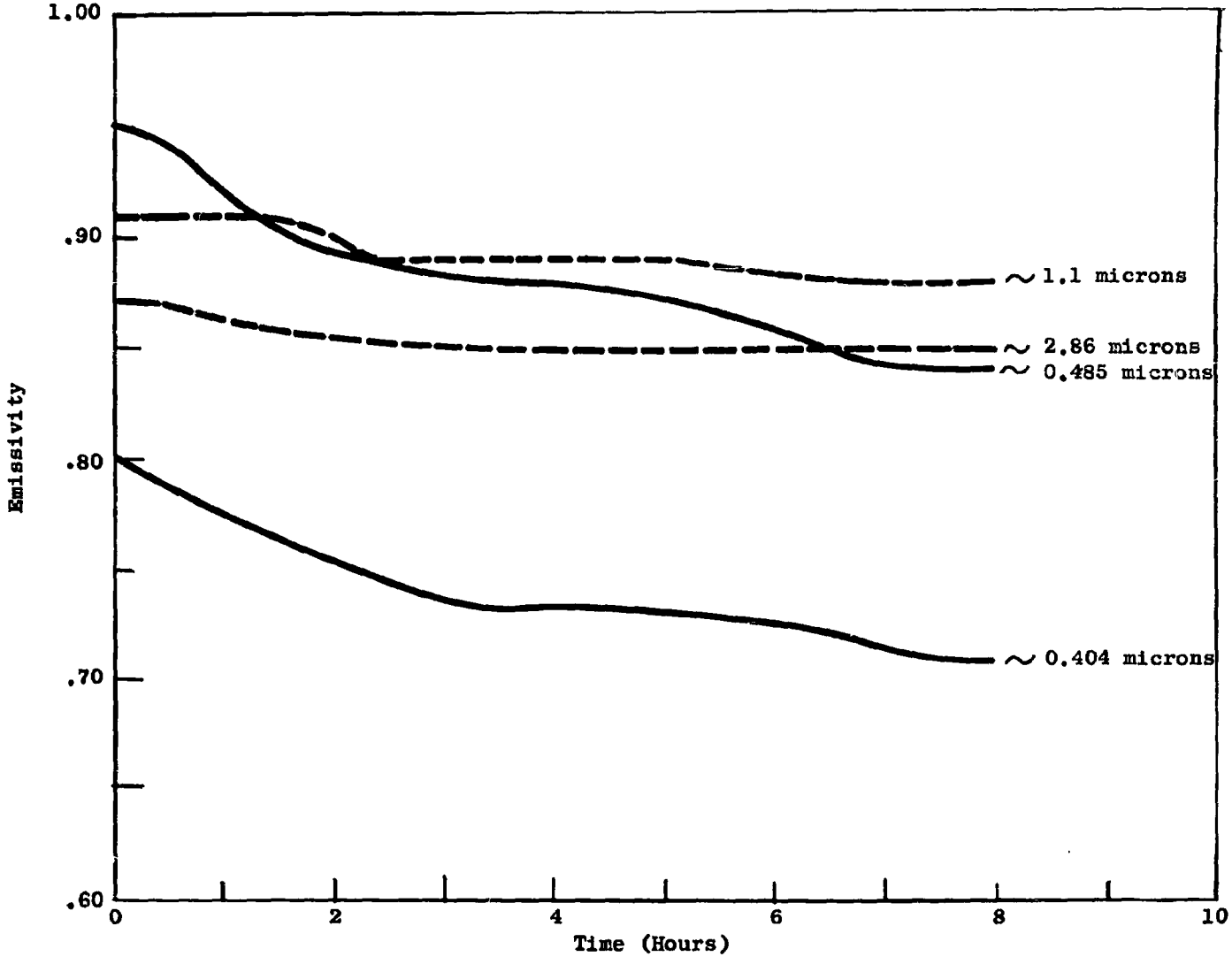

Figure 27 Variation with Time of Normal Spectral Emissivity of W-2 Coating at 1600°K in Air

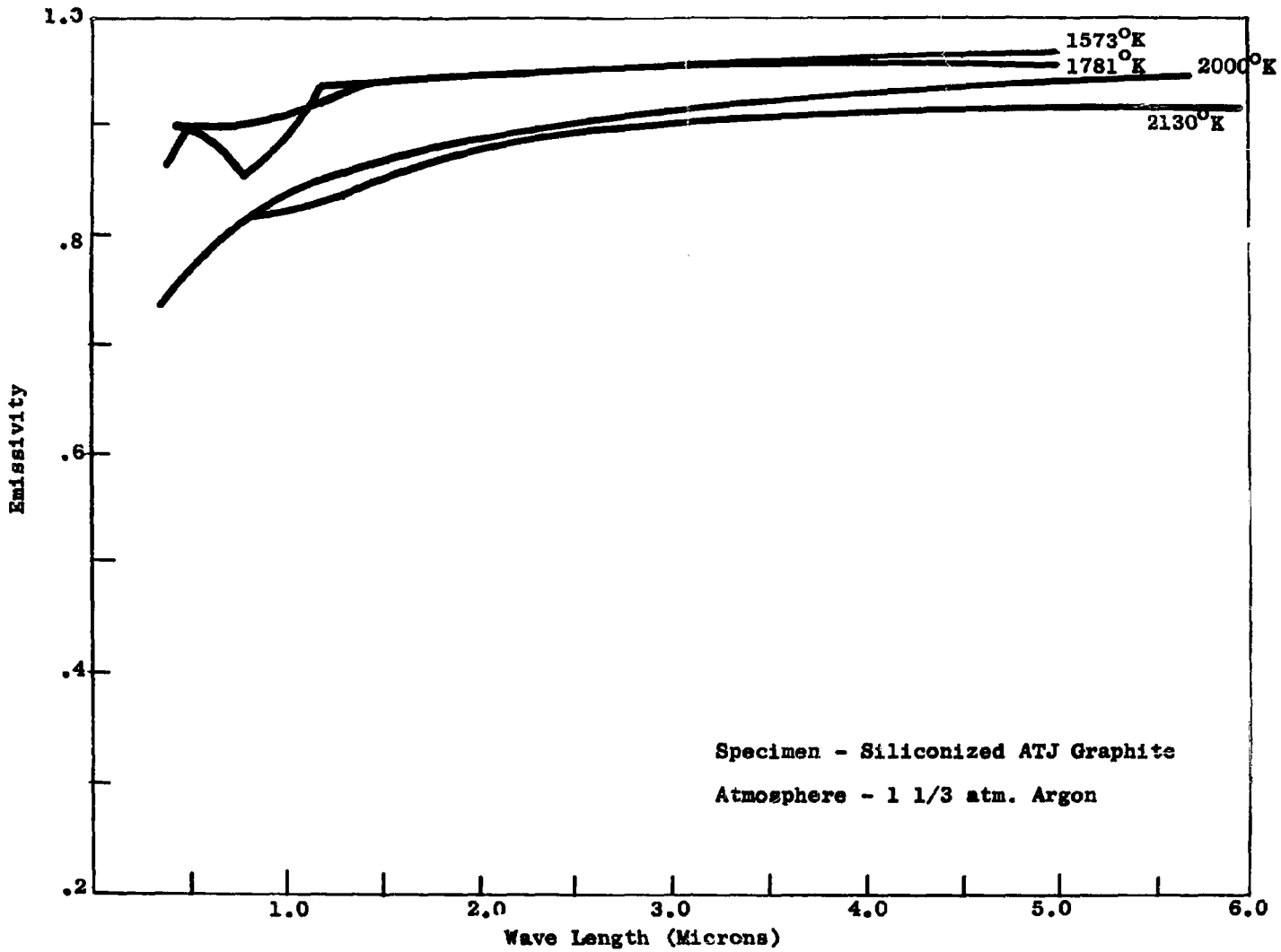

Figure 28 Normal Spectral Emissivity of Siliconized ATJ Graphite in Argon

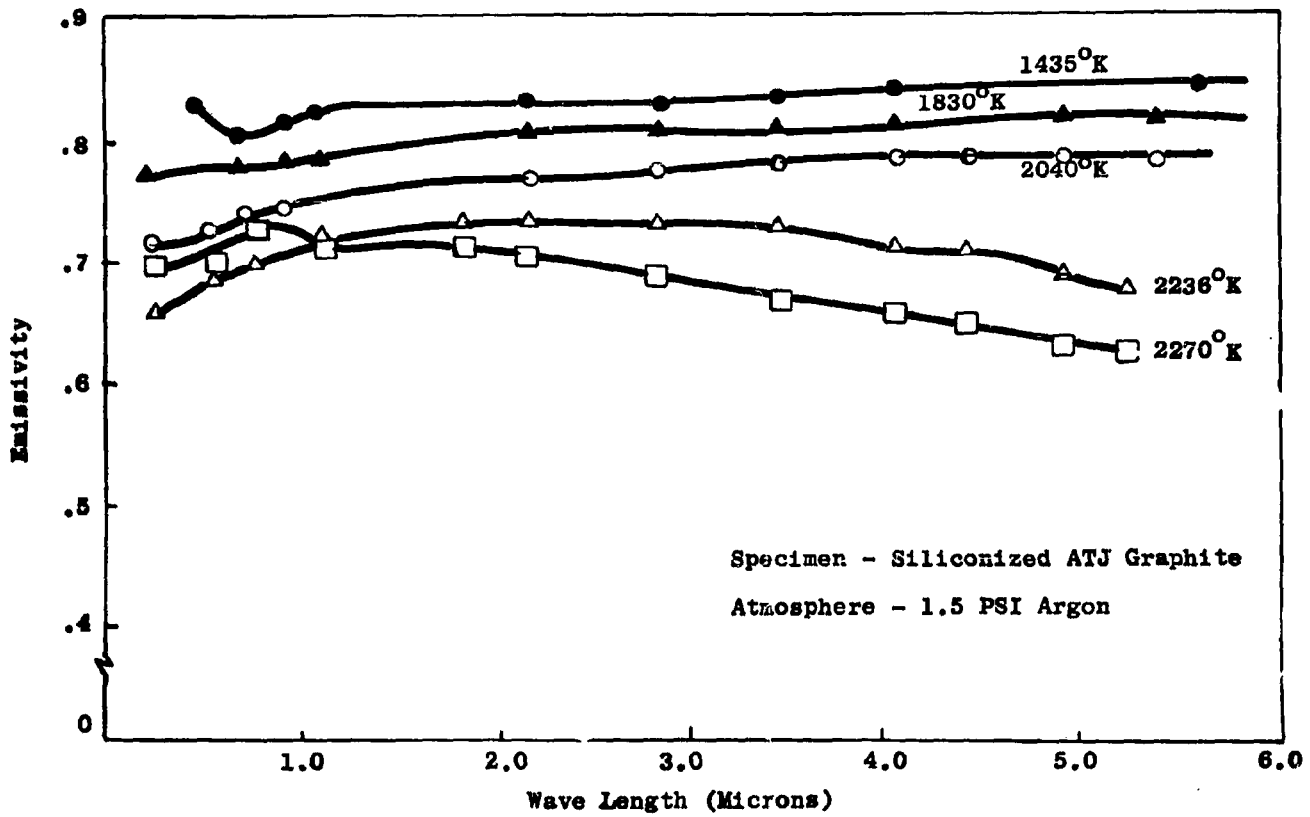

Figure 29 Normal Spectral Emissivity for Siliconized ATJ Graphite

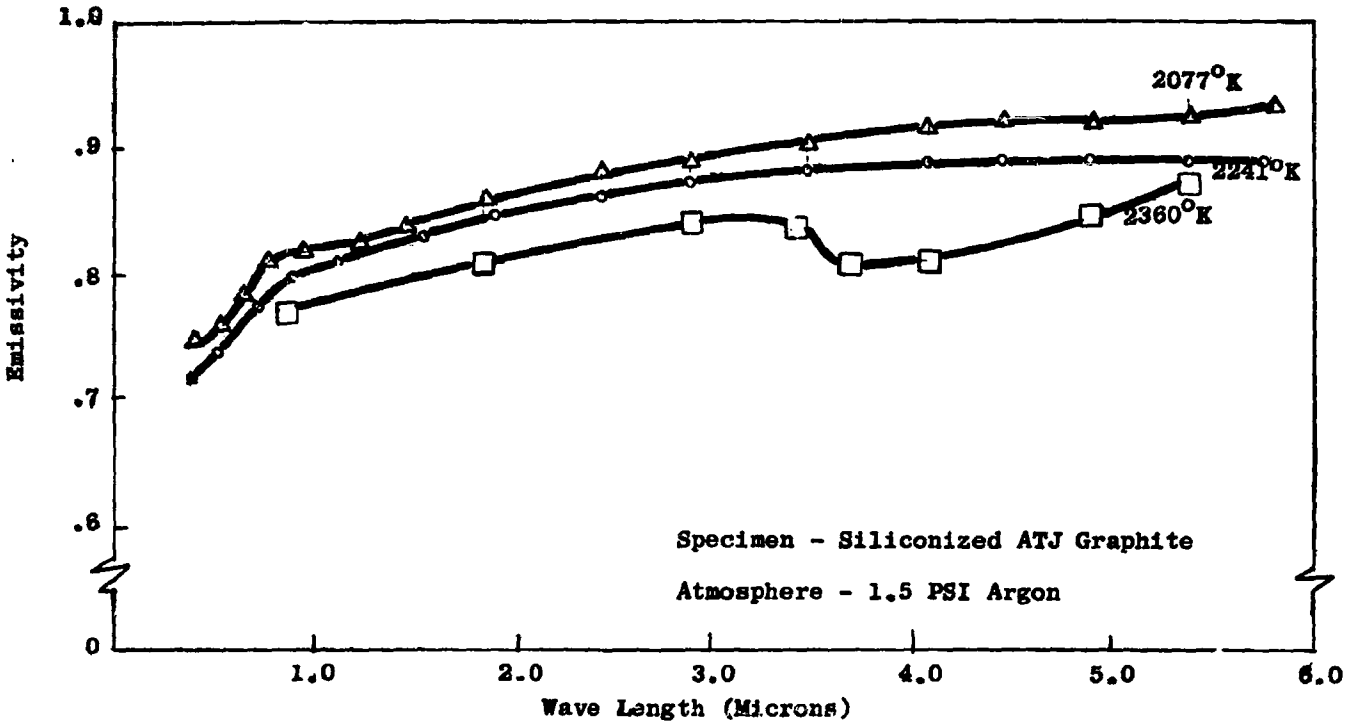

Figure 30 Normal Spectral Emissivity for Siliconized ATJ Graphite

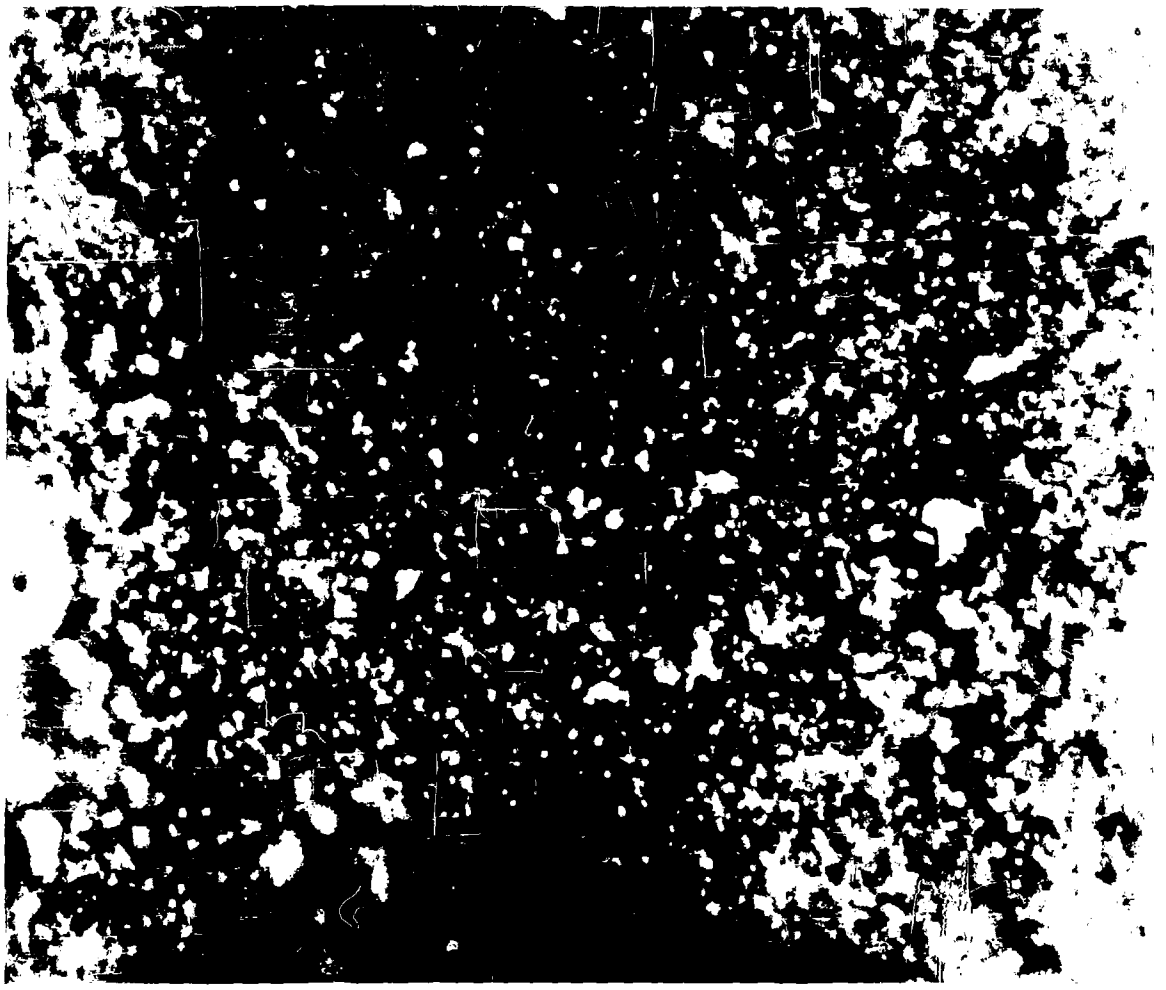

FIGURE 31. UNPOLISHED SILICONIZED ATJ GRAPHITE PRIOR TO HEATING (200X).

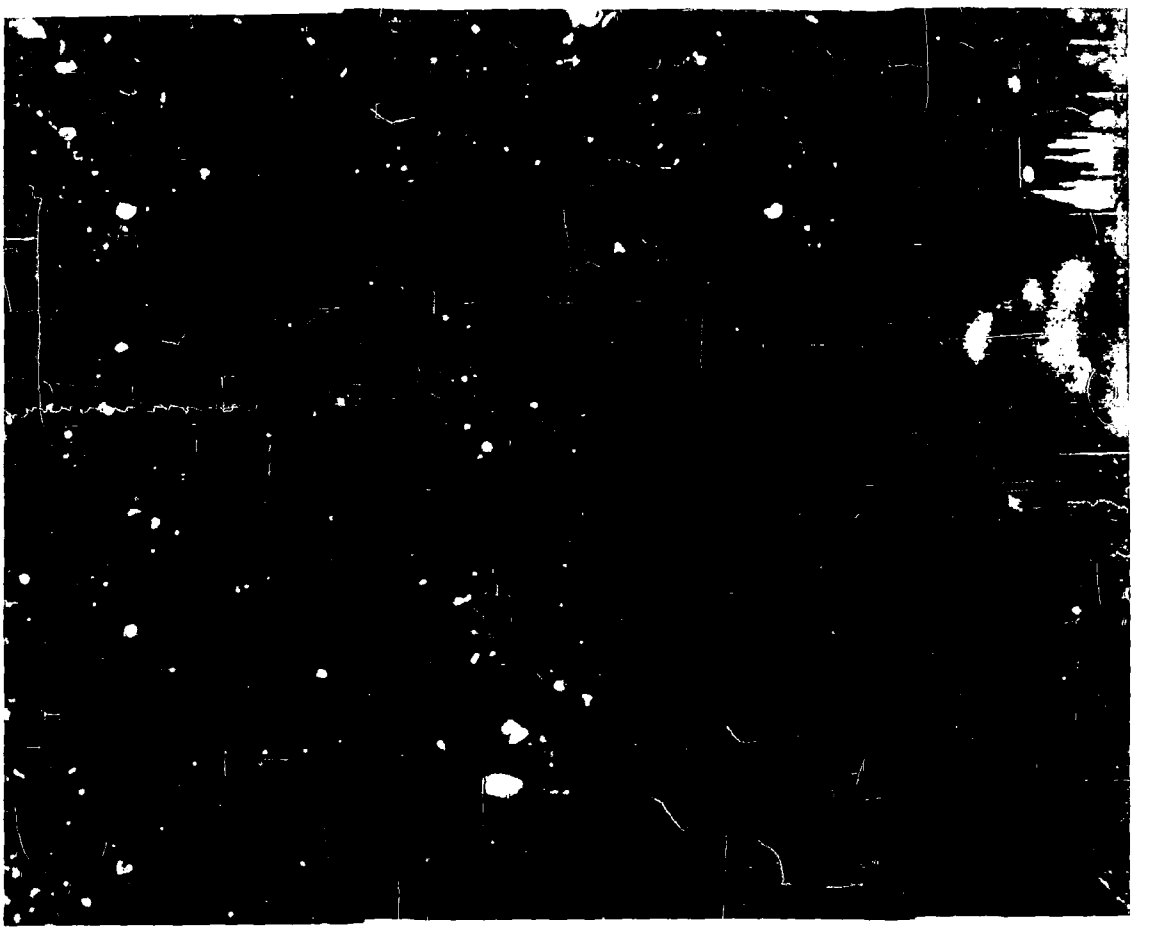

FIGURE 32. SILICONIZED ATJ GRAPHITE AFTER MEASUREMENT (200X).

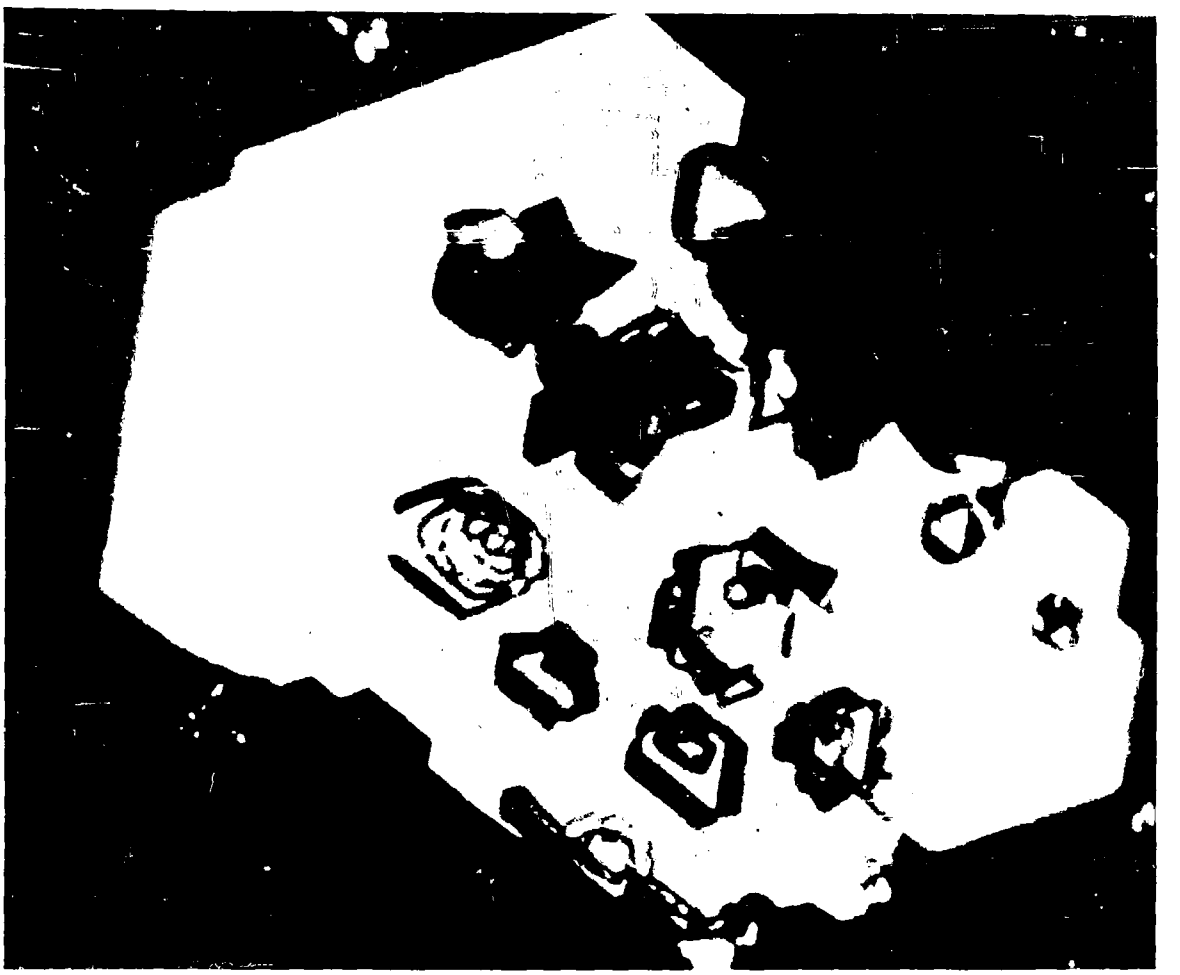

FIGURE 33. CRYSTALS FORMED ON SURFACE OF SILICONIZED ATJ GRAPHITE AFTER MEASUREMENT (200X).

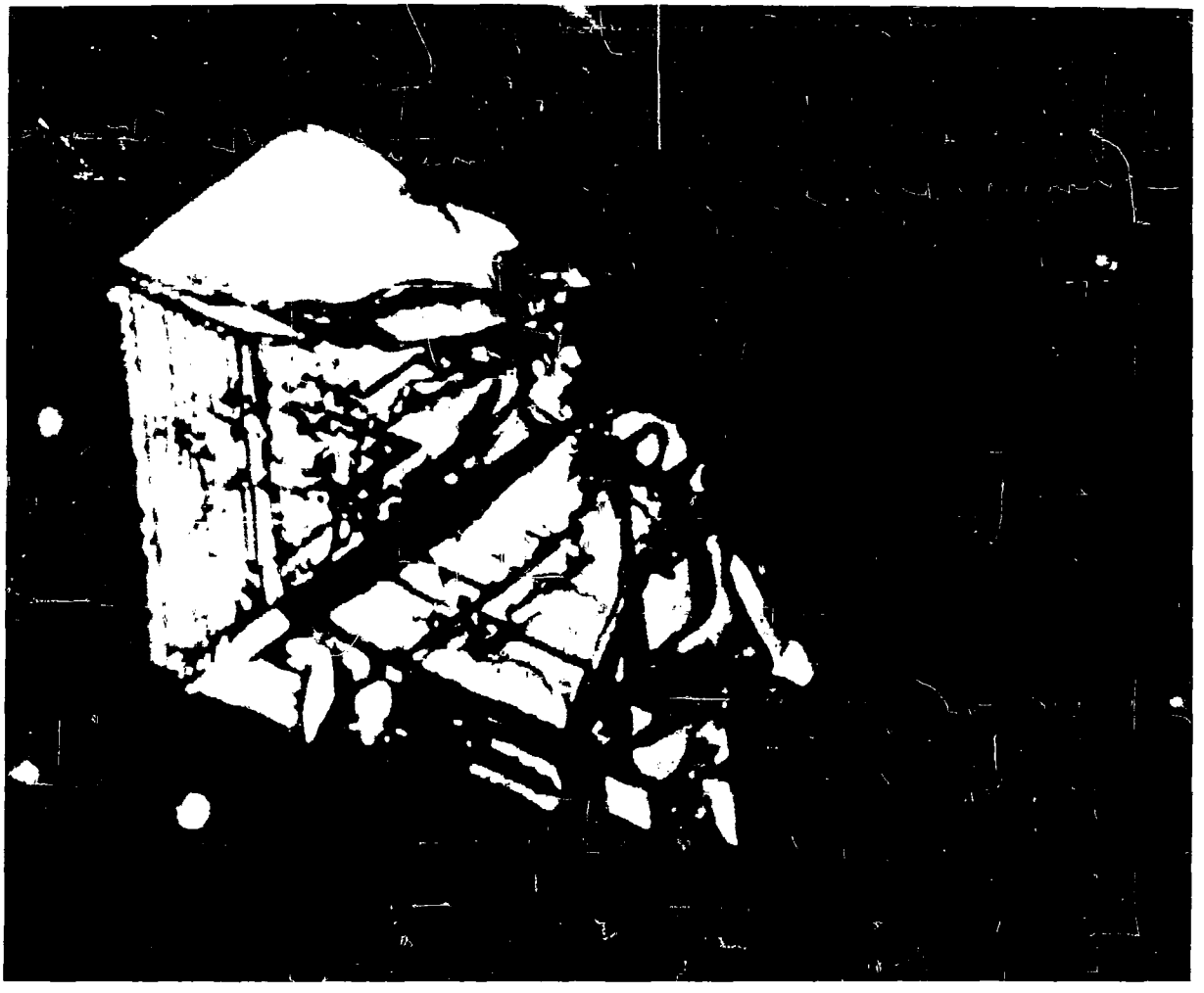

FIGURE 34. CRYSTALS FORMED ON SURFACE OF SILICONIZED ATJ GRAPHITE AFTER MEASUREMENT (200X).

Attempts were made to measure the emissivity of ATJ graphite in air. After noting large decreases in temperature in short periods of time, it was discovered that the graphite was being removed from the black-body cavity, probably in the form of CO_2, leaving a hollow shell. One of these shells was ground into a homogeneous mixture for X-ray diffraction analysis and the results shown only silicon carbide.

3. Tantalum

Tantalum specimens were studied both in an argon atmosphere and in vacuum. The results complement each other not only in reproducibility of emissivity but also in the formation of a "film" on the surface of the specimen. The term "film" is applied because no visible damage had occurred. In fact, the surface appears even more highly polished - one might even say "glassy-like".

The X-ray diffraction run prior to heating shows the crystalline tantalum pattern. After the specimen was heated, the diffraction lines disappeared, indicating an amorphous material.

Figure 35 shows a picture of the tantalum surface prior to heating, magnified 200x. Surface imperfections and polishing lines show up rather clearly. Figure 36 is a picture of tantalum after it was heated. It is noted that the scratches appear smoothed over. The dark lines seem to indicate the presence of a layer of some kind of material since it is possible to focus down into these "cracks". This layer is sufficiently thick to prohibit the X-rays from displaying a diffraction pattern.

Figure 37 shows the emissivity of tantalum at some elevated temperatures. The dashed line indicating emisssivity at 1700°K is the first run made, probably before the coating was formed. The other curves were made after the specimen had been heated to 2400°K. It does not appear that the coating affects the emissivity in the long wavelength spectral region. An x-point for the coated material is seen at about 0.7 micron, with an emissivity of about 0.4.

4. Molybdenum

During the tests, molybdenum specimens underwent rapid vaporization at temperatures above 2200°K. The metal which evaporated subsequently deposited on the calcium fluoride window in the form of a black deposit. This decreased the amount of energy the monochromator received and at the same time affected the pyrometer readings, thereby giving erroneous temperature measurements. Hence, extensive measurements were first made over a temperature range of 1600°K to 2000°K, temperatures being kept relatively low so as to minimize vaporization. Then the temperature was increased rapidly to 2800°K and a measurement was made at this latter temperature. This permitted an accurate temperature measurement before the deposit formed on the window.

FIGURE 35. TANTALUM PRIOR TO HEATING (200X).

FIGURE 36. TANTALUM AFTER MEASUREMENT (200X).

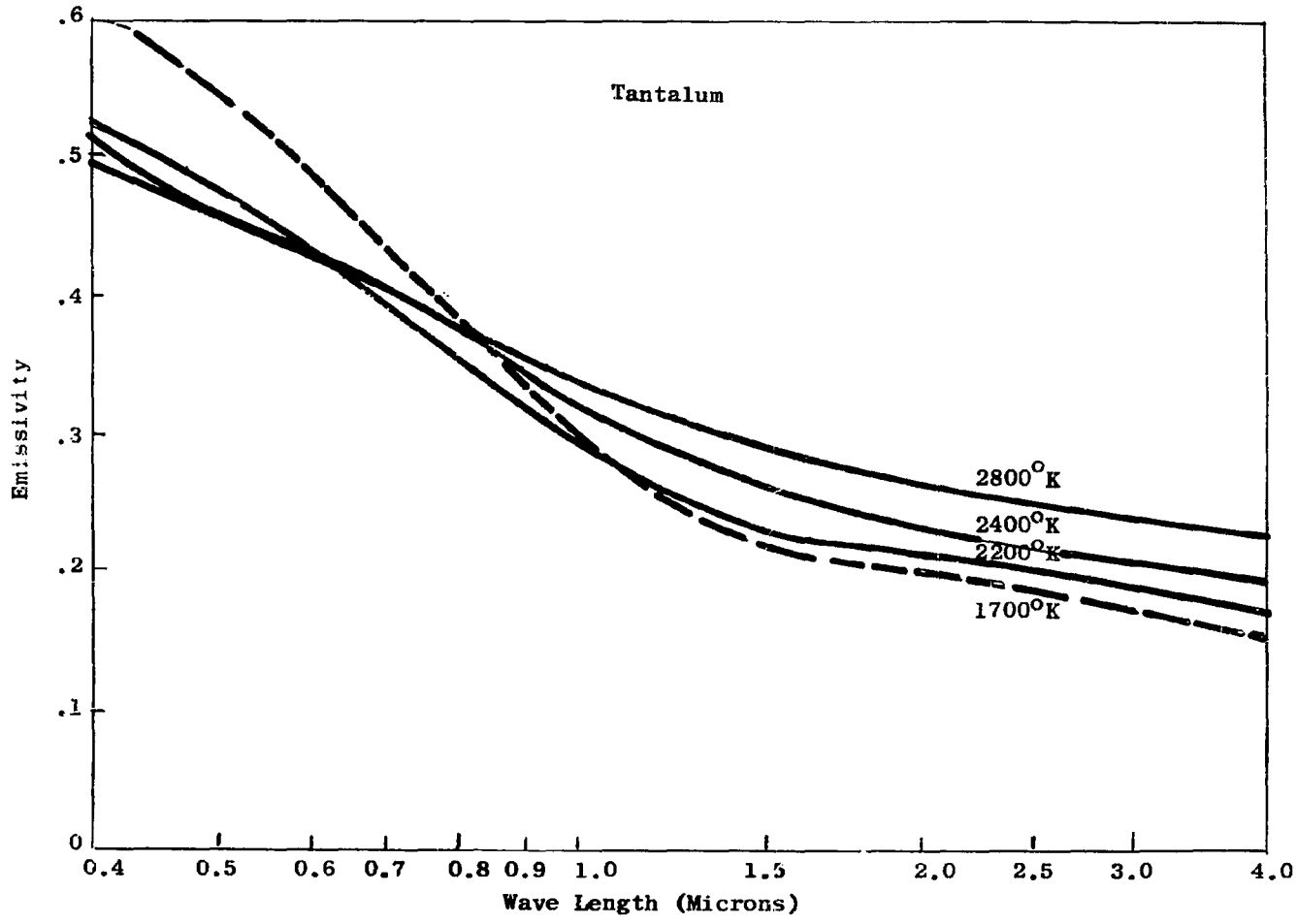

Figure 37 Normal Spectral Emissivity of Tantalum

Figure 38 is a plot of the emissivity of molybdenum at 1600°K, 2000°K and 2800°K obtained in this manner. Molybdenum displays typical metallic characteristics with the temperature independent point on the emissivity curve occurring around 1.3 microns, and indicating an emissivity of 0.22.

5. Tungsten

Tungsten specimens underwent considerable testing from 1600°K to 3100°K. In Figure 39 appears a typical plot of the emissivity of tungsten as a function of wavelength. The expected decrease of emissivity with increasing wavelength occurs, but the cross-over point has considerable scatter.

In order to establish the cross-over point more accurately, the data were further analyzed in the following manner. A plot of emissivity E versus temperature T was made of all available data, the wavelength in each case being constant. A linear regression curve was fitted, by the method of least squares, to these data points, and the slope dE/dT of the regression curve was determined. This was repeated for a number of wavelengths. Finally, a plot of dE/dT versus wavelength was made and, by definition, the cross-over point is that wavelength at which dE/dT = 0. It can be seen from Figure 40 that the cross-over point obtained by this method for tungsten is 1.28 microns. The emissivity at the cross-over point is between 0.32 and 0.33, which compares favorably with the values obtained by DeVos, [5] and earlier in this program. [1]

Both molybdenum and tungsten underwent the same type of change during heating. In both cases there was a crystallite growth and a preferred orientation of the crystals.

Figure 41 shows a picture of polished tungsten magnified 200x. This is much the same as the polished tantalum displayed in Figure 35. Both, incidentally, resemble molybdenum. Figures 42 and 43 are pictures of tungsten and molybdenum, respectively, after they have been heated. In both cases, the crystal structure can clearly be seen.

6. Tungsten Carbide

Tungsten carbide is a difficult material to work with because of the ease with which it decomposes at elevated temperatures. Even at temperatures below which decomposition rates per se became appreciable (see Section III) emissivity studies have shown that significant changes in surface composition do occur in the 1400 - 2000°K range.

All samples of this material, as received, were proved, by X-ray diffraction measurements, to be WC. Figure 44 presents the emissivity of WC from 1400°K to 1800°K. There is little evidence that composition changes occurred within this region. As the figure shows, there is very little variation in emissivity with temperature between 0.4 microns and 0.7 microns, but beyond 0.7 microns, the emissivity increases with temperature within this range. At 2000°K, and possibly beginning at 1800°, the

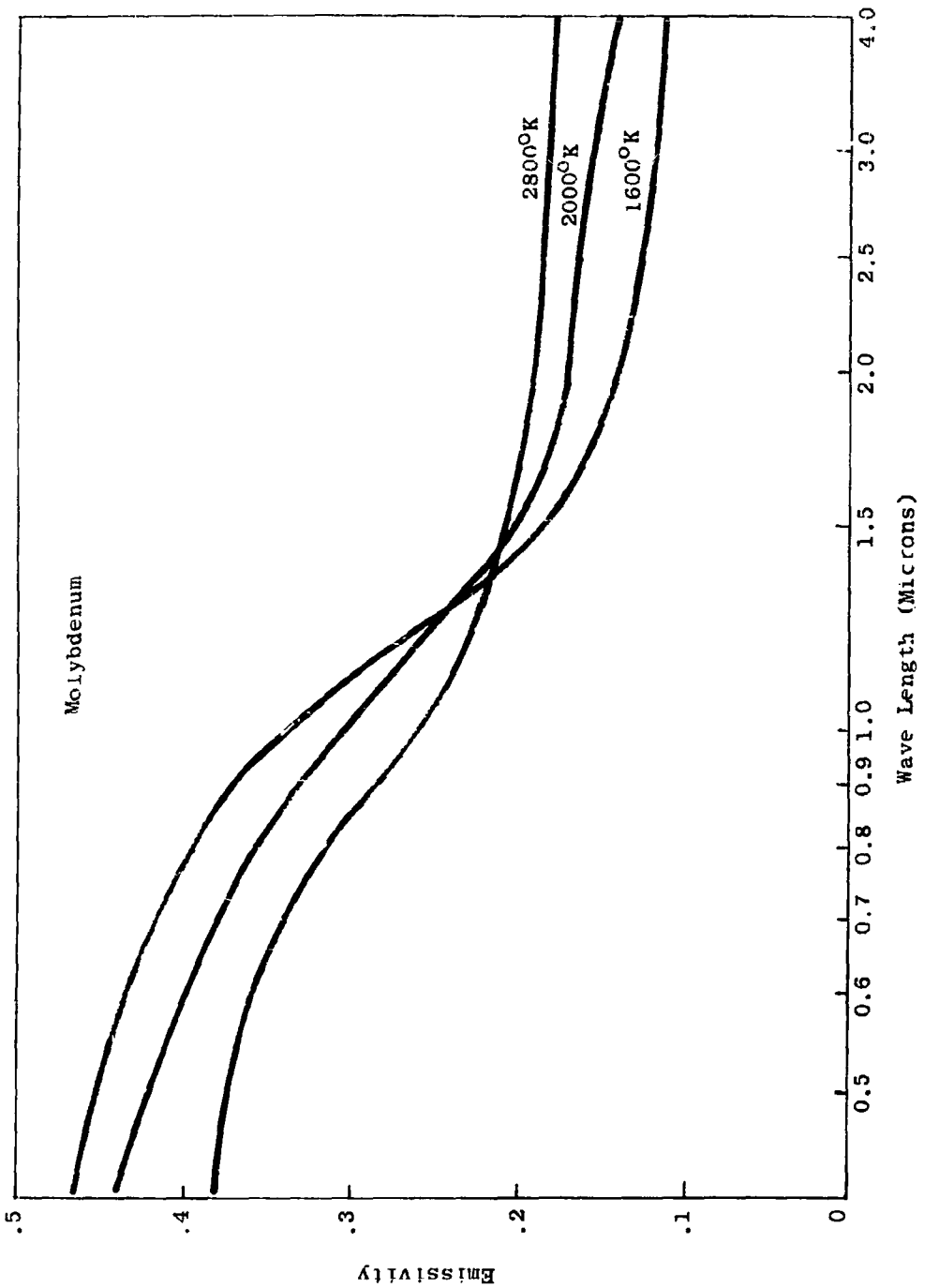

Figure 38 Normal Spectral Emissivity of Molybdenum

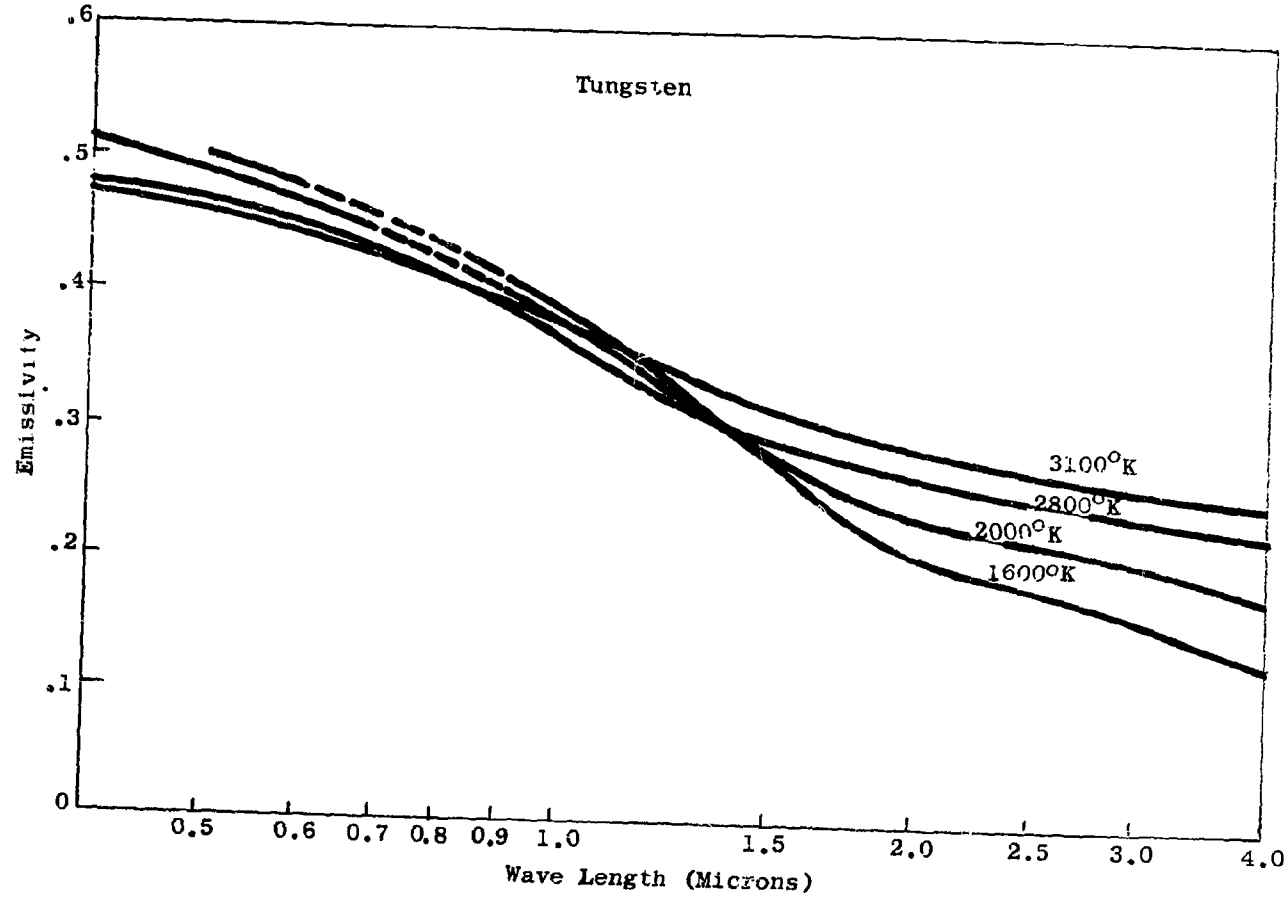

Figure 39 Normal Spectral Emissivity of Tungsten

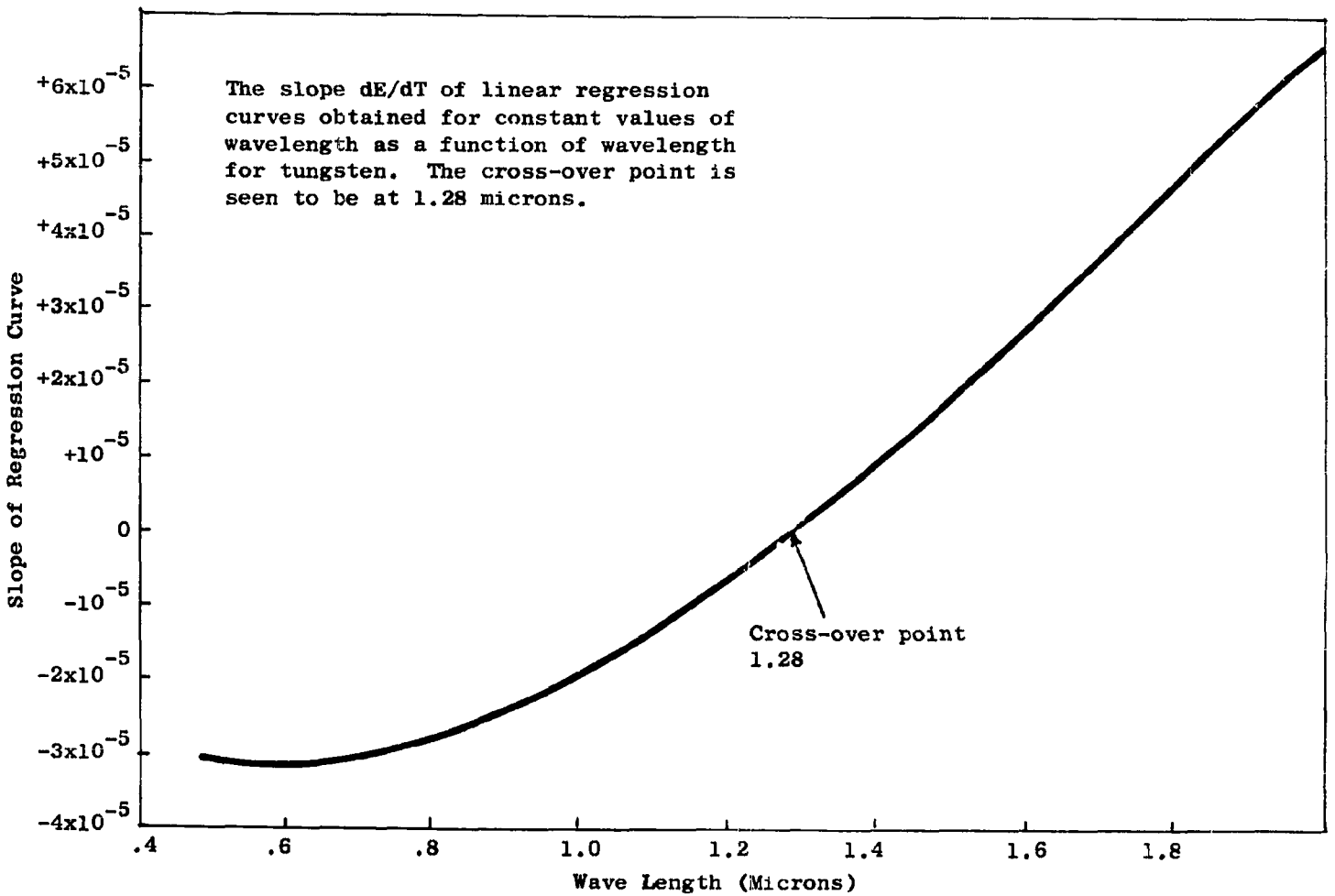

Figure 40 Cross-Over Point, Tungsten Emissivity

FIGURE 41. POLISHED TUNGSTEN SPECIMEN BEFORE HEATING.

FIGURE 42. TUNGSTEN SPECIMEN AFTER HEATING.

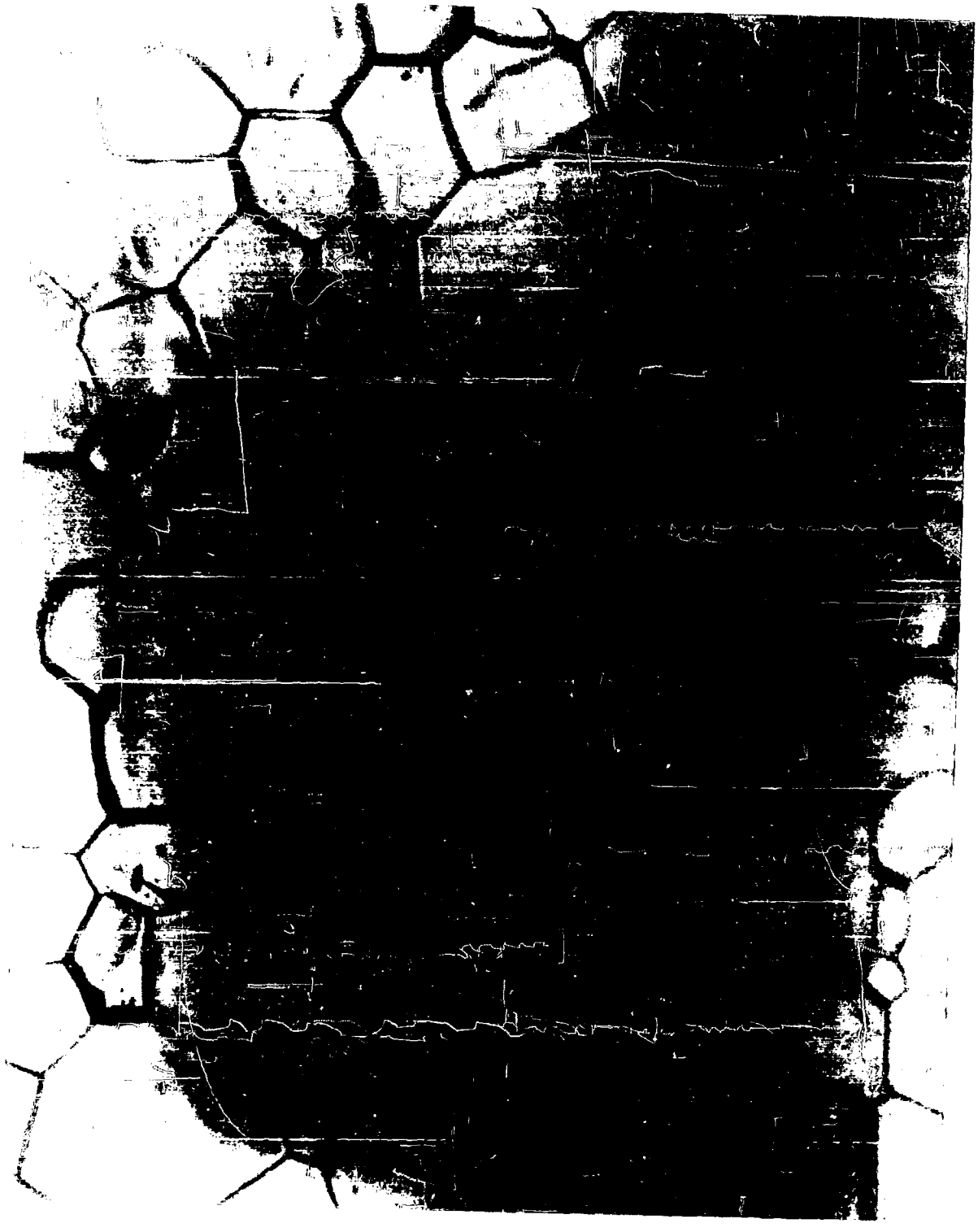

FIGURE 43. MOLYBDENUM SPECIMEN AFTER HEATING.

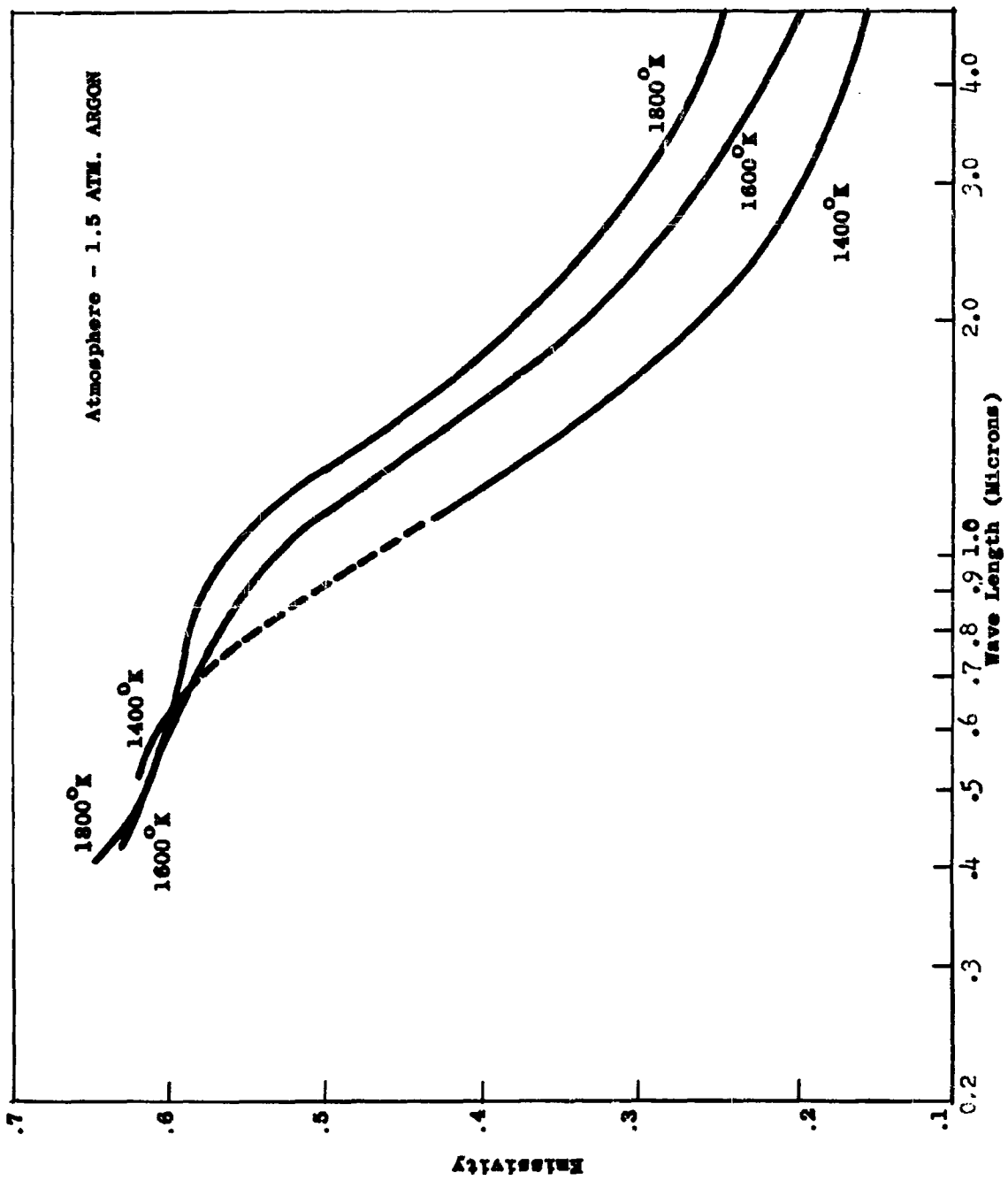

Figure 44 Normal Spectral Emissivity Of WC

emissivity changes quite markedly and irreversibly, after which the emissivity from 1400°K to 1800°K has also changed.

Two of the specimens which were removed from the chamber after they were heated to 2000°K were X-rayed and found to have undergone a change from WC to W_2C. Whether this is an α phase or a β phase W_2C is uncertain. It was suggested by Becker [9] that a high temperature modification of W_2C (β-W_2C) exists above 2400°C. However, Pearson [10] claims that this has not since been confirmed. Becker stated that the β - W_2C high temperature modification produced X-ray diagrams similar to α - W_2C except that many lines were missing.

The X-ray patterns produced from these samples were observed to be very similar to the patterns expected from α - W_2C except that they were far less complex. This seemed to indicate the presence of β - W_2C phase as described by Becker. It was found that all diffraction lines, with the exception of one (d = 2.27Å), checked out well with Becker's data. The additional line had a relative intensity of about 30%. This line can be accounted for in the diffraction pattern of α - W_2C. There is some hesitancy to labeling these specimens β - W_2C because of uncertainty as to its existence and because of the presence of the relatively strong line not observed by Becker.

No reference has been found to indicate that W_2C exhibits long range order. However, it may be that α - W_2C is a highly ordered phase and the phase that Becker calls β - W_2C is a disordered or random phase. If this is the case then the phase observed here may have a Bragg-Williams long range order parameter between zero and unity. More work would be required to establish whether W_2C truly exhibits long range order.

Figure 45 shows the emissivity of W_2C after it had been heated repeatedly from 1600°K to 2400°K. This specimen displayed the same pattern as Figure 44 when first heated, i.e., when it was still WC. There is a radical change in emissivity between 1800°K and 2000°K. This is a reversible phenomenon for when the specimen is cooled, the emissivity at 1600°K and 1800°K will repeat.

When this specimen was X-rayed, it was at first believed that a new phase of tungsten-carbon was present. From trial and error method and by fitting of data on Hull-Davy [11] charts it was found that the sample can be satisfactorily indexed in the tetragonal system. It turns out that the indices of the diffraction lines when based on a tetragonal system are the same as those for the case of similarly positioned lines in hexagonal α - W_2C. So far, the structure of this phase has not been completely elucidated, i.e., the number and position of W and C atoms in the tetragonal unit cell has not been determined.

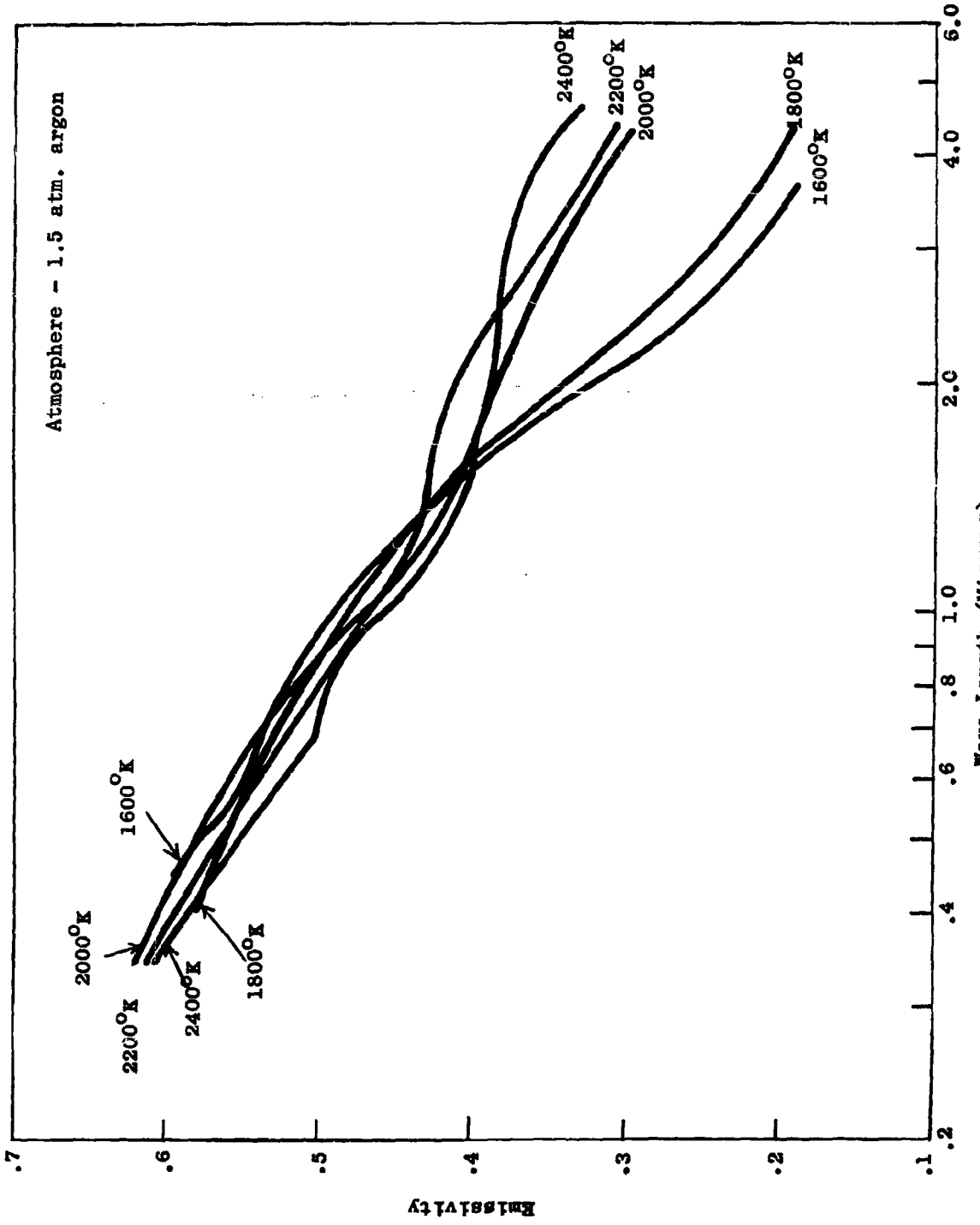

Figure 45 Normal Spectral Emissivity of α W_2C

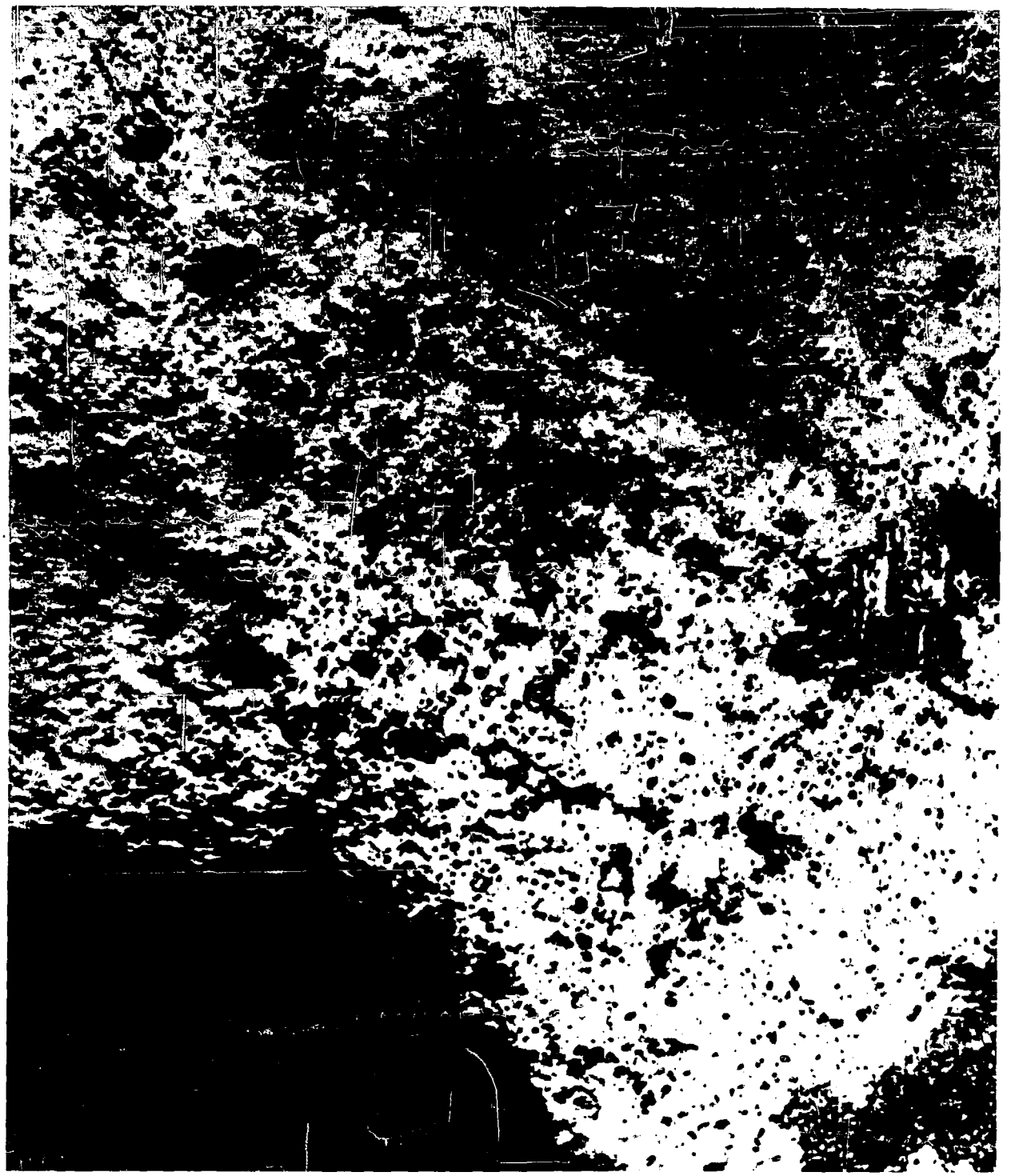

FIGURE 46. TUNGSTEN CARBIDE SPECIMEN BEFORE HEATING.

FIGURE 47. TUNGSTEN CARBIDE SPECIMEN AFTER HEATING TO 2000°K (NOW W_2C SURFACE).

FIGURE 48. TUNGSTEN CARBIDE SPECIMEN AFTER HEATING TO 2400°K.

7. Zirconium

Since zirconium melts at slightly above 2100°K, none of the measurements were made above 2000°K. An attempt was made at 2100°K (Zr#5), but a sudden surge in line voltage heated the specimen to its melting point. Examination by X-ray diffraction indicates that the specimens, prior to heating, are alpha zirconium. Photomicrography of these polished specimens reveal a smooth, fine grained surface (Figure 49).

All the specimens were heated in vacuum with a pressure of 10^{-6} mm. In all cases, when the specimen was first heated, the surface became blackened.

The first specimen was removed soon after it had blackened (heating time = 0.25 hr). It was photomicrographed (Figure 50) and X-rayed. The X-ray diffraction pattern obtained from this specimen was considerably more complex than the pattern obtained from the specimen before thermal treatment. In addition to the alpha-zirconium diffraction lines, the "extra" diffraction lines appear to fit well into the standard ASTM diffraction data for ZrB.

With each of the remaining specimens, when its surface became blackened, the temperature was raised to 2000°K under hard vacuum for about half an hour. This removed the black deposit from the surface of the specimen.

Figures 51, 52 and 53 give the emissivity of some zirconium specimens from 1400°K - 2000°K. The curves displayed in Figures 51 and 52 are quite similar. The curves shown in Figure 53, while somewhat smoother, are also higher

The specimen used in Figure 53 is the one mentioned previously as having melted. Extensive tests could not be made with this specimen and no X-ray diffraction examination was made after heating.

From the measurements made thus far, zirconium does not seem to exhibit typical metallic behavior, i.e., there is no x-point unless it occurs around 3 or 4 microns. However, it is quite possible that these curves are deceiving since there is a tremendous crystallite growth and a preferred orientation taking place in the specimens. Photomicrographs of zirconium specimens #2 and #4 can be seen in Figures 54 and 55.

The following table shows the X-ray diffraction data for specimens #2, 3, and 4 after they had been heated.

	Zr#2			Zr#3			Zr#4	
d	I/i_L	(hkl)	d	I/i_L	(hkl)	d	I/i_L	(hkl)
2.81	100	100	-	-	-	-	-	-
1.40	50	200	1.61	50	110	-	-	-
.934	80	300	1.01	100	114	1.01	100	114

FIGURE 49. POLISHED ZIRCONIUM SPECIMEN PRIOR TO HEATING.

FIGURE 50. ZIRCONIUM SPECIMEN AFTER HEATING TO 1160°K. BLACK DEPOSIT FORMED ON SURFACE.

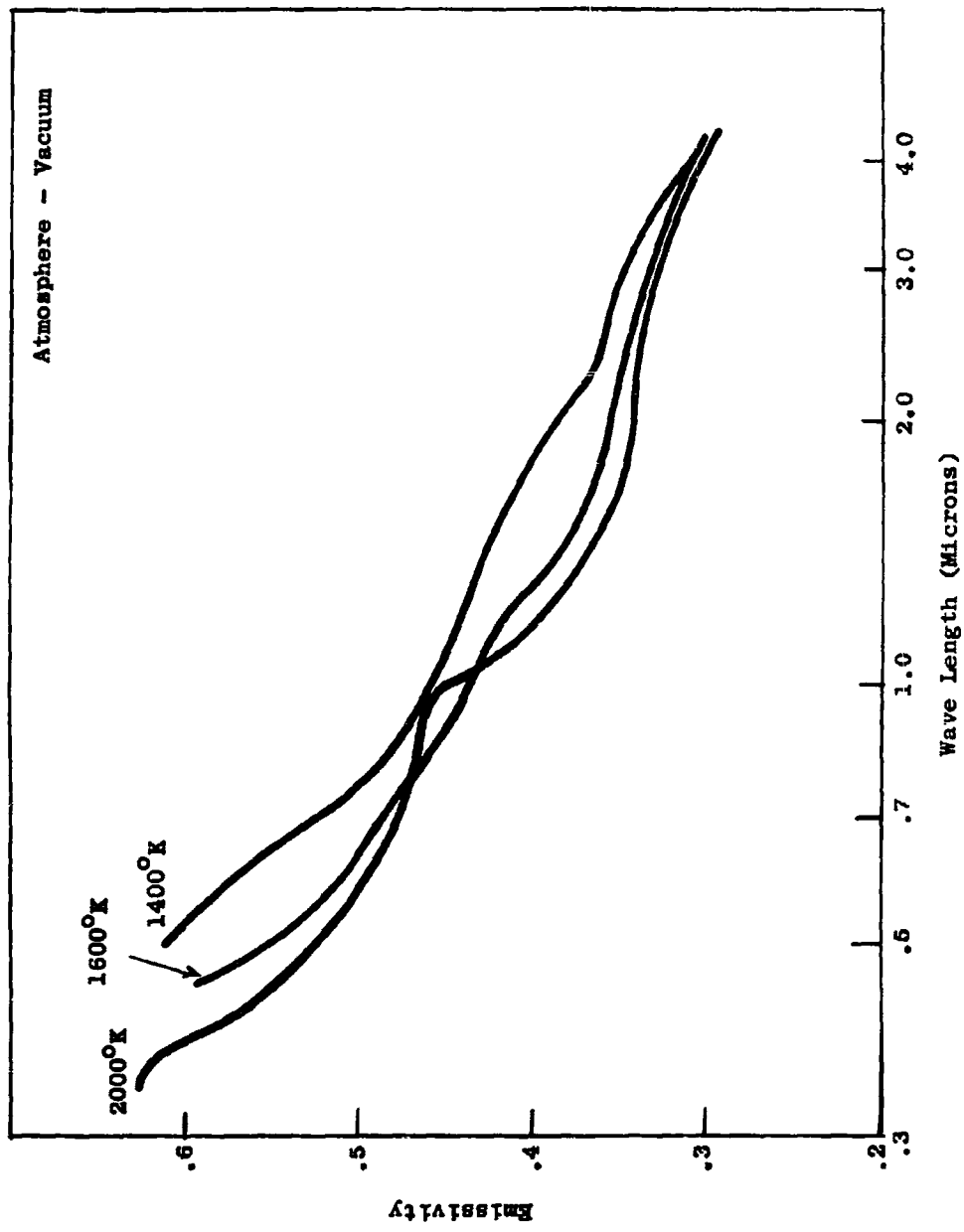

Figure 51 Normal Spectral Emissivity of Zirconium Specimen #2

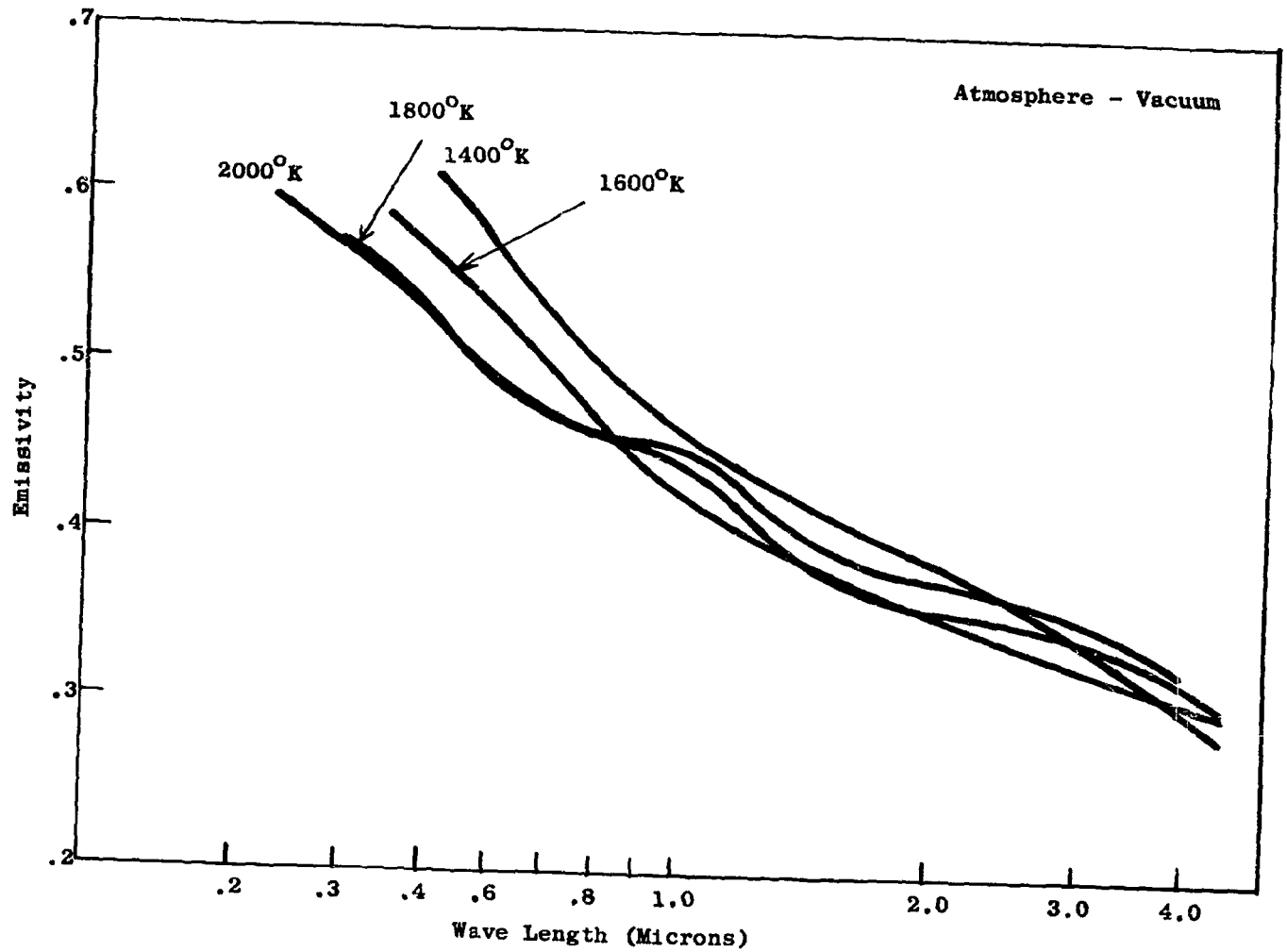

Figure 52 Normal Spectral Emissivity of Zirconium Specimen #4

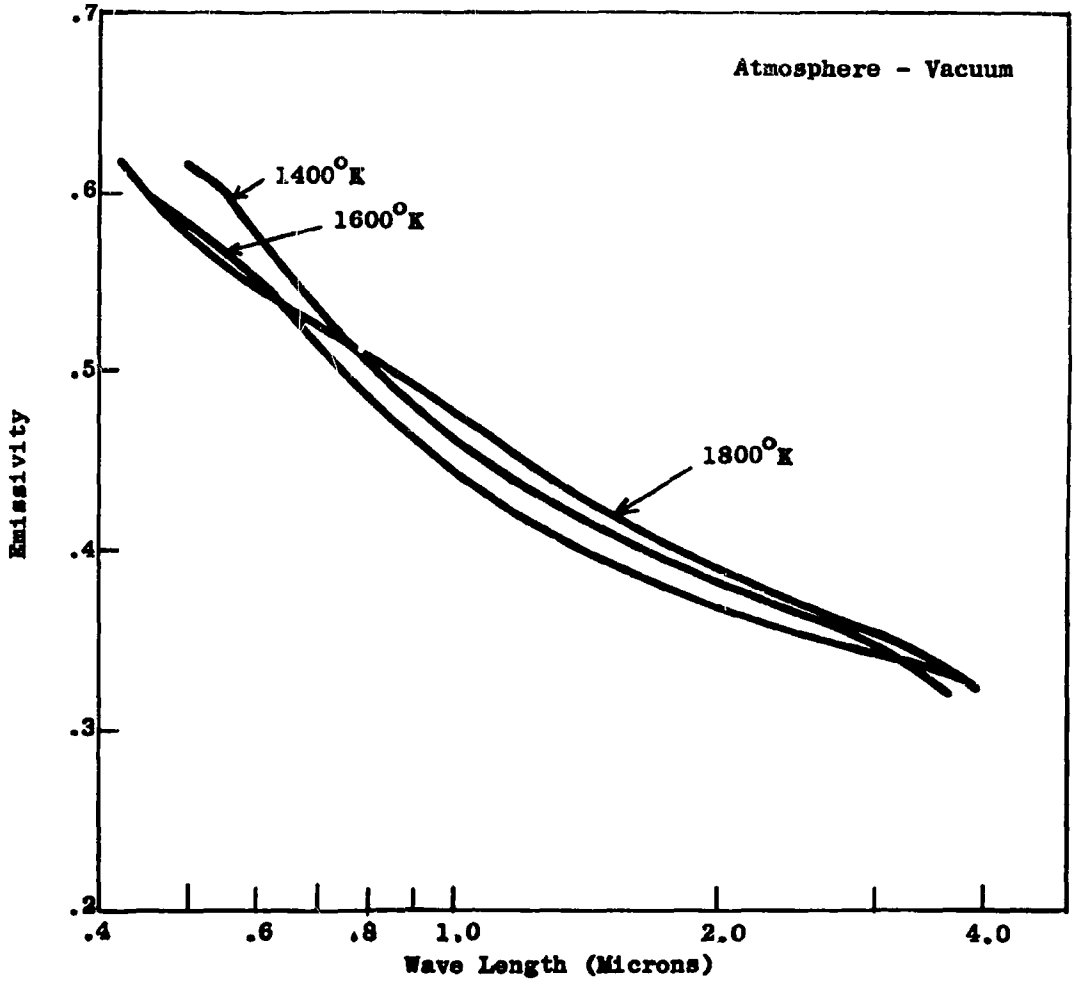

Figure 53 Normal Spectral Emissivity of Zirconium Specimen #5

FIGURE 54. ZIRCONIUM SPECIMEN AFTER HEATING TO 2000°K, SHOWING EXTENSIVE CRYSTAL GROWTH.

Figure 55. Zirconium Specimen After Heating To 2000°K, Shows Some Crystal Growth

FIGURE 56. ZIRCONIUM SPECIMEN HEATED A SHORT TIME SHOWING VARIANCE OF CRYSTAL STRUCTURE.

These data indicate that for Zr#2, the crystallites after testing have become preferentially oriented such that the "c" direction is normal to the surface of the specimen. On the other hand, Zr#3 and Zr#4 indicate preferentially oriented crystallites with the (114) planes parallel to the specimen surface. The degree of preferred orientation in Zr#3 appears to be less than that for sample Zr#4. The angle between (110) and (114) planes in a hexagonal system is

$$\varphi\ (110),\ (114) = \cos^{-1}\left[1 + \left(\frac{2a}{c}\right)^2\ \right]^{-1/2}$$

For Zr, c/a =1.593 and therefore $\varphi_{(110),\ (114)}$ is approximately 51.5^{o}.

8. Calculation of Total Emissivities

The calculation of total emissivity is discussed in reference 1. The conversion table (Table 34) of spectral emissivity to total emissivity is reprinted here to show how the total emissivities in Figure 57 were computed.

Plotted in Figures 58, 59 and 60 are total emissivities of ZrC, TaC, WC. The dashed curves are the results reported by Southern Research Institute, [12] while the solid curves represent our efforts. The discrepancy is quite large being as much as a factor of three in some instances (TaC at 1600^{o}K). Reason for the discrepancy is not known. It is conceivable that the specimens used by SRI had free carbon forming on their surfaces, especially when one considers the total emissivity of carbon. It is also noted that chemical analysis was not completed at SRI after heating. Tungsten carbide (WC) was found, here, to be unstable at temperatures above 1800^{o}K. It may have been that SRI experienced an extensive carbon loss for this specimen which would account for their curve in Figure 60 being lower than 58 and 59.

The method employed by SRI in determining total emissivity was by measuring the total radiation of the heated specimen and comparing it to the total radiation of a blackbody. Since

$$J\ (T) = \varepsilon_{(T)}\ \sigma\ T^4$$

the temperature must be monitored very carefully or the error will be magnified to the fourth power.

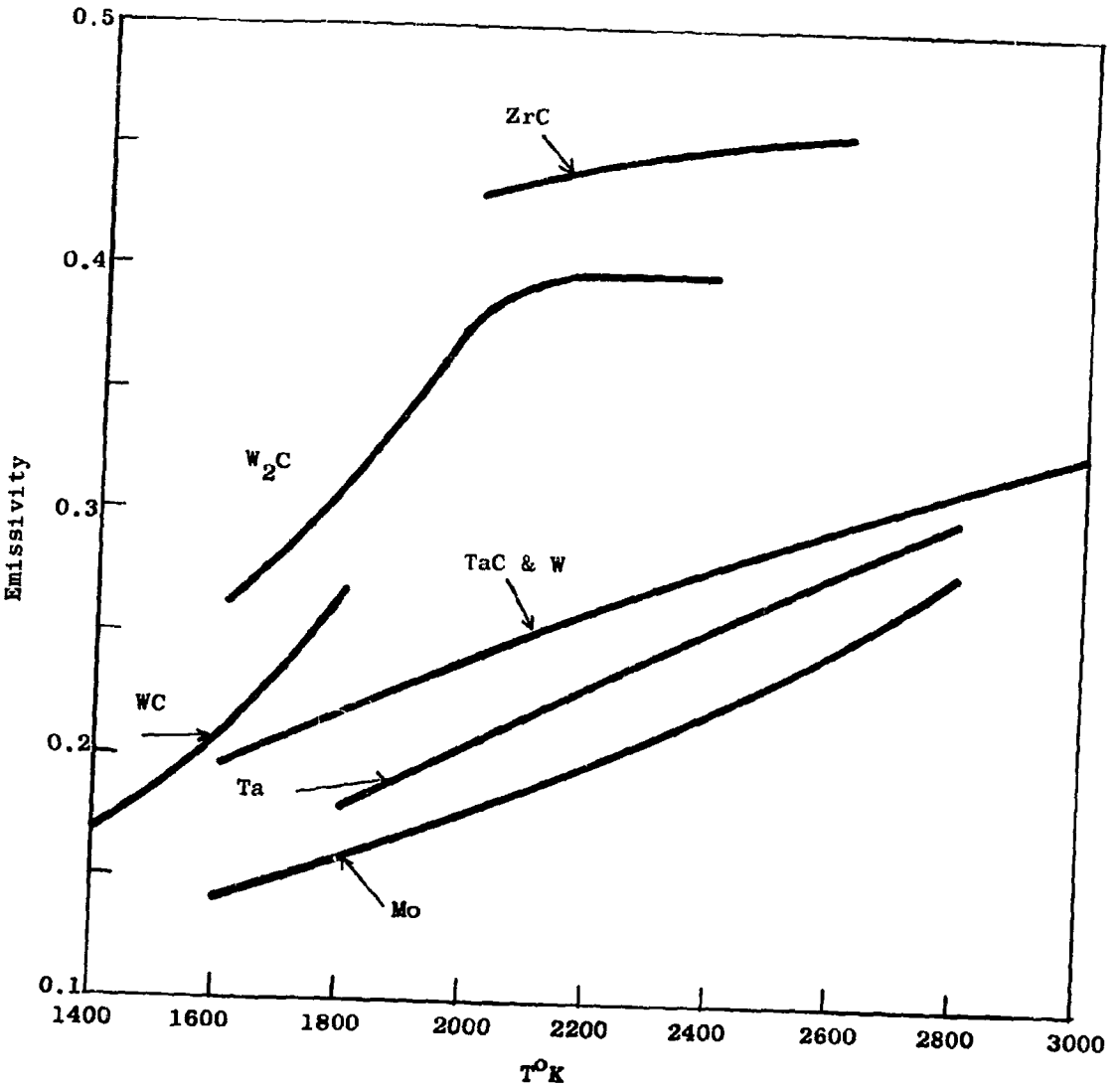

Figure 57 Normal Total Emissivity of Various Materials

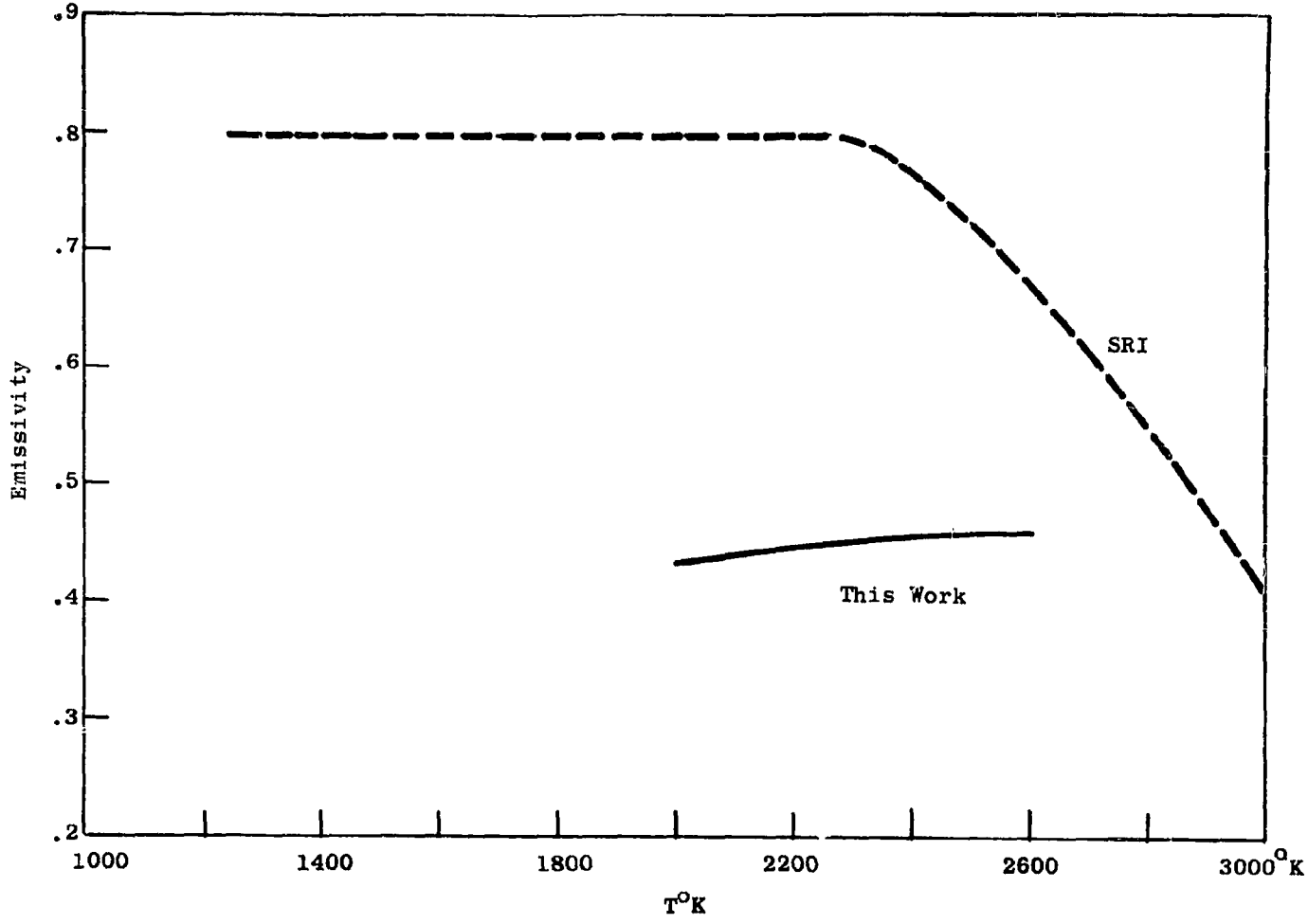

Figure 58 Normal Total Emissivity of ZrC

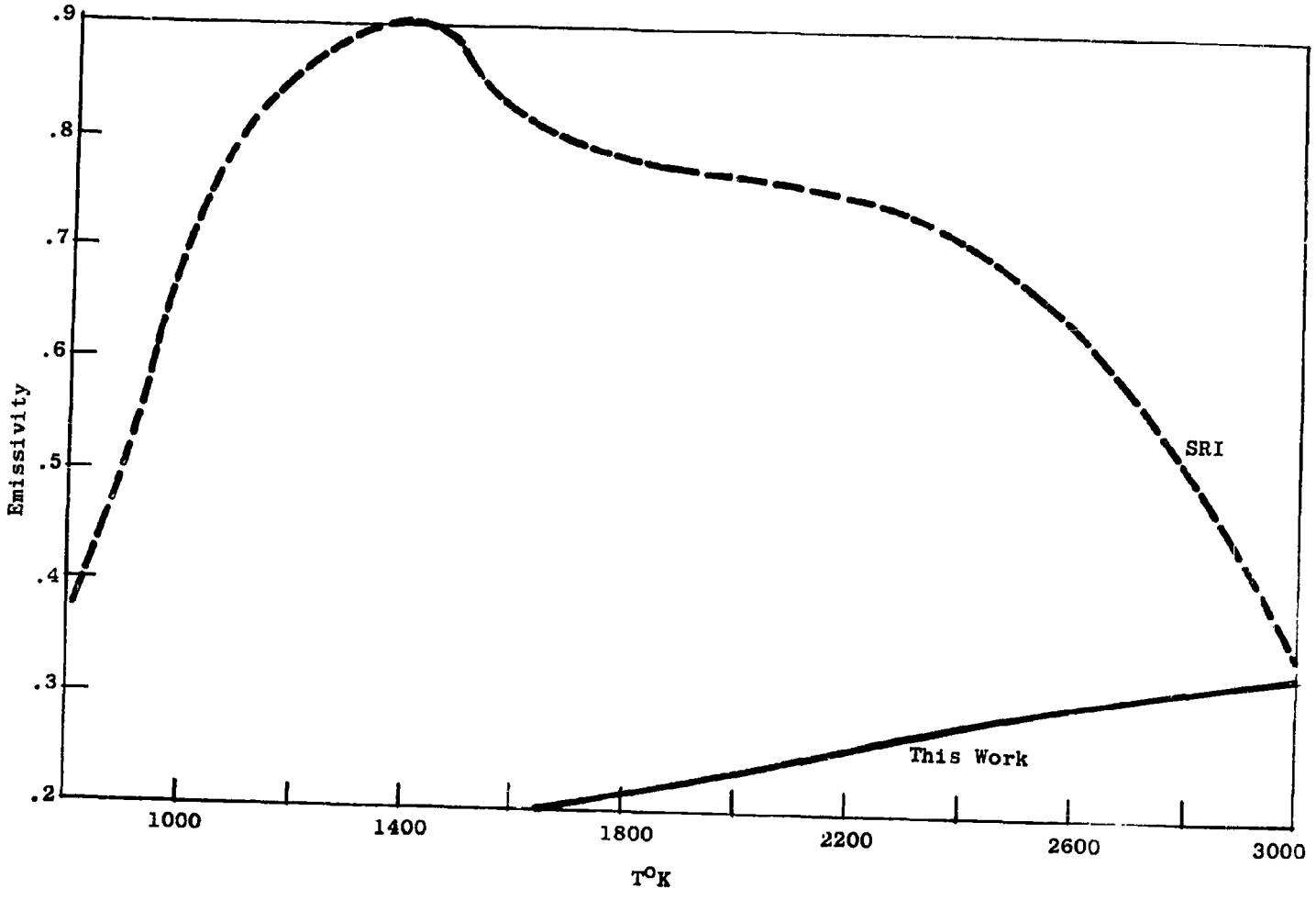

Figure 59 Normal Total Emissivity of TaC

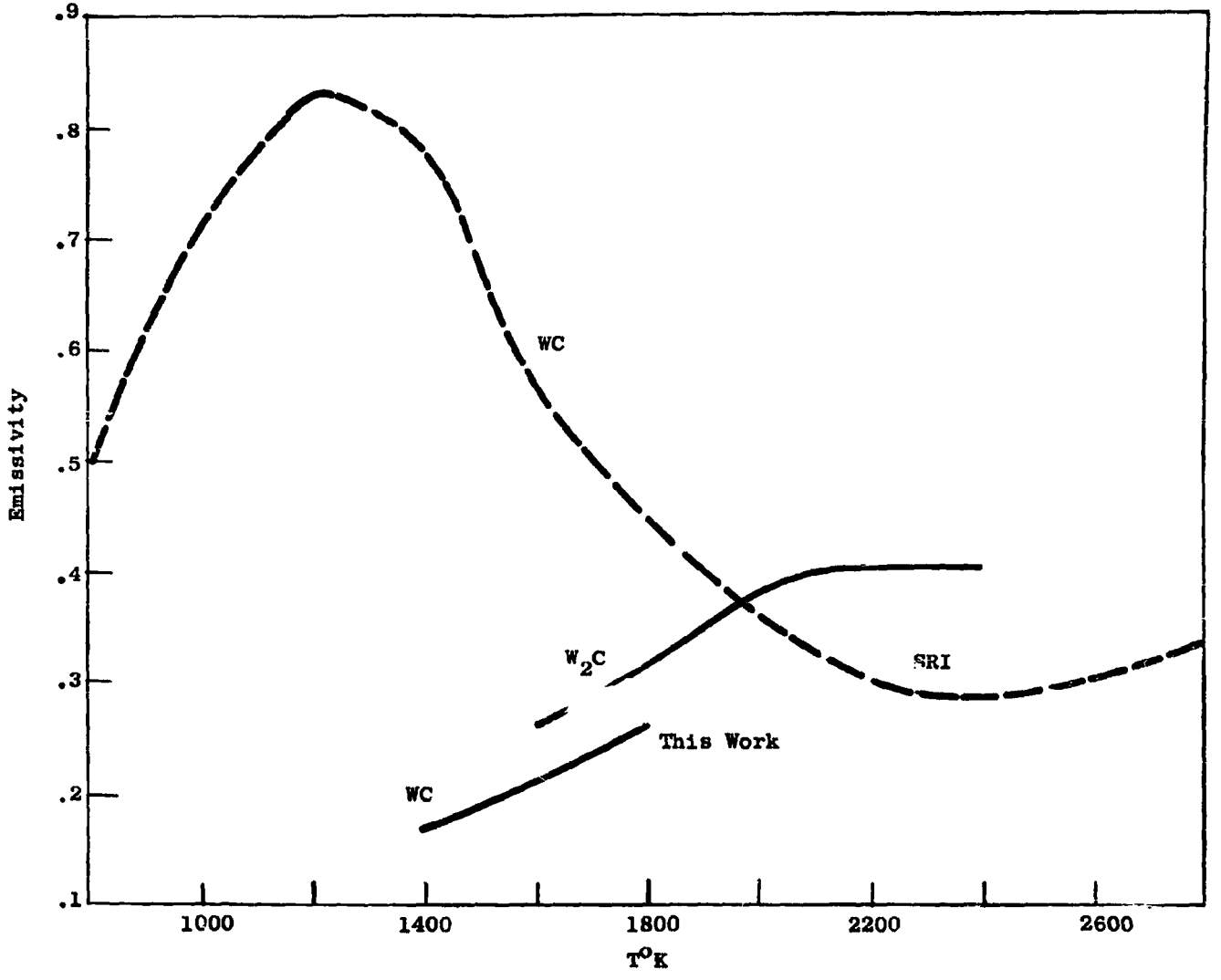

Figure 60 Normal Total Emissivity of Tungsten Carbides

TABLE 34 - CONVERSION OF SPECTRAL EMISSIVITY TO TOTAL EMISSIVITY

Mean Wavelength[1] or Wavelength Interval (in microns)	Fraction of Total Energy at Effective Mean Wavelength								
	1400°	1600°	1800°	2000°	2200°	2400°	2600°	2800°	3000°K
0.5[2]	-	-	-	-	-	-	.01	.01	.01
0.6[2]	-	-	-	-	.006	.01	.01	.02	.03
0.7[2]	-	-	-	.01	.014	.02	.025	.03	.04
0.8[2]	.001	.004	.01	.01	.02	.03	.035	.05	.06
0.9	.002	.006	.01	.02	.03	.04	.05	.06	.07
1.0	.007	.01	.02	.03	.03	.04	.06	.06	.06
1.1	.02	.04	.06	.07	.09	.11	.11	.13	.13
1.3	.03	.05	.07	.07	.10	.09	.12	.11	.12
1.5	.05	.07	.08	.09	.10	.09	.10	.09	.09
1.7	.06	.07	.08	.09	.08	.09	.08	.08	.07
1.9	.035	.08	.08	.08	.08	.07	.06	.06	.06
2.2	.155	.13	.13	.12	.12	.11	.10	.09	.08
2.6	.11	.10	.10	.10	.08	.07	.07	.06	.05
3.0	.10	.09	.08	.08	.06	.05	.04	.04	.04
3.4	.07	.07	.06	.05	.04	.04	.03	.03	.02
3.8	.06	.05	.04	.04	.04	.03	.02	.04	.02
4.5	.11	.09	.07	.06	.04	.04	.04	.02	.02
Above 5.0 [3]	.19	.14	.11	.08	.07	.05	.04	.04	.03
All Wavelengths	1.00	1.00	1.00	1.00	1.00	1.00	1.00	1.00	1.00

(1) Mean wavelengths are not spaced equally but rather are spaced to adequately reflect rate of emissivity variation with wavelength for many opaque solid materials.

(2) Shortest wavelength used is a function of temperature and includes all radiation below that wavelength.

(3) Spectral emissivity varies slowly at the long wavelength end of the spectrum where only a small fraction of the energy remains - particularly at the higher temperatures.

D. References

1. Coffman, J. A., Kibler, G. M., Riethof, T. R., Watts, A. A., Carbonization of Plastics and Refractory Materials Research, WADD Technical Report 60-646, Part I, (1961).

2. Worthing, A. G., "Temperature Radiation Emissivities and Emittances," p. 1164 in Temperature, Its Measurement and Control in Science and Industry, New York, Reinhold, 1941.

3. Blau, H. H., Jr., "Measurement of Flux, Emittance, and Related Properties," p. 45, Proceedings of International Symposium on High Temperature Technology, McGraw-Hill, October 1959.

4. Brugel, W., "Strahlungsmessungen on Elektrisch Geheizten SiC Staben," Z. Physik 127, 400 (1959).

5. DeVos, J. C., "A New Determination of the Emissivity of Tungsten Ribbon," Physica 20, 690 (1954).

6. Marple, D. T. F., "Spectral Emissivity of Rhenium," J. Opt. Soc. Am. 46, 490 (1956).

7. Riethof, T. R. "High Temperature Spectral Emissivity Studies," Proceedings of Conference on "Radiative Transfer from Solid Materials," Boston, December 1960.

8. Harrison, W. N., Richmond, T. C., Plyler, E. K., Stair, R., and Skranstad, H. K., Standardization of Thermal Emittance Measurements, WADC Technical Report 59-510, March 1960.

9. Becker, K., Z. Metallkunde 20, 437 (1928)
   Z. Physik 51, 481 (1928)

10. Pearson, W. B., A Handbook of Lattice Spacings and Structures of Metals and Alloys, Pergamon Press, 965 (1958).

11. Battelle Indexing Charts for Diffraction Patterns of Tetragonal, Hexagonal and Orthorhombic Crystals, J. C. Bell and A. E. Austin, Battelle Memorial Institute, Columbus, Ohio.

12. The Thermophysical Properties of Refractory Materials from 2000°F to their Destruction Temperature, Aeronautical Systems Division, Wright-Patterson Air Force Base, Contract No. AF 33(616)-7319.

APPENDIX A - THE VAPORIZATION OF GRAPHITE, TiC, ZrC AND HfC*

Guido L. Vidale

I. THE VAPORIZATION OF GRAPHITE

The most recent information available on the vapor pressure of carbon molecules over graphite is summarized below. These data are based primarily on the recent study by Drowart et al. [1] which generally confirms most of the most recent studies of this system.

It is assumed, therefore, that five molecular species are significant components of the vapor in equilibrium with the solid phase:

$$C_1,\ C_2,\ C_3,\ C_4 \text{ and } C_5.$$

Vapor pressure and equilibrium constants are given below for the temperature range 2500 - 4100°K. At the higher temperatures the data given become increasingly uncertain because they are based on long extrapolations of results obtained at lower temperatures, and because higher molecular weight molecules which are ignored here probably become increasingly important.

The vapor pressure of carbon atoms is known to a high degree of accuracy, and no improvement of the values listed in Stull and Sinke [2] need be made. The vapor pressure of C, given by equation (43) has, therefore, been obtained by fitting the data from 2500 - 3000°K.

$$\log P_{C_1} = 8.115 - \frac{37,170}{T} \qquad (43)$$

Vapor pressure values for the other four molecules are considerably less certain. They may be calculated from data given in Reference 1 by three methods.

In method (1) it is assumed the vapor pressure curves given in Reference 1 are correct and may be extrapolated linearly up to 4100°K. This implies, among other things, that the ionization cross section used by Inghram is correct at all temperatures.

Method (2) instead makes use of the assumption that the ionization cross section is roughly correct at a single temperature and relies on the free energy functions from estimated molecular parameters. This is the so called "Third Law" method of determining the vapor pressure.

---

* These calculations were performed under this contract, AF 33(616)-6841 prior to the experimental work presented in the body of this report.

Method (3) makes no use of ionization cross section, but uses heavily the assumptions that temperature dependence of the vapor pressure is given correctly by the experiment and that the free energy functions are correct. This is the so called "Second Law Method".

Values calculated using the three methods are given in Table 35. Two sets of values of the vapor pressure of some molecules are given in order to show what errors would be expected as a result of uncertainties in the knowledge of the appropriate free energy functions of the gaseous species.

Methods (2) and (3) are somewhat more logically consistent, since any error is due only to uncertainties in the knowledge of the basic thermodynamic properties, while approximation (1) also contains a linear extrapolation not justified by theory.

The discrepancy in the vapor pressures listed using "Second Law" and "Third Law" calculations cannot be resolved, since it is not apparent to this author that either method is inherently superior to the other in mass spectroscopy determinations of vapor pressure. In view of the magnitude of this discrepancy, it seems that the use of approximation (1) does not diminish significantly the reliability of the calculated pressures.

TABLE 35

$\log_{10}$ of the Vapor Pressure of Carbon Polymer Molecules

Molecule	T = 2000	2500	3000
	Method (1) - Linear Extrapolation		
C_2	-11.64	-7.39	-4.56
C_3	-10.53	-6.51	-3.83
C_4	-14.40	-9.48	-6.21
C_5	-14.31	-9.27	-5.91
	Method (2) - Third Law		
C_2	-11.67	-7.37	-4.54
C_3	-10.57	-6.52	-3.86
C_4	-14.61	-9.41	-5.98
	-14.55	-9.42	-6.04
C_5	-14.45	-9.25	-5.83
	-14.34	-9.27	-5.94
	Method (3) - Second Law		
C_2	-11.43	-7.18	-4.38
C_3	-10.42	-6.40	-3.76
C_4	-13.41	-8.45	-5.18
	-13.68	-8.72	-5.45
C_5	-13.60	-8.57	-5.26
	-14.14	-9.11	-5.81

Note: Where two values of log P are given, they have been obtained using different, but equally probable, values of the molecular parameters.

This simpler method of computation, which is almost identical to the "Third Law" method, is used in calculating the vapor pressures given in Tables 36 and 37.

TABLE 36

Log P (C_n)

T°K	n = 1	n = 2	n = 3	n = 4	n = 5	Log P Total
2000	-10.47	-11.64	-10.53	-14.40	-14.31	-10.18
2100	- 9.59	-10.63	- 9.58	-13.23	-13.11	- 9.26
2200	- 8.78	- 9.71	- 8.71	-12.17	-12.02	- 8.42
2300	- 8.05	- 8.87	- 7.91	-11.19	-11.02	- 7.65
2400	- 7.37	- 8.10	- 7.18	-10.30	-10.11	- 6.94
2500	- 6.75	- 7.39	- 6.51	- 9.48	- 9.27	- 6.28
2600	- 6.18	- 6.74	- 5.89	- 8.73	- 8.50	- 5.68
2700	- 5.65	- 6.13	- 5.32	- 8.03	- 7.78	- 5.11
2800	- 5.16	- 5.57	- 4.79	- 7.38	- 7.11	- 4.59
2900	- 4.70	- 5.05	- 4.30	- 6.77	- 6.49	- 4.10
3000	- 4.28	- 4.56	- 3.83	- 6.21	- 5.91	- 3.64
3100	- 3.88	- 4.10	- 3.40	- 5.68	- 5.37	- 3.21
3200	- 3.50	- 3.67	- 3.00	- 5.18	- 4.86	- 2.81
3300	- 3.15	- 3.27	- 2.61	- 4.72	- 4.38	- 2.43
3400	- 2.82	- 2.89	- 2.26	- 4.28	- 3.94	- 2.07
3500	- 2.51	- 2.54	- 1.92	- 3.86	- 3.51	- 1.73
3600	- 2.21	- 2.20	- 1.60	- 3.47	- 3.11	- 1.41
3700	- 1.93	- 1.88	- 1.30	- 3.11	- 2.73	- 1.20
3800	- 1.67	- 1.58	- 1.01	- 2.76	- 2.37	- 0.82
3900	- 1.42	- 1.29	- 0.74	- 2.42	- 2.03	- 0.55
4000	- 1.18	- 1.02	- 0.48	- 2.11	- 1.71	- 0.28
4100	- 0.95	- 0.76	- 0.24	- 1.81	- 1.40	- 0.04

TABLE 37

Composition of C_n Vapor (Method 1)

T°K	Total P	Ave. M.W.	N_C	N_{C_2}	N_{C_3}	N_{C_4}	N_{C_5}
2500	5.255×10^{-7}	27.0	.336	.077	.585	.0006	.001
2700	7.773×10^{-6}	28.0	.287	.095	.615	.001	.002
2900	8.009×10^{-5}	28.8	.248	.112	.634	.002	.004
3100	6.177×10^{-4}	29.4	.216	.128	.645	.003	.007
3300	3.740×10^{-3}	30.0	.190	.143	.651	.005	.011
3500	1.861×10^{-2}	30.5	.168	.157	.651	.007	.016
3700	7.810×10^{-2}	31.1	.150	.169	.647	.010	.024
3900	2.853×10^{-1}	31.5	.134	.180	.640	.013	.032
4100	9.231×10^{-1}	32.1	.121	.189	.630	.017	.043

These pressures, which are shown in Figure 61, were calculated from the following equations:

$$\log P_{C_2} = 9.605 - \frac{42,490}{T} \quad (44)$$

$$\log P_{C_3} = 9.571 - \frac{40,210}{T} \quad (45)$$

$$\log P_{C_4} = 10.184 - \frac{49,170}{T} \quad (46)$$

$$\log P_{C_5} = 10.889 - \frac{50,400}{T} \quad (47)$$

From equations 43-47, the equilibrium constants relating the equilibrium pressures of the various gaseous species are calculated:

$$2C(g) = C_2(g)$$

$$\log K_2 = \log \frac{P_{C_2}}{P_C{}^2} = -6.625 + \frac{31,850}{T} \quad (48)$$

$$3C(g) = C_3(g)$$

$$\log K_3 = \log \frac{P_{C_3}}{P_C{}^3} = -14.774 + \frac{71,300}{T} \quad (49)$$

$$4C(g) = C_4(g)$$

$$\log K_4 = \log \frac{P_{C_4}}{P_C{}^4} = -22.276 + \frac{99,510}{T} \quad (50)$$

$$5C(g) = C_5(g)$$

$$\log K_5 = \log \frac{P_{C_5}}{P_C{}^5} = -29.686 + \frac{135,450}{T} \quad (51)$$

These log K values are tabulated in Table 38.

It is clear that the second decimal digit of log P is most uncertain in all cases.

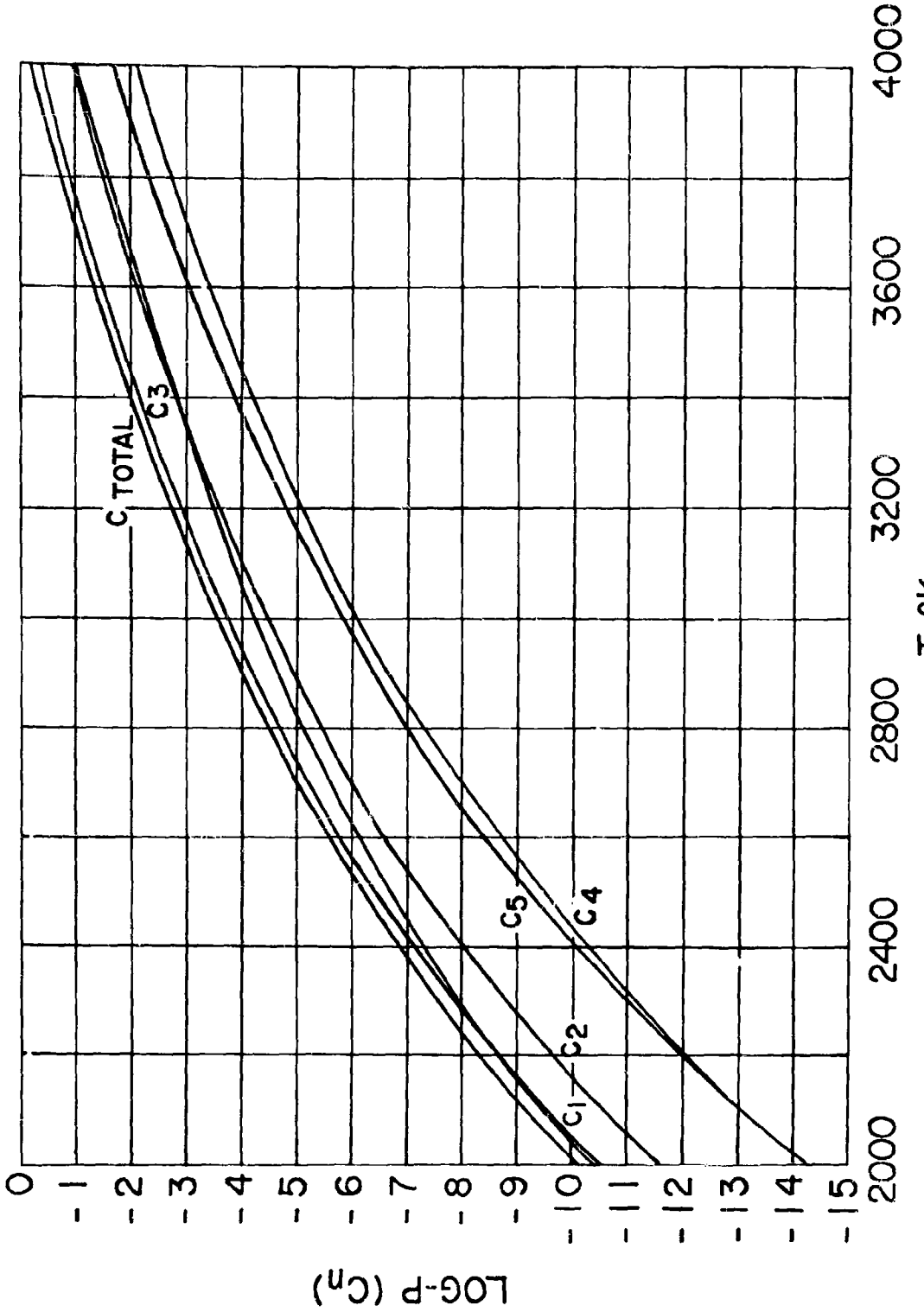

Figure 61. The Vapor Pressure Of C_n Over Graphite

TABLE 38

Logarithms of Equilibrium Constants for Carbon Vapor Equilibria

T°K	log K_2	log K_3	log K_4	log K_5
2000	9.300	20.876	27.479	38.039
2100	8.542	19.178	25.110	34.814
2200	7.852	17.635	22.956	31.882
2300	7.223	16.226	20.989	39.205
2400	6.646	14.934	19.186	26.752
2500	6.115	13.746	17.528	24.494
2600	5.625	12.649	15.997	22.410
2700	5.171	11.633	14.580	20.481
2800	4.750	10.690	13.263	18.689
2900	4.358	9.812	12.038	17.021
3000	3.992	8.993	10.894	15.464
3100	3.649	8.226	9.824	14.008
3200	3.328	7.507	8.821	12.642
3300	3.027	6.832	7.878	11.359
3400	2.743	6.196	6.992	10.152
3500	2.475	5.597	6.155	9.014
3600	2.222	5.032	5.366	7.939
3700	1.983	4.496	4.618	6.922
3800	1.757	3.989	3.911	5.959
3900	1.542	3.508	3.239	5.045
4000	1.337	3.051	2.602	4.176
4100	1.143	2.616	1.995	3.350

II. THE VAPORIZATION OF TiC, ZrC AND HfC

A. Introduction

In this section it is desired to calculate the vapor pressure of TiC, ZrC and HfC by making use of available thermal data for these compounds and the known vapor pressure of the pure elemental substances.

The equimolar carbides listed above are known to be particularly high melting substances, as may be seen in Table 39, and they have a particularly low vapor pressure. They are, therefore, among the few possible materials for use at temperatures in excess of 2500°C.

TABLE 39

Melting Points and Eutectic of Carbides of Ti, Zr and Hf

Metal	Melting Point of Carbide °C	Eutectic on Carbon Side
Ti	3250	N = 0.63 2900°C
Zr	3100 - 3530	N = ? 2430°C
Hf	3890	N = ? 2800°C

A computation of their vapor pressure requires the following information:

1. The phase diagram of the binary system under consideration.

2. The formula of the various gaseous species present in the equilibrium vapor.

3. Thermal data of the condensed carbide phase and of the gaseous species. These data may consist either of the free energy function and free energy of formation of all relevant species, or of the enthalpy and entropy of formation of these species. These two sets of data are equivalent, and are readily interconverted. In this case, the use of enthalpy and entropy values is more convenient as will be seen below.

B. Phase Diagrams

The phase diagram of the Ti - C system has been studied in some detail[3]. A single compound is present having an ideal formula of TiC. This compound is known to dissolve titanium metal, forming a variable composition phase, but does not dissolve excess carbon. The compound forms simple eutects with both excess titanium and excess carbon. This behavior is shown in Figure 62, which is the phase diagram in question reproduced from Reference 3.

Less information is available about the other two systems (see Reference 3). As might be expected, however, zirconium and hafnium behave very similarly to titanium. Both form an interstitial carbide similar in structure to the TiC phase. While these carbides also do not appear to dissolve excess carbon, it is known that HfC dissolves excess metal, and it seems reasonable to suppose that ZrC does also. This behavior is also predicted on the basis of theoretical arguments [4]. In these cases also, the melting point maximum occurs at, or very close to, the

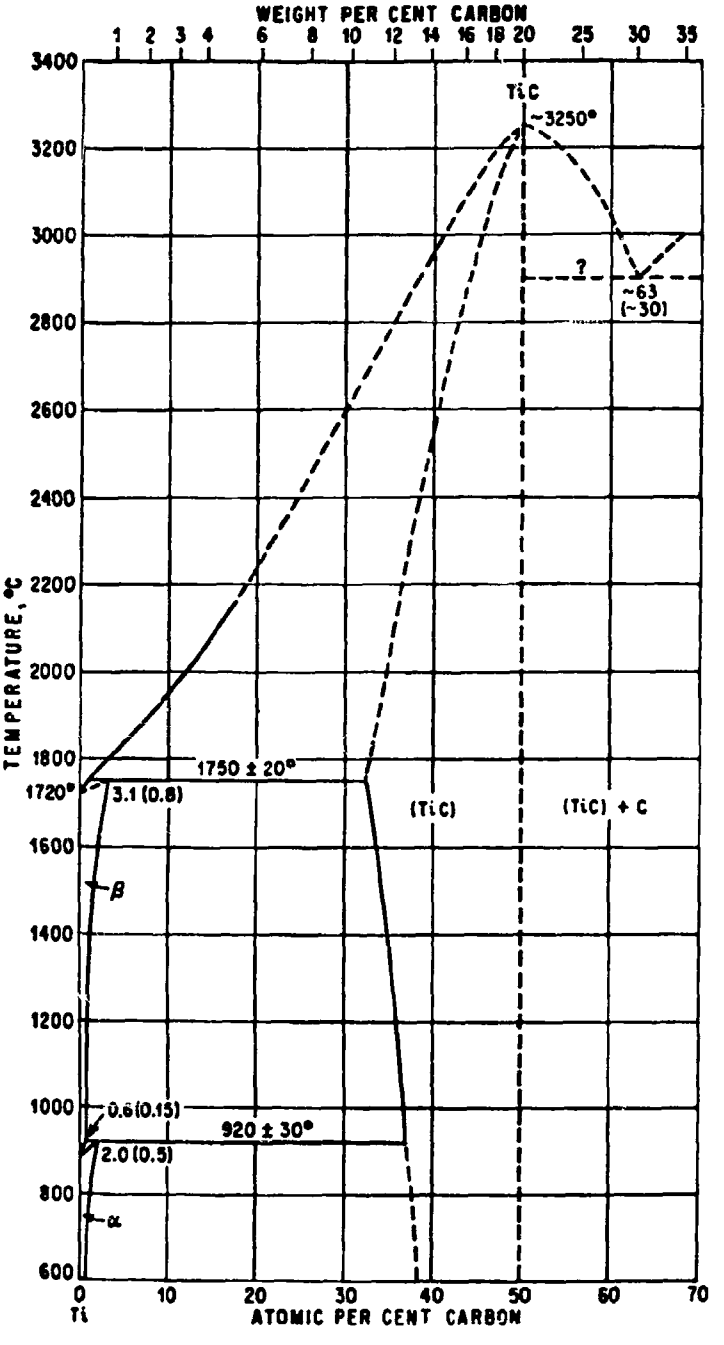

Figure 62. Phase Diagram Of Carbon-Titanium System

equimolar composition, and simple eutectics are formed with both excess metal and excess carbon. The melting point and eutectic temperatures of the three systems are listed in Table 39.

From these diagrams it can be seen that, if the metal has a volatility of the same order as carbon, the vaporization of the equimolar carbide phase proceeds congruently until the whole sample is vaporized. If the metal is much more volatile than carbon, a carbon-rich phase forms during the vaporization process, and the vapor pressure remains constant until enough material has vaporized to convert all of the carbide phase to the carbon rich phase. This latter phase can be a liquid solution or a solid carbon phase saturated with carbide.

If the metal is less volatile than carbon, the equilibrium vapor composition over the carbide phase may change continuously with time, because the composition of the condensed phase is also changing continuously as a result of preferential loss of carbon from this phase. In this case, it may be necessary to know the partial molar thermodynamic properties as a function of the precise composition of the condensed phase. These are not known even approximately for the systems in question. It has therefore been necessary to ignore the presence of solid solubility in all cases. This approximation does not affect the calculated vapor pressure of TiC, is not likely to lead to serious errors in the case of ZrC, but may be quite serious for HfC.

C. Composition of the Gas Phase

TiC, on vaporizing, has been reported to form only titanium and carbon atoms[5] as well as the carbon polymer molecules discussed in the first part of this report. At 2500°K, for example, the ratio of titanium atoms to all possible titanium carbide molecules is greater than 40 to 1[5]. Although, at higher temperatures gaseous carbide molecules are more likely to be important constituents of the equilibrium vapor[6], they can probably be safely ignored at temperatures lower than the boiling point of TiC.

No definite information is available for ZrC and HfC. No gaseous carbide molecules of these carbides have been sought or have been observed accidentally in mass spectroscopic studies. It is clear, however, that at temperatures lower than 2500°C, no detectable vapor pressure of such species is encountered for tungsten, molybdenum or tantalum[7]. From this information, and from estimates of vapor pressure of MC_2 molecules based on the suggestion[5] that the heat of

$$M(g) + C_2(g) = MC_2(g) \qquad (52)$$

is approximately 30 kcal less than that of

$$M(g) + O(g) = MO(g), \qquad (53)$$

it seems likely that these gaseous carbides can be ignored at temperatures lower than 3000°C. MC_2 and MC may, however, become as important as gaseous M at 4000°.

In the absence of any precise information it has been decided to ignore such species, and to calculate the vapor pressure only of atomic species and of carbon polymer molecules. These are unaffected by the presence or absence of other molecules and probably account for most of the vapor pressure in the temperature range of greatest interest (2500-3000°).

D. Thermodynamic Equations Used

The vapor pressure of metal and of carbon can be obtained from the following thermodynamic equations for the vaporization reaction in question:

$$\Delta F^{o}_{T} = - RT \ln K \tag{54}$$

$$\Delta F^{o}_{T} = \Delta H^{o}_{T} - T\Delta S^{o}_{T} \tag{55}$$

The enthalpy and entropy changes for the reaction are obtained from the standard molar entropy and enthalpy of formation of each product (i) and reactant (j) by:

$$\Delta H^{o}_{T} = \sum_{i} \Delta H^{o}_{fT}(i) - \sum_{j} \Delta H^{o}_{fT}(j) \tag{56}$$

and

$$\Delta S^{o}_{T} = \sum_{i} \Delta S^{o}_{fT}(i) - \sum_{j} \Delta S^{o}_{fT}(j) \tag{57}$$

or alternately

$$\Delta S^{o}_{T} = \sum_{i} S^{o}_{T}(i) - \sum_{j} S^{o}_{T}(j) \tag{58}$$

The temperature dependence of these quantities is obtainable from heat capacity data by:

$$\Delta H^{o}_{fT} = \Delta H^{o}_{f298} + \int_{298}^{T} \Delta C_p \, dT \tag{59}$$

$$\Delta S^{o}_{fT} = \Delta S^{o}_{f298} + \int_{298}^{T} \frac{\Delta C_p}{T} \, dT \tag{60}$$

or

$$\Delta S^{o}_{T} = \int_{o}^{T} \frac{C_p}{T} \, dT; \tag{61}$$

If a phase transition should occur in the temperature interval of the integration, or if residual entropy should be present at 0°K, a term must be added to equations 59, 60 and 61 which is independent of temperature.

Therefore, it is necessary to know ΔH^{o}_{f298}, ΔS^{o}_{f298}, C_p and ΔS^{o}, and ΔH^{o} of transition for each gaseous and condensed species which appears in the vaporization reaction under consideration.

If any of the species should exist as variable composition phases, all of the thermodynamic quantities mentioned should be known as a function of composition (partial molar functions).

Since it is assumed here that the vaporization reaction forms only atomic species, thermodynamic data are required only for the condensed carbide phase, and for the pure elements in the gaseous and condensed phases. A survey of data available in the literature has yielded reasonably reliable information on the value of ΔH^{o}_{f298} and ΔS_{f298} of the carbides and of the gaseous atomic species, and on the temperature dependence of the various thermodynamic properties of the gaseous and condensed phases of the pure elements.

E. Thermodynamic Data

The thermodynamic properties of zirconium, hafnium and carbon atoms in the gaseous and condensed phases have been compiled in a convenient form in Reference 2. Values of all necessary thermodynamic quantities are tabulated at 100° intervals for temperatures as high as 3000°K, and are, therefore, not reproduced here. For titanium, the more recent and probably more accurate data given in Reference 8 are used instead. The data for carbon polymeric species given earlier in this report are also used.

Information regarding the carbide phases is instead more fragmentary. The heat and the entropy of formation of these carbides at 298°K has been measured or estimated by others and the most reliable data available are given in Table 40.

TABLE 40

Heats and Entropies of Formation for TiC, ZrC and HfC

Carbide	ΔH^{o}_{f298}	Reference	ΔS^{o}_{f298}	Reference
TiC	-43.85 ± 0.4	8	-2.90 ± 0.07	8
ZrC	-44.4 ± 1.5	9	-2.7 ± 1	10
HfC	-47 ± 5	10	-4 ± 1	10

Although the value of ΔH^{o}_{f298} is only imperfectly confirmed by mass spectroscopic data[5], these data are probably fairly accurate for TiC.

ΔH^{o}_{f298} of ZrC is also based on reliable combustion calorimetry measurements[9]. Data for HfC and ΔS^{o}_{f298} of ZrC are instead highly approximate and are based on estimates[10]. Their uncertainty is obviously greater.

All these data refer to the stoichiometric compound having the ideal formula MC. No information whatsoever is available for other compositions. Therefore, the existence of the solid solution phases must be ignored.

Reliable data on the heat capacity of TiC are available up to a temperature of 1800[11], but no experimental data at all are available at higher temperatures, or for ZrC and HfC. In the absence of such information, two courses may be followed in extrapolating thermodynamic properties to higher temperatures:

1. A more or less arbitrary shape may be assumed for the reation between T and Cp, which is chosen on the basis of the known behavior of structurally similar compounds. (See, for example, Reference 8.) Such a procedure has been used for TiC[8] and ZrC[10].

2. A second alternative consists of assuming that $\Delta Cp = 0$ at all temperatures higher than those at which experimental data are available. Such an assumption cannot be satisfactory when the products of reaction are gaseous, and the starting materials are condensed phases, but is is often acceptable when all species are condensed phases. (See Reference 12.)

The first course was chosen by the authors of Reference 8, who devised a technique for extrapolating thermodynamic data for $TiC_{(s)}$ and $Ti_{(s,l)}$ to temperatures above the region where experimental information is available. Their data is used unmodified in this report.

For ZrC and HfC, it has been assumed that $\Delta C_p = 0$ for the reaction

$$MC_{(s)} = M(s,l) + C(s) \qquad (62)$$

at all temperatures higher than 298°K. Values of ΔH and ΔS of melting given in Reference 1 are included, however. In Section III, it is shown that only minor errors are introduced in the calculated vapor pressures by this assumption.

F. Titanium Carbide Vaporization

The vaporization reaction may be considered to be:

$$TiC(s) = Ti(g) + C(s) \qquad (63)$$

This reaction, the sum of

$$TiC(s) = Ti(s,l) + C(s) \qquad (64)$$

and of

$$Ti(s,l) = Ti(g) \qquad (65)$$

and the vapor pressure of Ti is calculated by combining the information given in Reference 8 for equation 64 and in Reference 1 for equation 65.

These data are given in Table 41. Here it is assumed that a solid carbon phase is present which maintains the pressure of the various carbon molecules at the values listed in the first section of this report. This is the situation encountered if the vaporized material initially contains a sufficient amount of free carbon, or if pure TiC is vaporized at temperatures lower than 2800°K.

TABLE 41

Vaporization of TiC - Graphite Phase Present

$T^{o}K$	$\Delta F_T^{o}(64)$	$\Delta F_T^{o}(65)$	$\Delta F_T^{o}(63)$	log P_{Ti}
1800	38.02	51.35	89.37	-10.85
1900	37.65	48.20	85.85	- 9.87
2000	37.21	45.13	82.34	- 9.00
2100	36.67	42.18	78.85	- 8.20
2200	36.13	39.25	75.38	- 7.49
2300	35.58	36.32	71.90	- 6.83
2400	35.05	33.40	68.45	- 6.23
2500	34.49	30.50	64.99	- 5.68
2600	33.92	27.58	61.50	- 5.19
2700	33.38	24.66	58.04	- 4.70
2800	32.88	21.76	54.64	- 4.27
2900	32.38	18.86	51.24	- 3.86
3000	31.80	16.00	47.80	- 3.48
3100	31.05	13.11	44.16	- 3.11
3200	30.25	10.22	40.47	- 2.76
3300	29.72	7.33	37.05	- 2.45
3400	29.46	4.44	33.90	- 2.18

When pure TiC is vaporized at temperatures of 2800°K or higher instead, the vaporization process becomes congruent, according to the data given here. The partial pressure of titanium is then higher than that listed in Table 41, and the pressure of the various carbon species is lower than the equilibrium pressure over graphite.

The value of the various equilibrium pressures is then obtained by solving simultaneously the equilibrium constant expressions for the following reactions:

$$TiC(s) = Ti(g) + C(g) \quad (66)$$

$$2C(g) = C_2(g) \quad (67)$$

$$3C(g) = C_3(g) \quad (68)$$

$$4C(g) = C_4(g) \quad (69)$$

$$5C(g) = C_5(g) \quad (70)$$

together with the condition for conservation of mass

$$P_C + 2P_{C_2} + 3P_{C_3} + 4P_{C_4} + 5P_{C_5} = P_{Ti}. \quad (71)$$

When this is done, it is found that the composition of the equilibrium vapor is that given in Table 42.

TABLE 42

Vaporization of TiC -
No Graphite Phase Present

T^oK	log P_{Ti}	log P_C	log P_{C_2}	log P_{C_3}	log P_{C_4}	log P_{C_5}
2800	-4.25	-5.18	-5.61	-4.85	-7.46	-7.21
2900	-3.82	-4.74	-5.12	-4.41	-6.92	-6.68
3000	-3.42	-4.32	-4.67	-4.03	-6.47	-6.24
3100	-3.04	-3.95	-4.25	-3.62	-5.98	-5.74
3200	-2.67	-3.59	-3.85	-3.26	-5.54	-5.31
3300	-2.34	-3.26	-3.49	-2.95	-5.16	-4.84
3400	-2.04	-2.96	-3.18	-2.68	-4.85	-4.65

Notice that applying equation 71 to congruent vaporization implies that the gas phase has the same stoichiometry as the solid. This condition is not satisfied in the cases of Knudsen cell effusion or Langmuir vaporization, and some correction must be made for mass selection effects accompanying effusive flow.

G. Zirconium Carbide Vaporization

Zirconium carbide behaves in exactly the same way as titanium carbide. However, the vaporization of zirconium carbide turns out to be congruent at all of the temperatures considered, so a single vaporization reaction is of interest.

$$ZrC(s) = Zr(g) + C(g) \quad (72)$$

(Here again the solid solution phase is ignored.)

The vaporization reaction given above can again be represented as the sum of the three following reactions:

$$ZrC(s) = Zr(s) + C(s) \quad (73)$$

$$Zr(s) = Zr(g) \quad (74)$$

$$C(s) = C(g) \quad (75)$$

The thermodynamic properties of the three above reactions are given in Table 43.

TABLE 43

Vaporization of ZrC

T^oK	$\Delta H^o(73)$*	$\Delta H^o(74)$	$\Delta H^o(75)$	$\Delta S^o(73)$	$\Delta S^o(74)$	$\Delta S^o(75)$	$\Delta F^o(72)$	$\log P_{Zr}P_C$
1800	45.2	143.8	171.0	3.1	32.07	37.56	229.1	-27.81
1900	45.2	143.7	170.9	3.1	32.02	37.51	221.8	-25.51
2000	45.2	143.6	170.8	3.1	31.97	37.46	214.5	-23.44
2100	45.2	143.5	170.7	3.1	31.92	37.40	207.3	-21.57
2200	49.2	139.5	170.6	5.0	30.00	37.35	200.1	-19.87
2300	49.2	139.4	170.5	5.0	29.97	37.30	192.9	-18.34
2400	49.2	139.3	170.4	5.0	29.94	37.25	185.6	-16.90
2500	49.2	139.2	170.3	5.0	29.91	37.21	178.4	-15.59
2600	49.2	139.2	170.2	5.0	29.89	37.16	171.3	-14.40
2700	49.2	139.1	170.0	5.0	29.87	37.11	170.0	-13.27
2800	49.2	139.1	169.9	5.0	29.85	37.07	156.7	-12.23
2900	49.2	139.1	169.8	5.0	29.84	37.03	149.7	-11.28
3000	49.2	139.0	169.7	5.0	29.83	36.99	142.4	-10.37
3100	49.2	139.0	169.7	5.0	29.83	36.99	137.3	- 9.68
3200	49.2	139.0	169.7	5.0	29.83	36.99	128.1	- 8.75
3300	49.2	139.0	169.7	5.0	29.83	36.99	120.9	- 8.01
3400	49.2	139.0	169.7	5.0	29.83	36.99	113.7	- 7.31
3500	49.2	139.0	169.7	5.0	29.83	36.99	106.5	- 6.65
3600	49.2	139.0	169.7	5.0	29.83	36.99	99.3	- 6.03
3700	49.2	139.0	169.7	5.0	29.83	36.99	92.2	- 5.45
3800	49.2	139.0	169.7	5.0	29.83	36.99	85.0	- 4.89
3900	49.2	139.0	169.7	5.0	29.83	36.99	77.8	- 4.36
4000	49.2	139.0	169.7	5.0	29.83	36.99	70.6	- 3.86

* Superscript numbers indicate equation numbers.

The composition of the equilibrium congruently boiling vapor over ZrC is given in Table 44. Notice that the polymeric carbon species are of less importance in this case.

TABLE 44

Vaporization of ZrC

T^oK	$-\log P_{Zr}$	$-\log P_C$	$-\log P_{C_2}$	$-\log P_{C_3}$
1800	13.91	13.91		
1900	12.76	12.76		
2000	11.72	11.72	14.14	14.28
2100	10.78	10.79	13.04	13.19
2200	9.93	9.94	12.03	12.17
2300	9.16	9.18	11.14	11.31
2400	8.44	8.46	10.27	10.45
2500	7.78	7.81	9.50	9.68
2600	7.18	7.22	8.81	9.01
2700	6.61	6.66	8.15	8.35
2800	6.08	6.15	7.55	7.76
2900	5.60	5.68	7.00	7.23
3000	5.14	5.23	6.47	6.70
3100	4.80	4.88	6.15	6.47
3200	4.32	4.43	5.53	5.78
3300	3.94	4.07	5.11	5.38
3400	3.59	3.72	4.70	4.96
3500	3.25	3.40	4.32	4.60
3600	2.93	3.10	3.98	4.27
3700	2.64	2.81	3.64	3.93
3800	2.35	2.54	3.32	3.63
3900	2.07	2.29	3.04	3.36
4000	1.82	2.04	2.74	3.07

The value of ΔH^o_{1800} (eq. 73), and of ΔS^o_{1800} (eq. 73), was calculated using the estimated heat capacity of ZrC(s) given by Krikorian [10] and the enthalpy and entropy values of Zr(s) and C(s) given in Reference 2. At temperatures higher than 1800°, the assumption that ΔH^o (eq. 73) and ΔS^o (eq. 73) are constant is made. Above 3000°K, the further assumption is made that ΔH^o (eq. 74), ΔH^o (eq. 75), ΔS^o (eq. 74) and ΔS^o (eq. 75) are also constant.

H. Hafnium Carbide Vaporization

In exactly the same manner the vaporization reaction in question

$$HfC(s) = Hf(g) + C(g) \qquad (76)$$

is taken as the sum of the following:

$$HfC(s) = Hf(s) + C(s) \quad (77)$$

$$C(s) = C(g) \quad (75)$$

$$Hf(s) = Hf(g) \quad (78)$$

The resulting thermodynamic data are given in Table 45.

In this case also, the vaporization is congruent over the whole temperature range considered. In this case, the concentration of all polymeric species of carbon is so low that it is ignored in calculating the total pressure of boiling HfC, which is given in Table 46.

TABLE 45

Vaporization of HfC

T^oK	$\Delta H^o(77)$	$\Delta H^o(75)$	$\Delta H^o(78)$	$\Delta S^o(77)$	$\Delta S^o(75)$	$\Delta S^o(78)$	$\Delta F^o(76)$	$\log P_{Hf}P_C$
2000	47	170.8	166.6	4.0	37.46	31.96	237.6	-25.96
2100	47	170.7	166.5	4.0	37.40	31.91	230.2	-23.95
2200	47	170.6	166.4	4.0	37.35	31.86	222.9	-22.14
2300	52	170.5	161.1	6.3	37.30	29.51	215.4	-20.48
2400	52	170.4	161.0	6.3	37.25	29.48	208.1	-18.95
2500	52	170.3	161.0	6.3	37.21	29.44	200.9	-17.56
2600	52	170.2	160.9	6.3	37.16	29.40	193.7	-16.28
2700	52	170.0	160.8	6.3	37.11	29.36	186.3	-15.07
2800	52	169.9	160.7	6.3	37.07	29.33	179.0	-13.97
2900	52	169.8	160.6	6.3	37.03	29.30	171.8	-12.95
3000	52	169.7	160.5	6.3	36.99	29.26	164.5	-11.98
3100	52	169.7	160.5	6.3	36.99	29.26	157.3	-11.09
3200	52	169.7	160.5	6.3	36.99	29.26	150.0	-10.25
3300	52	169.7	160.5	6.3	36.99	29.26	142.8	- 9.46
3400	52	169.7	160.5	6.3	36.99	29.26	135.5	- 8.71
3500	52	169.7	160.5	6.3	36.99	29.26	128.3	- 8.01
3600	52	169.7	160.5	6.3	36.99	29.26	121.0	- 7.35
3700	52	169.7	160.5	6.3	36.99	29.26	113.8	- 6.72
3800	52	169.7	160.5	6.3	36.99	29.26	106.5	- 6.12
3900	52	169.7	160.5	6.3	36.99	29.26	99.3	- 5.56
4000	52	169.7	160.5	6.3	36.99	29.26	92.0	- 5.03

TABLE 46

Vaporization of HfC

$T^{o}K$	log P Total
2000	-12.68
2200	-10.77
2400	- 9.18
2600	- 7.84
2800	- 6.69
3000	- 5.69
3200	- 4.88
3400	- 4.06
3600	- 3.38
3800	- 2.76
4000	- 2.22

III. VALIDITY OF ASSUMPTIONS

The following computation has been carried out in order to test the accuracy of various assumptions regarding the extrapolation of thermodynamic data to high temperatures when reliable heat capacity measurements are unavailable.

It was mentioned earlier that two assumptions may be made:

1. An approximate relation may be obtained between T and Cp based on known data for analogous phases.

2. ΔCp may be assumed to be zero for reactions involving only condensed phases at temperatures higher than those for which good data are available.

The free energy of formation of SiC[13], and TiC has been calculated from experimental Cp data, and using first one, then the other, of the two assumptions in order to determine their effect on calculated vapor pressures. Although SiC is not one of the carbides considered here, data for it are included in order to shed some light on this question. The values of ΔH and ΔS associated with known phase transitions are always included.

The relevant functions are tabulated in Tables 47 and 48, in which (1) is used to denote values obtained from reliable experimental data, and (2) to denote values computed using the assumption $\Delta Cp = 0$.

From the differences in ΔF_f^o given in the last column of Tables 47 and 48, it can be shown that, in the case of these two carbides, the assumption of $\Delta Cp = 0$ leads to an error in ΔF_f^o no greater than 0.5 kcal even when an extrapolation of 1500° is performed. Such an error leads to a difference in the calculated vapor pressures of about 10% at 2500°K. Its significance is small compared to other, more serious sources of error. The simpler assumption ($\Delta Cp = 0$) may therefore be used in predicting the vapor pressure of ZrC and HfC.

TABLE 47

SiC(hex) = Si(s,l) + C(graphite) (79)

T°K	$\Delta H_f^o(1)$	$\Delta H_f^o(2)$	$\Delta S_f^o(1)$	$\Delta S_f^o(2)$	$\Delta F_f^o(1)$	$\Delta F_f^o(2)$	$\Delta F_f^o(1)-\Delta F_f^o(2)$
298	12.3	12.3	1.96	1.96	11.7	11.7	0.0
400	12.3		2.05		11.5		
500	12.3		2.01		11.3		
600	12.3	12.3	1.98	1.96	11.1	11.1	0.0
700	12.2		1.89		10.9		
800	12.2		1.87		10.7		
900	12.2	12.3	1.85	1.96	10.5	10.5	0.0
1000	12.2		1.84		10.4		
1100	12.2		1.84		10.2		
1200	12.1	12.3	1.84	1.96	9.9	10.0	-0.1
1300	12.1		1.84		9.7		
1400	12.1		1.83		9.5		
1500	12.1	12.3	1.84	1.96	9.3	9.4	-0.1
1600	12.1		1.84		9.2		
1700	23.2		8.44		8.9		
1800	23.2	23.4	8.44	8.56	8.0	8.0	0.0
1900	23.3		8.44		7.3		
2000	23.3	23.4	8.43	8.56	6.4	6.4	0.0

TABLE 48

$$TiC(s) = Ti(\alpha, \beta, l) + C(graphite) \qquad (80)$$

T^oK	$\Delta H_f^o(1)$	$\Delta H_f^o(2)$	$\Delta S_f^o(1)$	$\Delta S_f^o(2)$	$\Delta F_f^o(1)$	$\Delta F_f^o(2)$	$\Delta F_f^o(1)-\Delta F_f^o(2)$
	(a)	(c)	(a)	(c)	(a)	(c)	
298	43.8	43.8	2.89	2.89	42.9	42.9	0.0
400	43.8		2.73		42.7		
500	43.7		2.56		42.4		
600	43.6	43.8	2.44	2.89	42.1	42.1	0.0
700	43.6		2.39		41.9		
800	43.6		2.38		41.7		
900	43.6	43.8	2.42	2.89	41.4	41.2	0.2
1000	43.6		2.46		41.1		
1100	43.7		2.53		40.9		
1200	44.7	44.8	3.41	3.71	40.6	40.3	0.3
1300	44.8		3.44		40.3		
1400	44.8		3.47		39.9		
1500	44.8	44.8	3.49	3.71	39.6	39.2	0.4
1600	44.9		3.51		39.3		
	(b)	(c)	(b)	(c)	(b)	(c)	
1800	44.9	44.8	3.53	3.71	38.5	38.1	0.4
2000	48.6	48.5	5.46	5.61	37.7	37.3	0.4
2200	48.6	48.5	5.46	5.61	36.6	36.2	0.4
2400	48.6	48.5	5.44	5.61	35.5	35.0	0.5

(a) Heat capacity experimental data used for all species.

(b) Heat capacity data of TiC and Ti extrapolated at temperatures higher than 1800°K.

(c) Calculated assuming $\Delta C_p = 0$, but including phase transitions.

IV. DISCUSSION AND CONCLUSIONS

The total vapor pressures over TiC, ZrC and HfC have been calculated. They are shown graphically in Figure 63. It is felt that the vapor pressure data referring to TiC should be relatively accurate. Data for ZrC are considerably more uncertain, and the calculated vapor pressure over HfC could be in error by as much as a factor of three or even five.

The presence of solid solution phases on the metal-rich side should have little effect on the vapor pressure of TiC; it could make much more difference in the case of ZrC and HfC. The assumptions made here would tend to make the calculated vapor pressure distinctly too low in the latter cases.

Furthermore, it is possible that gaseous carbide species are important constituents of the equilibrium vapor over ZrC and especially HfC. Ignoring these would again tend to underestimate the volatility of these carbides.

Therefore, the relative advantage of ZrC and HfC over TiC for high temperature applications may be offset to a large extent by the preferential vaporization of greater amounts of carbon than calculated here, and the resulting change in composition of the condensed phase which would lower greatly the melting point of the carbide.

There is obviously an urgent need for experimental information on the stability of gaseous carbide molecules, on the thermodynamic properties of the solid solution phases and of the phase diagram of the binary systems. Reliable experimental values of the heat and entropy of formation of hafnium carbide, and of the entropy of zirconium carbide are also necessary.

The heat capacity of the various condensed phases at elevated temperatures are probably less urgently needed, since they have less effect on the calculated vapor pressure values. This point is discussed in more detail in the foregoing Section III.

Notice that a recently published study of the vapor pressure of TiC[14] is not included here. Its findings appear to be seriously in error.

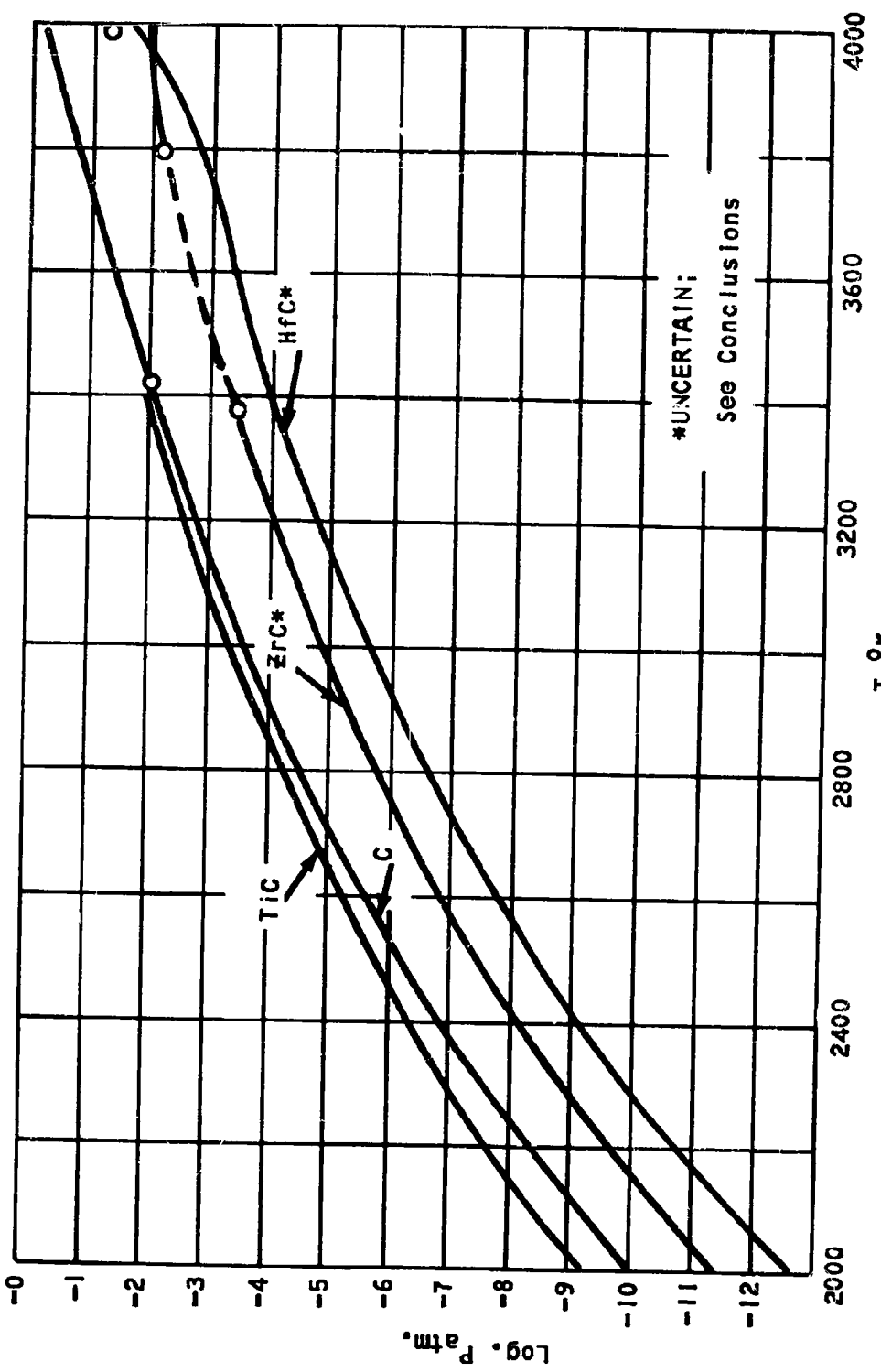

Figure 63. Total Vapor Pressure Over C, TiC ZrC And Hfc

V. LIST OF SYMBOLS

P	=	equilibrium vapor pressure in atmosphere
T	=	temperature in ^{o}K (unless otherwise indicated)
N	=	mole fraction
K	=	equilibrium constant, where pressures are in atmospheres, and all condensed phases have unit activity
(g)	=	gas
(s)	=	solid
(l)	=	liquid
ΔH_f^o	=	standard molar enthalpy of formation
ΔS_f^o	=	standard molar entropy of formation
ΔH_T^o	=	standard molar enthalpy change for the reaction at a temperature T
ΔS_T^o	=	standard molar entropy change for the reaction at T
ΔF_T^o	=	standard molar free energy change of reaction at T
ΔCp	=	difference in heat capacity at constant pressure between products of reaction and starting materials
log	=	logarithm - base 10
ln	=	logarithm - base ℓ
(i)	=	products of reaction
(j)	=	starting materials
R	=	gas constant

all values H and F in kcal/mole

all values of S in e.u./mole

VI. REFERENCES, Appendix A

1. Drowart, J., Burns, R. P., DeMaria, G. and Inghram, M. G., Jour. Chem. Phys., 31:1131 (1959)

2. Stull, D. R. and Sinke, G. C., "Thermodynamic Properties of the Elements," Advances in Chemistry Series, No. 18, Amer. Chem. Soc., 1956 (Washington, D. C.)

3. Hansen, J. and Anderko, K., Constitution of Binary Alloys, McGraw-Hill Book Co., 1958 (New York)

4. Rundle, R. E., Acta Cryst., 1:180 (1948)

5. Chupka, W. A., Berkowitz, J., Giese, C. F. and Inghram, M. G., Jour. Phys. Chem., 62:611 (1958)

6. Brewer, L. and Kane, J. S., Jour. Phys. Chem., 59:105 (1955)

7. Inghram, M. G. and Chupka, W. A., Private Communication

8. National Bureau of Standards - Report 6645, Preliminary Report on the Thermodynamic Properties of Selected Light Metal Compounds, April 1, 1960

9. Mah, A. D. and Boyle, B. J., Jour. Amer. Chem. Soc., 77:6512 (1955)

10. Krikorian, O. H., High Temperature Studies, UCRL Report 2888, April 1955

11. Kelley, K. K., "High Temperature Heat Content, Heat Capacity and Entropy Data for Inorganic Compounds," U. S. Bureau of Mines Bull. 476 (1949)

12. Brewer, L., et al., "Chemistry and Metallurgy of Miscellaneous Materials," Natl. Nuclear Energy Series IV - 19B Ed. L. L. Quill, McGraw-Hill Book Co., New York, 1950

13. Vidale, G. L., Standard Enthalpy of Formation of Silicon Carbide and Oscillator Strength of the Silicon 2516 Line, General Electric Co. TIS Rept. R60SD333, August 1960

14. Fujishiro, S. and Gokcen, N. A., Jour. Phys. Chem., 65:161 (1961)

APPENDIX B - SHAPE OF LINE FROM HOLLOW CATHODE SOURCE

Guido L. Vidale

A. Introduction

Previous reports in this series describe how absorption measurements of resonance lines have been used to determine the vapor pressure and heat of formation of some compounds or the value of the oscillator strength of atomic resonance lines. In this method, a sharp line is generated in a hollow cathode discharge tube, and its absorption by the hot equilibrium vapor is measured using suitable spectrophotometric equipment. The calculations for converting the measured absorption to the oscillator strength, or to vapor pressure have been made assuming that the line from discharge source is infinitely thin compared to the absorption line width.

Direct measurements of the line contour and half-width would provide the most conclusive information. They would require the detailed examination of the lines with an interferometer having a resolving power of 2×10^6. Such measurements require elaborate instrumentation, and are very time consuming. They have not been undertaken, since it is hoped that the following considerations will establish indirectly that the thin line assumption is satisfactory.

This appendix summarizes the evidence that has been obtained regarding the shape of the line from the source. Three arguments are advanced to show that the thin line assumption is very probably correct; they are:

(1) The method of operation of the source tends to minimize the magnitude of Stark, pressure and Doppler broadening, and of line reabsorption.

(2) Measurements of I/I_o as a function of lamp current show no drop in absorption at higher currents. This indicates that Stark broadening and reabsorption do not affect the results obtained.

(3) Measurement of the density of sodium vapor in equilibrium with sodium metal yields results which agree with more precise information found in the literature.

B. Experimental Equipment and Source Operation

The experimental source used in those studies has been described in report WADD TR 60-646, Part I.

The hollow cathode was patterned after the one described by Tolansky. It consists of a copper cathode cup region at the bottom, a ring anode made of nickel placed above it, and a vacuum tight glass envelope provided with a window at the top and with inlet and outlet tubes for the carrier gas. This design is most convenient when one desires to operate the discharge at a low temperature; the whole tube is then lowered in a refrigerant bath, leaving only the top part of the glass envelope and the window exposed. All the work carried out here has been performed with the cathode immersed in liquid nitrogen.

Constant line intensity can be obtained only if the liquid nitrogen level is held quite constant. An automatic constant level filler is therefore used to replenish the liquid nitrogen.

The discharge is operated in argon carrier gas at a pressure of 0.3 to 0.6 mm. of mercury as measured by a Pirani gauge. At this pressure the discharge tended to remain in the cup and was most stable. The argon gas used was a 99.97% pure Air Reduction Co. product, which was further purified before introducing it into the discharge tube by passing it over hot titanium turnings and through a liquid nitrogen trap. This purified argon was introduced into the top of the discharge tube through a needle valve, and was removed from the cathode cup by continuous pumping with a small diffusion pump.

The flow velocity under typical operating conditions is maintained at approximately 150 ml/sec. This high value was chosen in order to avoid the formation of a cloud of sputtered material in the area above the hollow cathode cup, because this cloud is the cause of possible reabsorption of the generated spectral lines.

The current through the discharge is controlled by varying the voltage generated in a 300 m.a., 500 volt DC source and by placing a 6000 ohm resistor in series with the discharge tube.

All of the lines used in the studies described in previous reports were very intense resonance lines. The intensity of these lines was sufficient even at the lowest currents which would support a stable discharge; these varied from 12 m.a. to 30 m.a. depending on the composition of the cup line and on the element under investigation. Currents only slightly higher than this lower limit were used, because the intensity of these lines was noticed to vary rapidly with the current in this region. At higher currents the intensity is more constant, indicating that line reabsorption may be becoming increasingly important. The observation that this drop in the rate of growth occurs at even higher currents for weaker lines confirms our interpretation of this effect.

Information available in the literature indicates that these conditions of operation tend to minimize line broadening, and that the line width so obtained is approximately what would be predicted for pure Doppler shapes for a temperature of 100°-300°K.

C. Dependence of Measured I/I_0 on Source Current

The fact that the intensity of the lines is strongly dependent on the current density has already been mentioned. Most likely the concentration of atomic species is in the cathode region, and so the amount of reabsorption will also depend strongly on the current.

If reabsorption caused excessive line broadening, the value of I/I_0 will depend on the current even if everything else is held constant.

This dependence has been investigated in some detail for the case of the copper 3247 line and especially the zirconium 3601 line.

The relevant data are tabulated below:

TABLE 49

Dependence of Absorption on Source Current, Cu 3247Å Line

Run No.	I/I_o	Lamp Current
78	0.31	30 m.a.
79	0.36	20
80	0.32	30
81	0.32	26
82	0.35	26
83	0.33	26
87	0.28	23
88	0.30	24
90	0.34	28
95	0.30	28
96	0.29	30
97	0.42	30
98	0.30	30
99	0.32	30

Although this variation in current changes the line intensity by more than a factor or two, no variation in I/I_o can be attributed to the changing current.

Similarly, in the case of zirconium, the value of I/I_o was measured as a function of current through the hollow cathode source. The furnace temperature and inert gas pressure were the same for all the runs listed, so any variation in I/I_o can be attributed solely to a change in the line shape.

TABLE 50

Dependence of Absorption on Source Current Zr 3601Å Line

Current Through Lamp m.a.	I/I_o	$-\log I/I_o$
30 m.a.	.443	.354
30	.439	.358
30	.432	.365
40	.448	.344
40	.422	.375
50	.413	.384
50	.432	.365
65	.445	.352
80	.409	.388

This remarkable constancy in $-\log I/I_o$ shows that the line width is not changed significantly even by operating lamp currents approximately three times as great as the normal operating value.

Clearly then, Stark broadening and line reversal do not affect the line shape sufficiently to render invalid the assumption that the emitted line is very thin.

D. Test of Method with Sodium Vapor

The final evidence supporting the assumption that the lines are thin compared to those absorbed by the hot atoms in the furnace is based on the agreement between the measured vapor pressure of sodium and the best values given in the literature. In the case of sodium, good values of the vapor pressure, oscillator strength, hyperfine structure, and pressure broadening constant are available. The good agreement therefore indicates that the assumptions which have been made are satisfactory, and that this method is capable of yielding satisfactory values for the vapor pressure. The demands on this method are fewer when it is used for measuring free energies of formation, since in this case errors tend to cancel almost completely.

E. Conclusions

A fairly safe assumption is that the line generated from a hollow cathode source operated as described above has a width typical of a Doppler shaped line for a temperature of approximately 100 - 300 K. Such a width has been shown to introduce an error of approximately 10-15% in measured vapor pressures calculated assuming the line is infinitely thin.

When the method is used for measuring free energies of formation, the vapor pressure ratio obtained has a probable error of 5% or less due to this assumption.

APPENDIX C - DETERMINATION OF FREE CARBON IN CARBIDES OF HAFNIUM, ZIRCONIUM, TANTALUM, TUNGSTEN, AND TITANIUM

F. H. Swearingen

Two methods were used interchangeably for the determination of free carbon in carbides. The procedure used for each method is briefly described. Both methods are based on the solubility of carbides in mixtures of hydrofluoric and nitric acid, and the insolubility of carbon in this acid mixture.

1. Monroe Crucible Method (O. H. Kriege, LA 2306, Los Alamos Scientific Laboratory, 1959)

   Transfer a 1 to 3 gm sample (depending on free carbon content previously estimated) to a 200 ml platinum dish. Add 10 ml hydrofluoric acid (48%) followed by sufficient nitric acid, dropwise, to dissolve the carbide completely. Some carbides (HfC, ZrC) are best dissolved in a mixture of 15 ml HNO_3 (3-5M) and 2 ml HF. Heat the solution to near boiling for 5 minutes. Filter through a weighed Monroe crucible supported in a plastic funnel with a rubber washer. Catch the filtrate in a polyethylene beaker inside a bell jar. Use only slight vacuum to prevent loss of solids through the filter surface. Rinse the dish and wash the filter surface with a solution of 10 ml HF and 10 ml HNO_3 in 500 ml H_2O.

   Replace the cap on the bottom of the Monroe crucible and dry in an oven at 150°C. Cool in desiccator and weigh. Then ignite the crucible in a muffle furnace at 1000°C until all carbon has burned away. Cool in a desiccator and weigh. Loss in weight after ignition is taken as the weight of free carbon in the sample.

2. LECO Crucible Combustion Method

   Dissolve sample containing a maximum of 20 mg free carbon and heat to near boiling as described in the method above. Add 6 gm boric acid (60 ml of solution saturated at 25°C) and heat again to near boiling. Filter through a LECO style No. 528-30 porous crucible, following the previous procedure (except for crucible). Wash the residue with water and dry at 150°C.

   Add 1 gm of LECO low carbon iron accelerator to the residue in the crucible and determine carbon in the LECO carbon analyzer by combustion to CO_2, followed by absorption and determination of the CO_2.

Aeronautical Systems Division, Dir/Materials and Processes, Physics Lab, Wright-Patterson AFB, Ohio. Rpt Nr WADD-TR-60-646, Pt II. CARBONIZATION OF PLASTICS AND REFRACTORY MATERIALS RESEARCH. Final report, Jan 63, 163p. incl illus., tables, 61 refs.
Unclassified Report

Presented in this report are the results of continuing investigations of the Carbonization of Plastics, Vapor Pressure of Refractory Materials and Spectral Emissivity of Refractories. Studies of thermal degradation of phenolic, epoxy, polyphenylene and polynaphthalene resins were made with the the arc-image furnace, the fluidized bed reactor and the thermogravimetric analysis technique. The effect of semicarbonized materials used as fillers has been studied and a Bendix time-of-flight mass spectrometer has been adapted to the study of transient and stable species resulting from the flash-

(over)

photolysed degradation of plastics. Properties of carbon residue have been measured.

Vapor pressure studies using the Langmuir evaporation technique, the matrix isolation method, and resonance line absorption spectroscopy have progressed. Rates of evaporation of tungsten carbides, hafnium carbide and titanium carbide have been measured; further conclusive measurements on zirconium carbide have been made. Preliminary application of the matrix isolation technique to thoria has been made. Resonance line absorption studies have been completed on zirconium carbide and titanium carbide and the accessible thermodynamic data have been deduced. Normal spectral emissivities of W-2 coated molybdenum, siliconized ATJ graphite, tantalum, molybdenum, tungsten carbide and zirconium have been measured in the temperature range of 1400 to 3100°K.

1. Carbonization of plastics
2. Refractory materials
3. Spectral emissivity
I. AFSC Project 4776
II. Contract AF 33(616)-6841
III. General Electric Co., Cincinnati, Ohio
IV. J. A. Coffman, et al.
V. Aval fr CTS
VI. In ASTIA collection

Aeronautical Systems Division, Dir/Materials and Processes, Physics Lab, Wright-Patterson AFB, Ohio. Rpt Nr WADD-TR-60-646, Pt II. CARBONIZATION OF PLASTICS AND REFRACTORY MATERIALS RESEARCH. Final report, Jan 63, 163p. incl illus., tables, 61 refs.
Unclassified Report

Presented in this report are the results of continuing investigations of the Carbonization of Plastics, Vapor Pressure of Refractory Materials and Spectral Emissivity of Refractories. Studies of thermal degradation of phenolic, epoxy, polyphenylene and polynaphthalene resins were made with the the arc-image furnace, the fluidized bed reactor and the thermogravimetric analysis technique. The effect of semicarbonized materials used as fillers has been studied and a Bendix time-of-flight mass spectrometer has been adapted to the study of transient and stable species resulting from the flash-

(over)

photolysed degradation of plastics. Properties of carbon residue have been measured.

Vapor pressure studies using the Langmuir evaporation technique, the matrix isolation method, and resonance line absorption spectroscopy have progressed. Rates of evaporation of tungsten carbides, hafnium carbide and titanium carbide have been measured; further conclusive measurements on zirconium carbide have been made. Preliminary application of the matrix isolation technique to thoria has been made. Resonance line absorption studies have been completed on zirconium carbide and titanium carbide and the accessible thermodynamic data have been deduced. Normal spectral emissivities of W-2 coated molybdenum, siliconized ATJ graphite, tantalum, molybdenum, tungsten carbide and zirconium have been measured in the temperature range of 1400 to 3100°K.

1. Carbonization of plastics
2. Refractory materials
3. Spectral emissivity
I. AFSC Project 4776
II. Contract AF 33(616)-6841
III. General Electric Co., Cincinnati, Ohio
IV. J. A. Coffman, et al.
V. Aval fr CTS
VI. In ASTIA collection

Aeronautical Systems Division, Dir/Materials and Processes, Physics Lab, Wright-Patterson AFB, Ohio. Rpt Nr WADD-TR-60-646, Pt II. CARBONIZATION OF PLASTICS AND REFRACTORY MATERIALS RESEARCH. Final report, Jan 63, 183p. incl illus., tables, 61 refs. Unclassified Report

Presented in this report are the results of continuing investigations of the Carbonization of Plastics, Vapor Pressure of Refractory Materials and Spectral Emissivity of Refractories. Studies of thermal degradation of phenolic, epoxy, polyphenylene and polynaphthalene resins were made with the the arc-image furnace, the fluidized bed reactor and the thermogravimetric analysis technique. The effect of semicarbonized materials used as fillers has been studied and a Bendix time-of-flight mass spectrometer has been adapted to the study of transient and stable species resulting from the flash-

(over)

1. Carbonization of plastics
2. Refractory materials
3. Spectral emissivity
I. AFSC Project 4776
II. Contract AF 33(616)-6821
III. General Electric Co., Cincinnati, Ohio
IV. J. A. Coffman, et al.
V. Aval fr OTS
VI. In ASTIA collection

Aeronautical Systems Division, Dir/Materials and Processes, Physics Lab, Wright-Patterson AFB, Ohio. Rpt Nr WADD-TR-60-646, Pt II. CARBONIZATION OF PLASTICS AND REFRACTORY MATERIALS RESEARCH. Final report, Jan 63, 183p. incl illus., tables, 61 refs. Unclassified Report

Presented in this report are the results of continuing investigations of the Carbonization of Plastics, Vapor Pressure of Refractory Materials and Spectral Emissivity of Refractories. Studies of thermal degradation of phenolic, epoxy, polyphenylene and polynaphthalene resins were made with the the arc-image furnace, the fluidized bed reactor and the thermogravimetric analysis technique. The effect of semicarbonized materials used as fillers has been studied and a Bendix time-of-flight mass spectrometer has been adapted to the study of transient and stable species resulting from the flash-

(over)

1. Carbonization of plastics
2. Refractory materials
3. Spectral emissivity
I. AFSC Project 4776
II. Contract AF 33(616)-6821
III. General Electric Co., Cincinnati, Ohio
IV. J. A. Coffman, et al.
V. Aval fr OTS
VI. In ASTIA collection

photolysed degradation of plastics. Properties of carbon residue have been measured.

Vapor pressure studies using the Langmuir evaporation technique, the matrix isolation method, and resonance line absorption spectroscopy have progressed. Rates of evaporation of tungsten carbides, hafnium carbide and titanium carbide have been measured; further conclusive measurements on zirconium carbide have been made. Preliminary application of the matrix isolation technique to thoria has been made. Resonance line absorption studies have been completed on zirconium carbide and titanium carbide and the accessible thermodynamic data have been deduced. Normal spectral emissivities of W-2 coated molybdenum, siliconized ATJ graphite, tantalum, molybdenum, tungsten carbide and zirconium have been measured in the temperature range of 1400 to 3100°K.

photolysed degradation of plastics. Properties of carbon residue have been measured.

Vapor pressure studies using the Langmuir evaporation technique, the matrix isolation method, and resonance line absorption spectroscopy have progressed. Rates of evaporation of tungsten carbides, hafnium carbide and titanium carbide have been measured; further conclusive measurements on zirconium carbide have been made. Preliminary application of the matrix isolation technique to thoria has been made. Resonance line absorption studies have been completed on zirconium carbide and titanium carbide and the accessible thermodynamic data have been deduced. Normal spectral emissivities of W-2 coated molybdenum, siliconized ATJ graphite, tantalum, molybdenum, tungsten carbide and zirconium have been measured in the temperature range of 1400 to 3100°K.

Aeronautical Systems Division, Dir/Materials and Processes, Physics Lab, Wright-Patterson AFB, Ohio. Rpt Nr WADD-TR-60-646, Pt II. CARBONIZATION OF PLASTICS AND REFRACTORY MATERIALS RESEARCH. Final report, Jan 63, 183p. incl illus., tables, 61 refs. Unclassified Report

Presented in this report are the results of continuing investigations of the Carbonization of Plastics, Vapor Pressure of Refractory Materials and Spectral Emissivity of Refractories. Studies of thermal degradation of phenolic, epoxy, polyphenylene and polynaphthalene resins were made with the the arc-image furnace, the fluidized bed reactor and the thermogravimetric analysis technique. The effect of semicarbonized materials used as fillers has been studied and a Bendix time-of-flight mass spectrometer has been adapted to the study of transient and stable species resulting from the flash-

(over)

1. Carbonization of plastics
2. Refractory materials
3. Spectral emissivity
I. AFSC Project 4776
II. Contract AF 33(616)-8841
III. General Electric Co., Cincinnati, Ohio
IV. J. A. Coffman, et al.
V. Aval fr OTS
VI. In ASTIA collection

Aeronautical Systems Division, Dir/Materials and Processes, Physics Lab, Wright-Patterson AFB, Ohio. Rpt Nr WADD-TR-60-646, Pt II. CARBONIZATION OF PLASTICS AND REFRACTORY MATERIALS RESEARCH. Final report, Jan 63, 183p. incl illus., tables, 61 refs. Unclassified Report

Presented in this report are the results of continuing investigations of the Carbonization of Plastics, Vapor Pressure of Refractory Materials and Spectral Emissivity of Refractories. Studies of thermal degradation of phenolic, epoxy, polyphenylene and polynaphthalene resins were made with the the arc-image furnace, the fluidized bed reactor and the thermogravimetric analysis technique. The effect of semicarbonized materials used as fillers has been studied and a Bendix time-of-flight mass spectrometer has been adapted to the study of transient and stable species resulting from the flash-

(over)

1. Carbonization of plastics
2. Refractory materials
3. Spectral emissivity
I. AFSC Project 4776
II. Contract AF 33(616)-8841
III. General Electric Co., Cincinnati, Ohio
IV. J. A. Coffman, et al.
V. Aval fr OTS
VI. In ASTIA collection

photolysed degradation of plastics. Properties of carbon residue have been measured.

Vapor pressure studies using the Langmuir evaporation technique, the matrix isolation method, and resonance line absorption spectroscopy have progressed. Rates of evaporation of tungsten carbides, hafnium carbide and titanium carbide have been measured; further conclusive measurements on zirconium carbide have been made. Preliminary application of the matrix isolation technique to thoria has been made. Resonance line absorption studies have been completed on zirconium carbide and titanium carbide and the accessible thermodynamic data have been deduced. Normal spectral emissivities of W-2 coated molybdenum, siliconized ATJ graphite, tantalum, molybdenum, tungsten carbide and zirconium have been measured in the temperature range of 1400 to 3100°K.

photolysed degradation of plastics. Properties of carbon residue have been measured.

Vapor pressure studies using the Langmuir evaporation technique, the matrix isolation method, and resonance line absorption spectroscopy have progressed. Rates of evaporation of tungsten carbides, hafnium carbide and titanium carbide have been measured; further conclusive measurements on zirconium carbide have been made. Preliminary application of the matrix isolation technique to thoria has been made. Resonance line absorption studies have been completed on zirconium carbide and titanium carbide and the accessible thermodynamic data have been deduced. Normal spectral emissivities of W-2 coated molybdenum, siliconized ATJ graphite, tantalum, molybdenum, tungsten carbide and zirconium have been measured in the temperature range of 1400 to 3100°K.

Aeronautical Systems Division, Dir/Materials and Processes, Physics Lab, Wright-Patterson AFB, Ohio. Rpt Nr WADD-TR-60-646, Pt II. CARBONIZATION OF PLASTICS AND REFRACTORY MATERIALS RESEARCH. Final report, Jan 63, 183p. incl illus., tables, 61 refs.
Unclassified Report

Presented in this report are the results of continuing investigations of the Carbonization of Plastics, Vapor Pressure of Refractory Materials and Spectral Emissivity of Refractories. Studies of thermal degradation of phenolic, epoxy, polyphenylene and polynaphthalene resins were made with the the arc-image furnace, the fluidized bed reactor and the thermogravimetric analysis technique. The effect of semicarbonized materials used as fillers has been studied and a Bendix time-of-flight mass spectrometer has been adapted to the study of transient and stable species resulting from the flash-

(over)

1. Carbonization of plastics
2. Refractory materials
3. Spectral emissivity
I. AFSC Project 4776
II. Contract AF 33(616)-6841
III. General Electric Co., Cincinnati, Ohio
IV. J. A. Coffman, et al.
V. Aval fr OTS
VI. In ASTIA collection

Aeronautical Systems Division, Dir/Materials and Processes, Physics Lab, Wright-Patterson AFB, Ohio. Rpt Nr WADD-TR-60-646, Pt II. CARBONIZATION OF PLASTICS AND REFRACTORY MATERIALS RESEARCH. Final report, Jan 63, 183p. incl illus., tables, 61 refs.
Unclassified Report

Presented in this report are the results of continuing investigations of the Carbonization of Plastics, Vapor Pressure of Refractory Materials and Spectral Emissivity of Refractories. Studies of thermal degradation of phenolic, epoxy, polyphenylene and polynaphthalene resins were made with the the arc-image furnace, the fluidized bed reactor and the thermogravimetric analysis technique. The effect of semicarbonized materials used as fillers has been studied and a Bendix time-of-flight mass spectrometer has been adapted to the study of transient and stable species resulting from the flash-

(over)

1. Carbonization of plastics
2. Refractory materials
3. Spectral emissivity
I. AFSC Project 4776
II. Contract AF 33(616)-6841
III. General Electric Co., Cincinnati, Ohio
IV. J. A. Coffman, et al.
V. Aval fr OTS
VI. In ASTIA collection

photolysed degradation of plastics. Properties of carbon residue have been measured.

Vapor pressure studies using the Langmuir evaporation technique, the matrix isolation method, and resonance line absorption spectroscopy have progressed. Rates of evaporation of tungsten carbides, hafnium carbide and titanium carbide have been measured; further conclusive measurements on zirconium carbide have been made. Preliminary application of the matrix isolation technique to thoria has been made. Resonance line absorption studies have been completed on zirconium carbide and titanium carbide and the accessible thermodynamic data have been deduced. Normal spectral emissivities of W-2 coated molybdenum, siliconized ATJ graphite, tantalum, molybdenum, tungsten carbide and zirconium have been measured in the temperature range of 1400 to 3100°K.

photolysed degradation of plastics. Properties of carbon residue have been measured.

Vapor pressure studies using the Langmuir evaporation technique, the matrix isolation method, and resonance line absorption spectroscopy have progressed. Rates of evaporation of tungsten carbides, hafnium carbide and titanium carbide have been measured; further conclusive measurements on zirconium carbide have been made. Preliminary application of the matrix isolation technique to thoria has been made. Resonance line absorption studies have been completed on zirconium carbide and titanium carbide and the accessible thermodynamic data have been deduced. Normal spectral emissivities of W-2 coated molybdenum, siliconized ATJ graphite, tantalum, molybdenum, tungsten carbide and zirconium have been measured in the temperature range of 1400 to 3100°K.